Title
Structural Characterization of the Ag/YBa{sub 2}Cu{sub 3}O{sub 7-x} Interface

Author
Tidjani, M.E.

Publication Date
1990-05-01

LBL-29843
UC404

Lawrence Berkeley Laboratory
UNIVERSITY OF CALIFORNIA

Materials & Chemical Sciences Division

Structural Characterization of the $Ag/YBa_2Cu_3O_{7-x}$ Interface

M.E. Tidjani
(Ph.D. Thesis)

May 1990

Prepared for the U.S. Department of Energy under Contract Number DE-AC03-76SF00098.

DISCLAIMER

LBL-29843

STRUCTURAL CHARACTERIZATION OF THE $Ag/YBa_2Cu_3O_{7-x}$ INTERFACE

Mohammed Elkhamis Tidjani

Ph.D. Thesis
May, 1990

University of California,
Dept. of Materials Science & Mineral Engineering
Berkeley, CA 94720

and

National Center for Electron Microscopy
Materials Science Division
University of California
Lawrence Berkeley Laboratory
Berkeley, CA 94720

This work was supported in part by the Director, Office of Energy Research, Office of Basic Energy Sciences, Materials Science Division of the U.S. Department of Energy under Contract No. DE-AC03-76SF00098.

"To my beloved son Ossama"

STRUCTURAL CHARACTERIZATION OF THE $Ag/YBa_2Cu_3O_{7-x}$ INTERFACE

Mohammed Elkhamis Tidjani

Abstract

Most applications of superconductors (i.e. power transmission cables and tapes, electronic circuits, supermagnets) require some interface with a power source or an electronic device that enables electrons to be injected into, and removed from the superconductor. The quality of metal-ceramic contacts is strongly dependent upon the structural properties of the metal-ceramic interface which depends on the processing conditions and the interaction between the two materials in contact. The present research is intended to characterize the interface microstructure and long term stability of the deposited silver metal in contact to the superconducting oxide $YBa_2Cu_3O_{7-x}$ (YBCO).

High resolution transmission electron microscopy (HRTEM) observations of the interfacial regions reveal that Ag contacts to YBCO occurred without any intermediate phase formation at the interface. The Ag metal exhibits a preferred orientation relationship with YBCO, in which the densely packed planes and directions of the metal are parallel to those of the superconductor. The formation of (111) interfaces and facets during deposition indicates that these planes are associated with the lowest interfacial energy. The as-deposited

Ag film exhibits a granular morphology, and the Ag grains are often twinned along the (111) plane while the surface of YBCO is mostly rough and structurally unstable.

Annealing of the Ag/YBCO interface resulted in outdiffusion of yttrium and oxygen at regions where the surface of YBCO was rough. This diffusion, however, did not result in the formation of continuous layers at the Ag/YBCO interface but only to growth of Ag_2Y and Ag_2O inclusions. Thus it is believed that the stability of the Ag/YBCO depends on the quality of the surface of YBCO, especially its structure. On the other hand, heat-treatment of the interface resulted in grain growth and a decrease in the density of structural defects within the deposited Ag.

Treatment of the surface of YBCO by ion-bombardment yielded flat surfaces but damaged a layer of about 30Å. Such a cleaning process improved the quality of the deposited Ag since the Ag grains were larger and contained low defects concentration. The same orientation relationships between Ag and YBCO were observed after cleaning the surface of YBCO which implied that the destruction of the structure at the surface is only partial. Further treatment of the surface of YBCO by sputter-etching did not result in any enhancement of the quality of the surface.

Deposition of Ag in the same chamber where YBCO was initially grown, to minimize the contamination of the surface of YBCO, also was not effective in enhancing the structure of the Ag/YBCO interface. The roughness of the surface of YBCO did not decrease while the quality of the deposited Ag by laser ablation was worse than that deposited by sputtering.

Any improvement of the morphology and structure of the Ag/YBCO interface and hence the contact resistivity of Ag to YBCO, requires a flat and perfect structure of the surface of YBCO prior to metal deposition. Thus finding a method to treat the surface of YBCO is the clue to establishing a good ohmic contact to the YBCO superconductor.

Acknowledgements

"This work would not have been possible without the blessings and support of Allah to whom I express my full submission and humble thanks."

The author would like to express his deepest gratitude to Professor R.Gronsky for his guidance, support and encouragement throughout the course of this research. He is also grateful to Professors L. C. De Jonghe, J. Clarke, and A. W. Searcy for their review of this manuscript. Thanks are also due to Professor J. Clarke, F. C. Wellstood, and J. J. Kingston for supplying the samples for this experiment. To Dr. M. D. Rubin and Eddie Yen goes my most sincere appreciation for their help in the process of metal deposition.

It is a privilege to acknowledge Professor R. Gronsky's research group, or research *family*, for the pleasant and fruitful time they offered me during my stay among them.

Finally I want to express my heartfelt gratitude to my immediate family, especially, my father, my mother, and my wife for the enduring support and encouragement.

This work was supported by the Director, Office of Energy Research, Office of Basic Energy Sciences, Materials Science Division of the U. S. Department of Energy under the contract No. DE-AC03-76 SF00098.

Table of Contents

I. INTRODUCTION

The characterization of the interface between the high critical temperature superconductor (HCTS) $YBa_2Cu_3O_{7-x}$ (YBCO) and metals is essential for technological applications. The discovery of high temperature superconductivity in LaBaCuO[1], LaSrCuO [2], and YBaCuO [3] systems triggered a burst of research activity in this field. Superconductive properties including transition temperature, Meissner effect, critical field, critical current, and tunneling characteristics etc. have been extensively studied along with the structural and electronic properties of this new class of materials. At the same time, there is concern about the stability of these superconducting materials as well as their technological applications.

Applications of the HCTS such as for electronic interconnects, power transmission lines, Josephson junctions and other devices, in addition to fundamental physics and chemistry studies, require (i) fabricating the material in forms and patterns that are suitable for applications, (ii) improving the superconducting properties such as critical current density J_c, and (iii) understanding and controlling the interface between the HCTS and other materials, e.g. metals for Ohmic contacts. In most technological applications of the HCTS some interface with a power source or an electronic device is required so that electrons can be injected into, and removed from the superconductor. And because $YBa_2Cu_3O_{7-x}$ is a ceramic oxide it has to be incorporated with a material that combines both thermal and electrical conductivity, ductility, and resistance to environmental degradation. However, this subject remains a major challenge due to the high contact resistance that usually occurs when external leads are attached to the superconductor.

Obtaining reliable and low resistance contacts to YBCO is of great concern for many investigators. The interaction between a ceramic oxide and a metal determines the structure of the interface and consequently determines the contact resistivity. Hence achieving a low contact resistance at the YBCO-metal interface requires that the structural details of this interface be studied down to the atomic level. Also, in order to preserve the stoichiometry of the HCTS and the conducting properties of the normal metal at the interface, the chemical reactions and interdiffusion of elements between the ceramic HCTS and the metal in contact must be well controlled.

Metal contacts to ceramic oxides have many characteristics chemical, structural, mechanical, electrical, however, this experiment is designed to study the structure and stability of the interface. The first step is to achieve a metal contact to the superconducting $YBa_2Cu_3O_{7-x}$ with the highest adhesion and structural regularity while preserving the superconducting properties of the ceramic substrate. Metals can be bonded to ceramic oxides by diffusion treatment but the interface may contain new phases that differ markedly from the starting materials but nevertheless are thermodynamically or kinetically stable. It is therefore essential to study the superconducting phase near the interface at the atomic level if possible. The structural and chemical nature of the superconductor-metal interface has to be well established for its best electrical performance. It is the purpose of this research effort to achieve a basic understanding of the metal interface by studying the structural and chemical character of the high T_c superconductor $YBa_2Cu_3O_{7-x}$/Ag interface.

There are three principal interfacial features of interest in this research. The first is the morphology of the interface. This may be characterized by direct examination of the interface using conventional transmission electron microscopy (TEM). The second feature of interest is the identification of

possible reaction product(s) at the interface. Even in the absence of bulk reaction products between the metal and the $YBa_2Cu_3O_{7-x}$ superconductor, the vicinity of the interface has to be carefully examined for possible interdiffusion. High resolution electron microscopy (HREM) will be used for detailed study of the morphology at the atomic scale including spatially defined orientation relationships at the metal/$YBa_2Cu_3O_{7-x}$ interface.

Once the characteristics of the as-deposited metal contact have been determined the stability of the interface will be investigated through the course of heat treatments in an oxygen atmosphere.

I.1. METAL CONTACTS TO CERAMIC OXIDES

Although the applicability of the new high T_c superconducting ceramic oxide YBCO relies heavily on its contact with other materials, especially metals, this subject has received little attention. However the general subject of the metal-ceramic interface has been extensively studied by many investigators. Metal-ceramic interfaces play an important role in electronic packaging systems for information processing [4], thin film technology [5], composites, and the joining with metals [6]. Also, metal- ceramic interfaces play a major role in the understanding of internal and external oxidation processes of metallic alloys. Finally, metal- ceramic interfaces are and will be extremely important in technological applications of the superconducting ceramic oxides.

There are well established physical theories governing the principles of adhesion and bonding of metals to ceramics. However, the quality of metal-ceramic contacts is strongly dependent on the structural properties of the metal-ceramic interface which depends on the processing conditions and the interaction between the two materials in contact. The structure of metal-

ceramic interfaces can best be studied using TEM. Recently HREM has been used to obtain structural details down to the atomic level.

The basic requirements for stable assemblies are chemical bonding across the interfaces and microstructures in the interfacial zones with favorable stress patterns [7]. Generally any two phases can form an acceptable assembly with a chemical bond if they are at stable chemical thermodynamic equilibrium at their interface and they are also compatible physically [8]. Several techniques have been developed for establishing direct contacts between ceramics and metals. The simplest is the direct solid joining of flat specimens [9] at sufficiently high temperatures and pressures, first to realize an intimate contact and second to provide sufficient thermal energy to cause a chemical reaction and obtain equilibrium at the interface. In the case of metallization of ceramic oxides, commonly used in electronic circuitry, metals are directly deposited on ceramic surfaces by metal evaporation, electron beam deposition or sputtering techniques. Metal deposition takes place in vacuum and at much lower temperatures than that used in diffusion bonding or brazing techniques. It is expected that the driving force for chemical reactions is limited and reactions will be diffusion controlled.

Chemical reactions at ceramic-metal interfaces are characterized mostly by mass transport across the interface and sometimes by charge transport [10]. The driving force for the reaction is the reduction in chemical potential of the species involved. Two particular types of reaction could take place at the interface: (a) redox and dissolution reactions and (b) reactions in a reducing gas.

The simplest reaction is the dissolution of one phase by the other to form an immediate equilibrium saturation at the interface. A continuation of the reaction is associated with diffusion into the bulk or diffusion bonding. Most

ceramic metal interfaces, however, are not compatible because redox reactions occur at the interface involving oxidation of the metal and reduction of the cations in the ceramic. Saturation of the interface with the oxide and subsequent formation of a layer oxide results in equilibrium and chemical bonding at the interfaces provided the oxide layer is compatible with both its base metal and the ceramic. When there is an undissolved oxide layer, chemical bonding may occur across the interface. With this structure, however, various physical effects complicate the thermodynamically predicted adhesion and bonding processes. The most important complicating factors are thermomechanical, structural, and dielectric compatibilities of the two bonded materials. Thermodynamically incompatible interlayers may be produced by high temperature growth of stable reaction layers between the metal and oxide ceramic. Furthermore, mismatch between coefficients of thermal expansion results in stress when the interface is heated or cooled from its initial temperature of formation.

A number of metal-ceramic assemblies have been studied in detail [11,12]. The Al_2O_3/Nb bond achieved at 1700°C exhibited good strength at the interface suggesting the formation of stable equilibrium compositions at the interface. Since both phases retain their crystallinity, the role that a possible good epitaxial fit at the interface plays is also a contributing factor. Direct bonding of copper to alumina has also been achieved in an inert gas atmosphere with a fractional percentage of oxygen [13]. The temperature is between the melting point of Cu and the Cu_2O eutectic, causing the formation of a thin film of essentially eutectic liquid on the interface of the copper. This liquid spreads on and reacts with the alumina to form $CuAlO_2$ at the interface.

In bonding ceramic oxides to metals two types of reaction have been observed [14]. Type 1 is a surface reaction between oxide ceramics and noble

metals (e.g. Fe, Co, Ni) which maintains a sharp discontinuity at the interface. Type 2 is a bulk reaction between oxide ceramics and other transition metals which produces a diffuse interface of compositional variations and shows penetration of the metal into the ceramic oxide.

For some non-reactive ceramic-metal systems it has been shown that geometric modelling of interface structures based on the coincidence crystal lattices is not generally applicable for predicting the structure with the lowest energy of a ceramic-metal interface [15]. The optimum interface properties are achieved if certain crystallographic planes of the ceramic and of the metal, including those of the reaction products, make a fit that involves little or no elastic strain [16-18]. This condition is thought to determine the growth of thin films on substrates and applies also to ceramic-supported metal catalysts and bulk ceramic-metal interfaces [19]. Small metal spheres were sintered onto substrates of alkali halides, alumina or magnesia such as to be free to rotate to form minimum energy interfaces [20-22]. In this experiment, parallelism of the close packed planes and directions across the interface was found to be the common characteristic of favored orientations. This occurred preceding high spatial coincidence density, even when such orientations were available. Hence it is thought that "locking in" of close packed rows at the interface is the principle by which nature constructs favoured interfaces between dissimilar solids, rather than high coincidence density. A study of interface dislocations in gold islands on MgO (001) confirmed the prevalence of lock-in orientations [23], and showed that the lattice misfit is taken up by interface dislocations.

On the other hand, there is a group of observations of small, but defined, angular offsets occur between close packed directions and/or planes in metal-ceramic interfaces. Diffusion-bonded Cu and Pt foils on oriented sapphire

crystals have been found to develop a preferential orientation where (111) planes of the metal were parallel to (0001) planes of the sapphire but with the metal crystals rotated in their own (111) plane by different angles for the two metals [24]. In the Nb/Al_2O_3 system the close-packed (0001) planes of Al_2O_3 and (001) planes of Nb were also found to be tilted with respect to each other by 3° [25,26]. This tilt occurs both in specimens grown by epitaxy and by diffusion bonding of samples in which their close-packed planes were initially oriented to be parallel.

I.2. $YBa_2Cu_3O_7$ SUPERCONDUCTOR

X-ray, neutron, and electron diffraction has shown that the superconducting phase $YBa_2Cu_3O_{7-x}$ is orthorhombic [27-29] and has been assigned to the space group Pmmm [30-41]. The orthorhombic phase forms on cooling from the high temperature tetragonal phase with a transition temperature around 700-800°C [42-52]. The $YBa_2Cu_3O_9$ tetragonal structure can be derived from three perovskite unit cells stacked one above the other along the z axis where a yttrium atom replaces the barium centered in the middle cube. For the superconducting phase $YBa_2Cu_3O_{7-x}$ the oxygens on the edges of this cube are removed as shown in figure 1a as well as those along one direction (a direction by convention) on the basal plane. Consequently, the center cube is compressed along the z axis to take up the space of the missing oxygens and the smaller size of yttrium. Another way to describe the structure of $YBa_2Cu_3O_{7-x}$ could be by its most important characteristic, namely, its layered aspect. As shown in figure 1b, the layering sequence is CuO/ BaO/ CuO_2/ Y/ CuO_2/ BaO/ CuO/.... with the two median planes adjacent to the yttrium much closer together (3.18Å) than they are to the basal plane (4.25Å). The basal planes CuO are coupled to the median layer CuO_2 through oxygens

whereas the median planes CuO_2 are not interconnected. Also the basal planes CuO are perfectly flat whereas the median planes CuO_2 appear to be puckered.

Several theories, put forward to account for the high T_c of $YBa_2Cu_3O_{7-x}$ rely on the change of Cu^{III}/Cu^{II} ratio and/or the oxygen deficiency caused by the sintering atmosphere [53]. The oxygens are disordered on the basal (z=0) plane sites in the orthorhombic phase and ordered to form chains in the tetragonal phase. High resolution electron microscopy reveals that oxygen vacancies arranged in ordered sets in Cu planes between Ba layers forming O-Cu-O chains with long-range order [54] resulting in a distortion of the tetragonal cell to an orthorhombic cell. For the superconducting phase $YBa_2Cu_3O_x$, x is close to seven ($6.9<x<7.1$). Beyond that range $YBa_2Cu_3O_x$ is either a low T_c superconductor or a semiconductor [55-57]. So the oxygen content has to be controlled to maintain the oxygen vacancies and hence the superconducting phase.

The high Tc superconducting phase $YBa_2Cu_3O_{7-x}$ exhibits different types of defects ranging from individual missing atoms to faults extending over tens of nanometers. Planar defects consist mainly of staking [58] faults and the insertion of extra plane(s) similar to the basal plane (CuO plane) separated by Ba or Y resulting in $(CuO)_2$ double layers between BaO planes, especially at the surface, which leads to a completely different stoichiometry [59,60]. Furthermore, electron microscopy revels [61-65] that $YBa_2Cu_3O_{7-x}$ contains a high density of twins along {110} planes. The a and b dimensions of the orthorhombic unit cell are almost equal and often interchange directions during the tetragonal to orthorhombic phase transition which results in these twins.

One of the major problems contributing in the instability of $YBa_2Cu_3O_{7-x}$ is its tendency to reversibly exchange oxygen with the surrounding

atmosphere in the temperature range of 600-1100°K. The surface of $YBa_2Cu_3O_{7-x}$ decomposes in oxygen-containing atmospheres above 150°C and is also succeptible to degradation through atmospheric H_2O and CO_2 [66]. The concentration of these defects increases with increasing temperature up to the loss of periodicity.

II. APPLICATIONS OF SUPERCONDUCTORS

II.1. Definitions

Superconductivity, discovered by Onnes in 1911 [67], is the complete loss of electrical resistance at some finite temperature defined as the critical temperature T_c. At T_c, the resistance drops sharply to zero and remains zero at all temperatures below T_c. Almost immediately after the discovery of superconductivity, Onnes found that superconductivity was destroyed by the passage of a transport current greater than a certain critical value I_c or by the application of an external magnetic field greater than a critical value H_c. A consequence of zero resistivity is that everywhere within a superconductor the electric field is zero. In 1933 Meissner and Ochsenfield [68] were able to show that magnetic fields are completely excluded from the body of a superconductor in its superconducting state. This is known as the Meissner effect. The magnetic induction does not fall abruptly to zero at the surface of the superconductor, but decreases exponentially over a characteristic distance, the penetration depth. The flux is excluded by supercurrents that flow in the penetration layer so as to produce a magnetic field within the superconductor that exactly cancels any externally applied field.

II.2. Applications of superconductors

Superconductors are employed in different electrical devices mainly because they can theoretically (and practically) carry extremely high overall current densities. These high current densities allow the construction of smaller and more compact machines. Compactness is aided by the fact that the

lack of power dissipation consequent upon the absence of electrical resistivity reduces the necessity for internal cooling. The reduced power requirements are an added attraction, though they must be balanced against the power consumed by refrigeration. The applications of superconductivity are basically of three types briefly listed below.

II.2.1. Generation of large magnetic fields

The most important application of superconductivity, in terms of quantity of material employed, has been the production of magnetic fields. Materials suitable for magnet construction are the irreversible type II superconductors, with high upper critical fields and high bulk current densities. The principal difference between the conventional copper-iron or resistive magnets and superconducting ones are twofold: (a) the field and current are not independent variables in superconducting magnets; and, of more practical significance, (b) the current density in superconducting magnets is higher than that of conventional magnets.

First, magnetic fields are used in physics laboratories for research purposes. Highly stable magnetic fields for NMR and for high-resolution, high-voltage electron microscopy are provided by superconducting magnets. Superconductors may also be used for the production of large magnetic fields. Large refers not only to the field intensity but also to the volume over which it is generated. Large magnetic fields are required in high-energy nuclear physics. Power generation by magnetohydrodynamic methods or thermonuclear fusion will require large fields that can only be provided by superconducting magnets. Superconducting motors and generators are devices in which the superconductor is used to generate high magnetic fields. Superconducting magnets have also been proposed for the levitation of high-speed tracked vehicles.

The first successful superconducting magnet was constructed by Yntema in 1955 by winding cold-worked niobium wire around an iron core. This magnet achieved a field of 0.7 T [69]. At the same time, laboratory magnets capable of producing 10 T were made from Nb_3Sn [70].

II.2.2. Superconductors for Power Transmission

Superconductors have been proposed for power transmission cables and tapes. The design of a superconducting transmission line consists of three interdependent parts: the cable itself; the refrigeration system; and the transmission line as a whole. For most cable designs the coaxial geometry is generally preferred because of compactness and lower eddy current losses. The cryostat may be either flexible or rigid.

Rigid conductors are the simplest, both conceptually and electrically, and were the first to be developed. They consist of rigid pipes held concentric by solid spacers. Each pipe is made of a composite incorporating a superconductor and a good metal. The coolant flows in the annular space between the conductors. Figure 2 shows an example of such composite cable which consists of concentric layers of copper and niobium. The niobium faces the annular space between inner and outer conductors and therefore under normal operation carries all the current. During faults, the current transfers to the copper layer. The copper also provides sufficient strength to withstand both the pressure of the coolant and the magnetic pressure during faults.

The basic design of a flexible cable is shown in figure 3. Conductors, either tapes or wires, and dielectric tapes are helically wound in cylindric forms. Flexibility results from butt gaps between individual conductor strands and dielectric tapes. Because of advantages such as longer fabrication lengths, higher dielectric strength, and accommodation of thermal contraction, most

designs of superconducting cables favor flexible coaxial conductors with lapped plastic tape as dielectric.

II.2.3. Superconductors for electronic circuitry

Superconductors can be employed in electronic circuitry. Devices were originally based on the idea of using the superconductor-normal transition as a switch. Devices based on the Josephson effect are also of great interest. The critical current that flows between two superconductors weakly coupled together through a weak link, which may be a very thin (2nm) oxide barrier, or a layer of nonsuperconducting metal, varies in an oscillatory fashion depending on the local value of the magnetic field of the weak link. This effect can be used as the basis of highly sensitive ammeters, gauss meters, and voltmeters, as well as logic and memory elements [71]. Superconducting thin-films are the basis for such applications.

II.3. Importance of metal contacts to superconductor :

Among the other requirements for good performance of supermagnets is superconductor stability. The simplest approach to the prevention of flux jumping is the use of "fully stabilized" or "cryostatically stable" conductors [72-74]. These consist of superconductors in close thermal and mechanical contact with sufficient normal metal of high electrical conductivity to smooth out local hot spots and to ensure an alternative current path during periods of instability.

It is obvious that the most important requirement of any conductor is that it be able to carry the highest possible current. However, during operation, power cables will occasionally be subjected to sudden rapid rises in current and/or voltage due to lightning strikes or to short circuits somewhere along

the network. The occurrence of these surges must be taken into account in the cable design. For conventional ac cables, surges of up to 10-20 times the normal rated current could occur and last for a few cycles before breakers open [75]. To cope with this problem, conductors are made of composites that incorporate a good normal conductor, such as pure copper or aluminum, and a hard superconductor with high critical current density. The conductor into which the superconductor is incorporated must be mechanically strong and able to withstand forces imposed by current and field. It must be stable against flux jumps and sudden changes in current, field, or temperature.

II.4. $YBa_2Cu_3O_{7-x}$/metal contacts

The fundamental discovery of superconductivity in $YBa_2Cu_3O_{7-x}$ has had a great impact on the application of superconductors in many technical fields. A number of fabrication techniques have been already proposed to produce superconducting wires [76-80]. Due to the inherent brittleness of ceramic materials and the difficulties in forming the HCTS into desired shapes thick-film fabrication techniques have been investigated such as coating by electrophoretic means [81]. The prospect of coating superconducting materials on a variety of substrates may offer some advantages for large scale as well as electronic device applications. Using electrophoretic deposition to make YBCO coatings on Cu, Ag, polycrystalline Al_2O_3, and single crystal MgO and YSZ substrates has been reported. For coatings on Ag, MgO(Ag), and YSZ(Ag) substrates, sharp superconducting transitions at about 90°K have been obtained. However, intermediate layers were formed on Cu, Al_2O_3 (Al), and YSZ(Ag) [82]. They are thought to occur as a result of interfacial reactions during firing. However, a prior condition for technical applications of a superconductor involving high currents are low resistance contacts. High

resistance contacts dissipate heat and may lead to low critical currents in the system. Even for fundamental studies of superconductivity, low contact metallic resistance is required for four-probe measurement techniques. Consequently, a great deal of research has been focussed on producing low resistivity ohmic contacts using diverse methods and different metals.

Several different contacts on the $YBa_2Cu_3O_{7-x}$ superconductor have been used to minimize the contact resistivity defined as the contact resistance times the contact area. Previous work in the literature includes silver epoxy [83], melted [84] or embeded [85] gold, pressed indium [86], and ultrasonic soldering [87]. Those methods applied to bulk superconductors have been found to exhibit high contact resistance, typically in the range of 10^{-2} ohm.cm^2, considered high for most practical applications and critical current measurements. Low contact resistivities have been obtained essentially by sputter deposition of gold or silver onto YBCO superconductor and annealing at 500-600°C in an oxygen atmosphere [88] which has given contact resistance of 10^{-10} ohm.cm^2. The same value has been also obtained using as-evaporated gold films on YBCO thin films [89]. However, evaporated metal contacts on bulk YBCO have been reported to give higher contact resistances [90,91]. Evaporation deposition of silver films on YBCO has achieved about 10^{-8} ohm.cm^2 [92] after annealing at 500°C in oxygen atmosphere. Plasma-sprayed silver metallization on YBCO has been also employed with which a contact resistance of about 10^{-8} ohm.cm2 has been obtained without additional heat treatment [93].

There are two processes with different physical origins that may contribute to the contact resistance on oxide superconductors. One relates to the modification in the detailed charge balance and carrier concentration at the interface induced by the proximity contact metal. The other is due to the

nature of carrier injection which depends on the nature of the free surface of the superconductor [94]. The contact resistance of different metals such as Al, Bi, Ag, and Au has been found to decrease as the temperature of the superconductor is decreased. On the other hand, the curent-voltage characteristics at the $Ag/YBa_2Cu_3O_7$ contact show nonlinearity, which has been attributed to the superconducting state of the interface [95].

Reactions between YBCO and other materials at elevated temperatures have also been investigated [96-99]. These studies have been focused on incorporating foreign atoms into the superconductor and examining their effect on the material. The interaction between Au and YBCO from 800 to 878°C in oxygen atmosphere has been studied [100]. It has been found that Cu and small amounts of Ba were removed from YBCO resulting in a different structure and leaving what has been thought of as $BaCuO_2$ and CuO on the surface of Au.

However, none of the updated publications has provided any structural details of YBCO-metal interfaces to be correlated with its electrical properties. Success of technological applications is likely to be based on a complete understanding of the morphology, microstructure, and orientation relationship of the metal/superconductor interface. Once this understanding has been achieved, the stability of the interface or enhancement of its quality by heat-treatment should be investigated and correlated with its electrical properties.

III EXPERIMENTAL PROCEDURES

III.1 Preparation of $YBa_2Cu_3O_{7-x}$

Superconducting thin films of $YBa_2Cu_3O_{7-x}$ were furnished by the research group under the supervision of Prof. J. Clarke in the Department of Physics at the University of California at Berkeley. The films, about 300nm thick, were deposited from 2.54mm diameter, pressed and sintered, stochiometric targets. A 0.15m focal length lens was used to focus 248nm pulses from a Questek series 2800 excimer laser onto the surface of the target at a 45° angle of incidence. Cleaved and polished [100]-oriented MgO, $12.5x12.5x1mm^3$, was used as a substrate. The substrate was mounted onto an Inconel heater block using silver paste. The heater block was mounted in a high vacuum chamber 60 mm from the target so as to intercept the normally directed ablation plume. The heater block and substrate were first outgassed, by raising the temperature of the substrate holder to 730°C as the chamber was pumped down to 5 μTorr. Once the silver paste was outgassed, oxygen was supplied to the system with an O_2 pressure maintained at 190mTorr. The surface of the target was then cleaned by 300 laser pulses at $1.2Jcm^{-2}$ and the YBCO layer was deposited using $1.2Jcm^{-2}$ pulses at 5Hz. Once the deposition was completed the chamber was filled with O_2 to 700Torr and the heater block was allowed to cool to 450°C in 15 min, after which the sample was cooled to 100°C.

III.2 Metallization of the superconductor

The microstructure, uniformity, and purity of the deposited metal are critical to achieve a good ohmic contact as well as for electron microscope sample preparation. Hence vacuum coating techniques have been used to deposit Ag on $YBa_2Cu_3O_{7-x}$ (YBCO). The most commonly used of these

techniques are evaporation and sputtering. For evaporation, the coating metal is heated to produce a free-flowing vapor which travels to the substrate and forms a deposit. This results in heating of the substrate and may cause the superconducting phase to lose its properties. In the case of sputtering, however, the coating material remains in its solid form and gaseous ions are accelerated towards the target at high energies to sputter away the target material. After sputtering, the microstructure of the coating tends to be denser than that produced by evaporation and the subtrate does not heat up, an important feature that is critical for the stabilization of the $YBa_2Cu_3O_{7-x}$ superconducting phase.

Sputtering: The basic sputtering process takes place in a partial vacuum. Two electrodes are mounted in a vacuum chamber. The cathode, or the target, which is the material to be deposited, is held at a potential of -2 to -5kV with respect to the grounded anode, to which the part to be coated is fixed. During the sputtering process, the vacuum pumps are throttled, and a gas such as argon is metered in to maintain a vacuum of about 10Pa. The positively charged gas ions are accelerated towards the cathode striking it at high velocity, dislodging target atoms which then travel to the anode.

Heat treatment of YBCO/Ag contact: The basic advantage of using sputtering is the adhesion of the deposited film. Heat treatment of the YBCO/Ag contact, which may improve its quality, is also performed subsequent to Ag deposition. The metal/superconductor contact is hence annealed in an oxygen atmosphere at 500°C for two hours.

Laser ablation of Ag: Silver was also deposited by laser ablation in a separate experiment. This procedure was used to reduce the degradation of the surface of YBCO when exposed to the ambient atmosphere. In this case, Ag was deposited within the same chamber where the YBCO film was grown.

III.3 Sample preparation for Transmission Electron Microscopy

Information obtained from plan-sectioned specimens is indirect and the accumulated data may be significant only after sufficient deconvolution. To obtain the maximum information about the the YBCO/Ag interface, preparation of cross-section specimens is required to achieve lateral resolution and to be able to view specimens parallel to the interface. Traditional techniques [101-103] of mechanical polishing and ion milling are used to prepare all the samples for the present experiment. The procedures for specimen preparation consist of three major steps as described below.

II.3.1 Cutting the materials to appropriate sizes

The first step is to cleave the trilayer (MgO, YBCO, and Ag), which is generally $10x10x1mm^3$, into two equal rectangular slabs. The slabs are then cemented together such that the Ag layers are facing each other as shown in figure 4. The glue used is "M-BOND 610 ADHESIVE" furnished by (Measurements Group, Raleigh, NC 27611). The advantages of using this type of glue are: its strength, its small thickness when properly applied, and its thinning rate which is very close to that of MgO. However, it must be thermoset under pressure for about one hour at 150°C. For this purpose a small vise is used that can be heated in an oven. The vise is designed such as to be able to apply pressure evenly to the brittle MgO substrate. This rectangular slab is then sectioned along its length such as to have two sandwiched samples each measuring about $10x2.5x2mm^3$. The last step is to cut off from each slab a number of slices approximately 300μm thick. The cutting procedure is accomplished with a diamond wafering saw. Before slicing, it was found that it is convenient to attach the sample with wax rather than using the clamps of

the saw. At this stage a $2.5x2mm^2$ sandwiched sample of 300μm thickness is ready for the process of mechanical thinning.

III.3.2 Mechanical thinning

Once the slices are obtained the process of thinning down to electron transparency begins. Each slice is mounted with a strong wax (i.e "Crystal-Bond") on a piece of glass. The wax helps protect the edges of the specimen from preferential polishing or cracking. On the other hand, using the glass enables the specimen to be viewed during sanding and polishing, to ensure that it does not come loose as well as to estimate its thickness by optical microscope. It is extremely important to mount the slice such that its surface is parallel to that of the supporting glass throughout the whole process. Starting with 600-grit sandpaper, the sample is ground to a thickness of about 200μm and then polished with 1.0μm diamond paste on a polishing cloth. No water is used, since water may react with the superconducting film; only alcohol or kerosine is used in this thinning step.

After thinning and polishing, a 3-mm copper grid with a single oval hole is glued onto the polished surface of the specimen. The brittle cross-section becomes much easier to transport and handle while mounted to the grid. The glass substrate is then heated and the specimen is removed. The other surface is then ground to a thickness of about 100μm and polished to about 60-70μm.

The final stage of mechanical thinning is accomplished by dimpling. In this process a concave impression is polished into the face of the specimen. The dimpling wheel must be centered as accurately as possible on the interface. This leaves the outer perimeter of the specimen thick, and thins only the center region containing the interface to the desired thickness. The final thickness of the specimen achieved with the dimpler is limited by the brittleness of the MgO substrate. Under the best conditions, when the specimen

is crack-free, a thickness of 20μm can be achieved. The sample is then cleaned by soaking in acetone and is ready for the final stage of thinning.

III.3.3 Ion-beam thinning

The last stage of thinning is accomplished by using an ion-beam milling apparatus. Initially the specimen is bombarded from both sides with argon ions accelerated with 5.5kV potential and at a specimen tilt of 16° for about two hours. Because the specimen consists of compounds with different sputtering rates, it is more effective to stop the specimen rotation, and set it in a position where the interface is perpendicular to the ion beam, as shown in figure 5. This step, however, is not intended to perforate the specimen but only to create a thin region at the interface. By using both guns the time required to perforate the specimen is reduced.

In the second step only one gun is used, and targeted on the undimpled side with accelerating voltage and specimen tilt reduced to 4kV and 12° respectively.

In the third and final step the specimen is ion-milled using both guns at low accelerating voltage (3-4kV) and a shallow angle (8-10°). The purpose of this step is to remove the damaged layer which may build up as a result of ion-bombardment. To obtain an adequate sample for lattice imaging some additional precautions need to be taken. (a) The specimen is mounted such that the interface is parallel to the short edge of the hole of the copper grid. In this configuration the edges of the grid intercept the ion flux when it is parallel to the interface. (b) The ion beam must be positioned accurately with respect to the specimen such that the thin region is centered on the interface. (c) Since the MgO substrate is transparent to light, the laser terminator can not be used and the process of thinning must be followed carefully to avoid excessive thinning or complete loss of the specimen. (d) To minimize the ion-beam

damage the specimen must be ion-milled at low temperature, i.e liquid N_2 temperature.

IV RESULTS

IV.1 Structure of the grown YBCO film

The high T_c superconductor YBCO, grown on (001)-oriented MgO substrate, was tested electrically and structurally before metal deposition. The resistivity versus temperature curve is shown in figure 6. The critical temperature T_c (zero resistivity) is 87 °K with a very narrow transition width.

The superconducting layer was found to be polycrystalline, however, large grains exhibiting specific orientation relationships with respect to the substrate were often observed. Most frequently the c-axis of the YBCO film was oriented normal to the interface. Figure 7 shows (a) a high resolution lattice image of a typical YBCO/MgO interface along with (b) its corresponding selected area electron diffraction (SAD) pattern. From the indexed SAD pattern, in figure 7c the following orientation relationship is readily obtained:

$$(001)_{YBCO} \,//\, (001)_{MgO} \quad (1)$$

$$(100)_{YBCO} \,//\, (100)_{MgO} \quad (2)$$

$$[010]_{YBCO} \,//\, [010]_{MgO} \quad (3)$$

In figure 7a the two sets of {100} planes are visible in both the YBCO grown film (above) and its MgO substrate. The interface lying parallel to the (001) planes is atomically flat in the entire micrograph. However, dark regions of about 20 Å are seen periodically along the interface representing the strain-fields due to lattice mismatch between $(010)_{YBCO}$ (3.89Å) and $(010)_{MgO}$ (4.21Å). The micrograph also shows that the first few atomic layers (about ten) of the grown YBCO contain different classes of defects ranging from insertion of extra planes as in region (i) to regions of completely different structure as in region (iii) as well as bending of atomic planes such as in region (ii). Away from the interface the regular periodicity of clearly resolved white dots in the

image, as seen in the upper right hand side of the micrograph, indicates that the lattice of YBCO is free of distortion. Whereas close to the interface rapid oscillation in contrast can be seen.

Deviations from the above orientation relationship are sometimes encountered, two examples of which are shown in figure 8. In the first micrograph, figure 8a, two grains (I) and (II) are oriented such that their c planes are respectively parallel and normal to the interface and perpendicular to each other. It can also be noticed that the $(001)_{YBCO}{}^{II}$ planes are heavily bent along the grain boundary. The corresponding SAD pattern shown in figure 8c and illustrated in figure 8d reveals that the c-axis is normal to the incident beam for both grains with the following orientation relationships:

$$(001)\ MgO \perp (001)YBCO^{I} \qquad (001)\ MgO \parallel (001)YBCO^{II}$$

$$(010)\ MgO \perp (010)YBCO^{I} \qquad (010)\ MgO \parallel (010)YBCO^{II}$$

$$[100]\ MgO \parallel [100]YBCO^{I} \qquad [100]\ MgO \parallel [100]YBCO^{II}$$

Figure 8b is a micrograph showing a second example showing two adjacent grains of YBCO in the [100] orientation. While their c-axes are, again, normal to the incident beam, they form a 44° angle. Grain II has the same orientation relationship as grain II in in figure 8a; however, grain I is inclined 44° to the interface. In both figure 8a and 8b the grains retain their specific orientation down to the MgO substrate which indicates that the nucleation of each grain took place separately. In both examples, however, there exist regions of overlap between the YBCO grains indicating that the grain boundaries are not sharp and/or not normal to the incident beam.

IV.2 YBCO/Ag interface

A thin film of silver of about 300 nm was sputtered onto YBCO and

examined by HREM to determine the morphology, structure, and orientation relationships at the YBCO/Ag interface.

IV.2.1 Morphology of the interface

A low magnification electron micrograph of a typical contact between silver and the high critical temperature superconductor $YBa_2Cu_3O_{7-x}$ is shown in figure 9a. It can be seen that YBCO is much thicker than Ag, due to the difference between their thinning rates in the ion mill. Large grains of Ag exhibiting particular orientation relationships with respect to YBCO are evident. Although the Ag film appears to be heavily twinned along the whole interface, no visible intermediate layer could be seen. The SAD pattern in figure 9b taken near the interface shows spots from both Ag and YBCO. The indexed pattern in figure 9c indicates that Ag is in the [011] zone axis twinned along the (111) plane, while YBCO is in a [100] zone axis.

At higher magnification, figure 9d, two sets of $\{111\}_{Ag}$ as well as $(001)_{YBCO}$ planes are resolved. There are, however, regions of different contrast frequently observed at certain parts of the interface representing, most probably, strain-fields due to mismatch between the two lattices. There is also a layer of variable thickness, 15 to 30 Å, extending along the interface. The SAD pattern, however, does not reveal any major spots that allow the identification of this intermediate layer. On the side of YBCO the (010) planes appear to extend through this layer without a distinct boundary. This implies that the surface of YBCO contains disordered regions prior to any Ag deposition.

Figure 10a shows another interface and illustrates the roughness of the surface of YBCO. In this micrograph YBCO is seen to have uniform structure up to the the interface, despite the roughness of its surface, and the Ag film

appears to have granular morphology. The SAD pattern in figure 10b taken from the interface shows that there is again a 9° offset angle between the close packed planes $(111)_{Ag}$ and $(001)_{YBCO}$. The indexed pattern in figure 10c shows that Ag is in a [123] zone and YBCO is in a [100] zone.

IV.2.2. Structure of the interface

Figure 11a shows a lattice fringe image of a Ag/YBCO interface where a sharp boundary can be seen extending over large areas without any intermediate layer. The SAD pattern in figure 11b is indexed in figure 11c and shows parallelism of the close-packed planes $(111)_{Ag}$ and $(001)_{YBCO}$ with an offset angle of about 1.5°. In this micrograph both close-packed planes $(111)_{Ag}$ and $(001)_{YBCO}$ are resolved as well as interfacial steps along the interface. Closer inspection of the silver planes indicates that $(111)_{Ag}$ planes change orientation along the steps of the YBCO surface. Regions of dark contrast result from the strain fields caused by mismatch between the two lattices. Linear defects crossing the c planes of YBCO are also seen extending sometimes up to the interface.

Figure 12a shows another orientation of the Ag/YBCO interface. Here again the close packed $(111)_{Ag}$ planes are stacked parallel to the $(001)_{YBCO}$ planes with no offset angle like that observed in the previous cases. Inspection of the SAD in figure 12b, indexed in figure 12c, shows that Ag is oriented along a [011] zone axis parallel to the $[100]_{YBCO}$ zone axis. Due to the thickness of this region of the sample, only the $(001)_{YBCO}$ is visible as well as the twin boundary on the silver side. While the contrast along the flat region of the interface is constant, it changes frequently along the the curved interface. It can be noticed also that the twin boundary starts near a step on the YBCO surface. However, no intermediate layer can be resolved as in the

previous orientation.

IV.2.3 Orientation relationship

Two unique orientations are found in all Ag/YBCO interfaces studied. In both the close packed $(111)_{Ag}$ planes are stacked parallel to those of YBCO, the $(001)_{YBCO}$ planes. The only variables are the orientations in which the interface is imaged and the offset angle between $(111)_{Ag}$ and $(001)_{YBCO}$ planes. However, this angle seems to decrease as the roughness of the surface of YBCO decreases and completely vanishes whenever there is a direct contact between Ag and YBCO. Those orientation relationships are summarized below:

Figure 9c	$[011]_{Ag}$ // $[100]_{YBCO}$	
	$(111)_{Ag}$ // $(001)_{YBCO}$	rotated 9°
Figure 10c	$[123]_{Ag}$ // $[100]_{YBCO}$	
	$(111)_{Ag}$ // $(001)_{YBCO}$	rotated 6°
Figure 11c	$[123]_{Ag}$ // $[100]_{YBCO}$	
	$(111)_{Ag}$ // $(001)_{YBCO}$	rotated 0°
Figure 12c	$[123]_{Ag}$ // $[100]_{YBCO}$	
	$(111)_{Ag}$ // $(001)_{YBCO}$	rotated 1.5°

IV.3 Heat-treatment of the interface

In order to study the stability of the Ag/YBCO interface the deposited Ag film was heat-treated for two hours in an oxygen atmosphere. The effect of this experiment on the morphology and structure of the interface is presented in the following sections.

IV.3.1 Effect on the morphology and structure of the interface

A lattice image of a typical region of the annealed Ag/YBCO is shown in figure 13a. Direct contact of Ag to YBCO can be seen in the entire micrograph in which the interface is well defined without any extended transition region between the two components. The Ag film shows much larger grains when compared to what was found prior to the heat treatment. The interface is still not atomically smooth. Apart from a flat region on the left side of the micrograph the Ag/YBCO interface is irregularly rippled due to local growth perturbations in the YBCO thin film. The corresponding SAD pattern is shown in figure 13e and indexed in figure 13f. The YBCO grain is in a [100] orientation while the Ag region consists of a [011] oriented grain and its twin along the (111) plane. Close-packed planes $(001)_{YBCO}$ and $(111)_{Ag}$ are stacked parallel to each other and to the interface. The twin boundary can be seen in the micrograph parallel to the (111)Ag planes consistent with the diffraction pattern. Only one set of {111} Ag planes is visible around the interface due to the misorientation (or bending) of Ag away from the exact zone axis condition. However, both sets of {111} Ag planes can be seen in the upper right hand side of the micrograph.

The inset box I is shown in figure 13b at higher magnification. In this figure both (010) and (001) YBCO planes are resolved; however, the c-planes are not smooth everywhere since bending of those planes and disturbances in the stacking parallel to the c-axis are evident in this image. The curvature of the interface clearly observable at lower magnification does not seem detrimental to the epitaxy of the deposited Ag film or to the structure of YBCO. The stacking sequence of both (010) and (001) YBCO planes is preserved up to a thin layer of about 20 Å at the interface wherein the structure of both YBCO

and Ag are distorted especially in YBCO. This becomes even clearer in figure 13c showing the specimen after tilting around $[010]_{YBCO}$, which brings the interface closer to an edge-on orientation. In this orientation, this layer shows interpenetration of the $(001)_{YBCO}$ and $(111)_{Ag}$ planes and bending of the $(001)_{YBCO}$ planes.

Figure 13d shows the inset box II in figure 13a at higher magnification. This micrograph shows an area where the Ag/YBCO is nearly free of curvature. The lattices of both Ag and YBCO can be clearly distinguished at the interface and the disturbed regions close to the interface are very narrow, i.e. only three to four lattice planes in YBCO. Closer inspection of the stacking sequence of the (111) Ag planes shows that there is a dark/bright contrast oscillation running along the interface at the right hand side of the micrograph. This oscillation seems to be regular in that there is one dark fringe every two bright fringes and might correspond to specific planar matching conditions at the interface.

A lattice image of another region of the annealed Ag/YBCO interface is shown in figure 14a. The SAD pattern in figure 14b taken near the interface shows spots from both Ag and YBCO. The indexed pattern in figure 14c again indicates that Ag is in the [011] zone axis twinned along the (111) plane while YBCO is along the [100] zone axis. In figure 14a crystallinity is maintained on both sides of the interface up to the boundary plane. The $(111)_{Ag}$ and $(001)_{YBCO}$ planes are resolved up to the interface and appear to be interlocked. The Ag/YBCO contact exhibits a sharp interface along the whole micrograph with occasional unit steps due to local growth perturbations of the YBCO film. The flat faces of the interface are atomically smooth in most regions and facets can clearly be identified in this micrograph, i.e at the arrow. The facet risers exhibit darker strain contrast.

IV.3.2 Orientation relationship at the annealed interface

In most of the interfaces observed after annealing, Ag is found to lie along a [011] zone axis. The predominant orientation relationship is consequently:

$$[011]_{Ag} \,//\, [[100]_{YBCO}$$

$$(111)_{Ag} \,//\, (001)_{YBCO} \quad (5)$$

However, an offset angle is sometimes encountered when the surface of YBCO shows irregularity and/or roughness. Figure 15 is an example where the orientation relationship (5) holds but the $(111)_{Ag}$ is rotated 4° with respect to the $(001)_{YBCO}$ as can be seen from the diffraction pattern in figure 15c. The indexed SAD in figure 15d shows three grains of Ag in the [011] orientation and YBCO in the [100] orientation with no extra spots. This is confirmed in the bright field image in figure 15a where three large grains of Ag can be seen and where the two sets of {111} Ag planes are resolved. The interface, however, does not look smooth everywhere and both YBCO and Ag overlap near the interface, i.e. at the arrow and in the inset box. At higher magnification, figure 15b, three major structural regions can be distinguished. At the left hand side of the micrograph the two set of {111} Ag planes are clearly in region I as well as $(001)_{YBCO}$ in region III, while the boundary in between looks sharp and atomically smooth. At the right hand side of the image, however, there is a region (II) where YBCO and Ag overlap. This shows that the surface of YBCO is not flat and explains the existence of the offset angle.

IV.3.3 Formation of new phases at the annealed interface

Formation of Ag_2Y: As was described above, the YBCO/Ag contact frequently shows no intermediate phase and Ag is directly bonded to YBCO. However, interdiffusion of certain species through the interface was

sometimes encountered, where the formation of new phases occurred at regions of rough and disturbed YBCO surface. In this section some examples of this phenomenon are reported.

Figure 16a is a HREM micrograph showing a [123] oriented grain of Ag in contact to YBCO in the [100] orientation. While certain parts of the YBCO/Ag contact exhibit smooth and flat interfaces, regions where the surface of YBCO appears to be rough show some inclusions between YBCO and Ag. The SAD pattern in figure 16b was taken at region (II) and indexed in figure 16c. Spots from both YBCO and Ag in the [100] and [123] orientations respectively are identified and used as an internal callibration to the remaining reflections. The extra spots coming from the inclusion could be indexed as silver yttrium Ag_2Y, a tetragonal phase, in the [331] zone axis. Figure 16f and 16g are the inset boxes (I) and (II) at higher magnification. In figure 16f a sharp interface between Ag and YBCO can be seen, both $(111)_{Ag}$ and $(001)_{YBCO}$ are resolved up to the interface. Lattice distortions at the contact are limited to a very narrow region, preferentially, in YBCO. Facets parallel to the incoming electron beam can clearly be identified due to the offset angle between $(111)_{Ag}$ and $(001)_{YBCO}$ planes. This offset angle is probably due to local growth perturbations of the grown YBCO as can be observed. Apart from this flat interface Ag and YBCO are separated by Ag_2Y. In figure 16g the cross lattice fringes of Ag_2Y and $(111)_{Ag}$ are clearly resolved and the contact between the two phases exhibit a sharp and atomically smooth interface at the arrow. This is not the case everywhere, a layer that appears to be amorphous separates Ag and Ag_2Y. Figures 16d and 16e illustrate the orientation relationships between YBCO and Ag_2Y and YBCO and Ag respectively which are:

$$[100]_{YBCO} \,//\, [331]_{Ag_2Y} \qquad [100]_{YBCO} \,//\, [123]_{Ag} \qquad (6)$$

$$(001)_{YBCO} \,//\, (111)_{Ag_2Y} \qquad (001)_{YBCO} \,//\, (111)_{Ag} \quad 3^\circ \text{ rotated}$$

Figure 17a is an other example where Ag_2Y forms along the whole interface seen in this micrograph with variable thickness. Close inspection of the bright field images figures 16a and 17a as well as their SAD patterns shows perfect structure in YBCO along the interface. This may imply that the silver diffused through the disordered surface of YBCO during the heat treatment procedure rather than yitrium diffusing out of YBCO. Figure 17b is the SAD pattern taken at the interface illustrated in figures 17c , 17d and 17e yielding the same orientation relationships as (6).

Formation of Ag_2O: Another phase found to form at the interface is the cubic Ag_2O. Figure 18a shows that a second phase particle has nucleated at the Ag/YBCO interface, at the arrow sign. The (111) planes belonging to the [123] oriented Ag as well as $(001)_{YBCO}$ are clearly visible up to the interface which can be seen as flat and sharp. Facets along the YBCO/Ag contact are also visible, as well as dark contrast images. Inspection of the SAD pattern shown in figure 18b and illustrated in figure 18c indicates three separate grains YBCO, Ag, and Ag_2O in the [100], [123], and [011] orientation respectively. From figures 18d and 18e the orientation relationships between YBCO and Ag_2O and YBCO and Ag are:

$$[100]_{YBCO} \;//\; [011]Ag_2O \qquad [100]_{YBCO} \;//\; [123]_{Ag} \qquad (7)$$

$$(001)_{YBCO} \;//\; (100)Ag_2O \qquad (001)_{YBCO} \;//\; (111)_{Ag} \qquad 3° \text{ rotated}$$

The structure of YBCO near the Ag_2O particle is clearly disturbed suggesting that oxygen diffused out of YBCO upon annealing the interface. It can also be noted in this micrograph that Ag in the [011] orientation has started to nucleate in specific location Ag.

IV.4 Laser ablated Ag on YBCO

In the previous sections it was reported that the surface of YBCO reacts easily with the ambient atmosphere. This leads to structural degradation which is detrimental for the superconducting properties of YBCO. The contact resistivity would also deteriorates if the metal is not deposited on a clean surface of YBCO and/or if the heat treatment leads to the formation of some reaction products at the interface. To cope with this problem an attempt has been made to deposit Ag before the surface of YBCO is exposed to the ambient atmosphere. Hence the Ag film was laser-ablated immediately after the YBCO film was grown. The deposition of both YBCO and Ag took place in the same chamber. The results of this experiment are presented below.

Figures 19a, 19b, and 19c are a series of HREM images taken at different regions of the YBCO/Ag contact following the procedure described above. Both close packed planes $(111)_{Ag}$ and $(001)_{YBCO}$ are visible in the three micrographs. There is, however, an intermediate layer of different thicknesses along the interface which could not be identified, but which could be an amorphous layer at the surface of YBCO that developed upon deoxygenation of the chamber prior to Ag deposition. This is also supported by the fact that the $(111)_{Ag}$ planes are randomly oriented with respect to the interface. Figure 19b shows cross lattice fringes belonging to YBCO in the [110] orientation as seen in figure 20b. Both (110) and (001) are clearly resolved without any observable distortion or bending of those planes.

A rather interesting result is presented in figure 20a where Ag_2Y is found to nucleate along the surface of YBCO. In this figure steps of one to four atomic layers are observed along the whole surface of YBCO illustrating once again its irregularity. The location, number and size of these steps are quite random.

The SAD pattern, in figure 20b, taken from this region and indexed in figure 20c indicates that YBCO is in the [110] orientation while the extra spots are found to belong to Ag_2Y in the [110] orientation yielding the following:

$$[110]\ YBCO\ //\ [110]Ag_2Y \qquad (8)$$
$$(001)YBCO\ //\ (001)Ag_2Y$$

The Ag_2Y phase does not seem to be continuous along the surface of YBCO but rather distributed as clusters. Dark contrast is observed at the steps of the surface of YBCO in which lattice fringes run normal to the $(001)YBCO$ planes. Those lattice fringes belong to Ag_2Y in full agreement with the SAD pattern in figure 20b.

IV.5 Treatment of the surface YBCO prior to Ag deposition

Despite the attempts made to do so, obtaining a direct contact between Ag and YBCO was very difficult to achieve. The surface of YBCO was found to be rough and exhibited different structure and/or composition over large areas compared to that observed in bulk films. In order to enhance the properties of the Ag/YBCO interface we tried to treat the surface of YBCO to make it flat and structurally stable. In the first stage the surface was "cleaned" by ion milling and in the second stage the surface was sputter-etched. Silver was subsequently sputtered onto the surface following each stage and structurally characterized.

IV.5.1 Deposited Ag on the ion milled surface of YBCO

Figure 21a and 21b show a typical YBCO/Ag interface, taken at low magnification, and the corresponding SAD pattern respectively. The micrograph illustrates the effect of ion-milling on the surface of YBCO before the metal contact is established. Three layers of distinguishable contrast are

observed representing the glue, Ag, and YBCO respectively from the top to the bottom of the micrograph. The sputtered Ag film extends along the whole interface (about 4000Å) having a nearly constant thickness (about 1200Å). Twins and other defects are clearly observed in Ag as well as a low angle grain boundary between two Ag grains. The SAD pattern indexed in figure 21c shows that both Ag grains are in the [011] zone axis while YBCO is in the [010] zone axis. For clarity only one Ag grain is indexed in figure 21c. Both Ag grains have their close-packed {111} planes stacked parallel to $(001)_{YBCO}$ planes, although one of them is slightly rotated (about 2°) around the [011] zone axis. The orientation relationship between YBCO and Ag is:

$$(111)_{Ag} \,//\, (001)_{YBCO}$$

$$[011]_{Ag} \,//\, [010]_{YBCO}$$

It can be noticed from the micrograph in figure 21a that an intermediate layer of constant thickness, about 30Å, extends along the whole interface exhibiting a uniform contrast. Lattice fringes are seen in some regions of this layer. Inspection of the SAD pattern shows a weak ring whose spacing, about 2.72Å, does not belong to Ag. The measured spacing corresponds to either (013) or $(103)_{YBCO}$ spacing. This, however, cannot be verified in the micrograph at this magnification.

Figure 22a is a lattice image of a region of the YBCO/Ag interface with its corresponding SAD pattern in figure 22b. In figure 22c the SAD pattern is indexed and shows strong spots relative to a twinned Ag grain and the YBCO in the [011] and [010] zone axes, respectively, along with few extra spots. The strong reflections are used as an internal calibration to determine the spacings of the weak spots. Those are found to match the (013) and $(103)_{YBCO}$ spacings relative to YBCO in the [331] zone axis. Lattice fringes, i.e. see arrow, are visible in some regions of the intermediate layer and seem to originate in

the YBCO and extend up to the Ag. Away from the interface both sets of $\{111\}_{Ag}$ planes as well as (001) and $(100)_{YBCO}$ planes are clearly resolved. Their spacings in the bright field image are used as a calibration to measure the spacing of the lattice fringes in the intermediate layer and agree with the result obtained from the SAD pattern. The micrograph also shows that the silver grain is heavily twinned along the interface. Stacking faults and bending of (001) are also observed in the YBCO film.

Examination of the interface at other regions shows that this intermediate layer is always present at the YBCO/Ag contact and Ag is in different orientations. Figures 23a and 23c show two examples of such orientations and their corresponding SAD patterns in figures 23b and 23d which are illustrated in figures 23e and 23f. Silver is in the [112] and [123] orientations, in figures 23a and 23b respectively, while YBCO is along the [010] zone axis. In both cases the close packed planes of Ag are stacked parallel to the $(001)_{YBCO}$ planes with an offset angle of about 8° and 15° in the first and second example respectively. In the two micrographs the lattice fringes of Ag and YBCO are clearly resolved whereas the intermediate layer seems to be completely disordered. The SAD patterns in figures 23b and 23d show only diffuse rings around the incident beam in agreement with the bright field images. Some defects are also detected in the YBCO such as in figure 23b wherein the $(001)_{YBCO}$ planes seem to be shifted against each other at two locations, i.e the arrows.

Although the process of ion milling seems to polish the surface of YBCO some regions of the interface are curved. The micrograph in figure 24a shows that the YBCO surface contains steps over a large area. Once again, an intermediate layer is observed which is crystalline in certain regions. The lattice fringes of both randomly oriented silver grains and YBCO are also

visible. The YBCO film seems to be free of defects except for an inclusion, i.e at the arrow, and a linear defect in region (I). Three different regions (I, II, and III) along the interface are examined at higher magnification in figures 24b, 24c, and 24d respectively. In figure 24b the lattice fringes in the upper part of micrograph are the (002) planes belonging to a Ag grain and those in the lower part are the $(001)_{YBCO}$ planes. Lattice fringes running across the intermediate layer are also visible. The spacing of those fringes is about 2.75Å corresponding to the spacing of $(103)_{YBCO}$ or $(013)_{YBCO}$, 2.72 Å and 2.75Å respectively. This implies that this intermediate layer is probably YBCO oriented in the [331] zone axis. In figure 24c the linear defect in YBCO represents a shift of the $(001)_{YBCO}$ planes in the [001] direction. Along the interface, in all three micrographs, there is a noticeable change in the contrast of Ag, the intermediate layer, and YBCO. While the resolution of $(001)_{YBCO}$ degrades, that of the intermediate layer is enhanced from left to right, figures 24b to 24d.

IV.5.2 Ag Deposited on ion-milled and sputter-etched YBCO

After ion-milling, the surface of YBCO was sputter-etched to improve its quality. Figures 25a and 25b show a typical YBCO/Ag interface at low magnification and a SAD pattern taken near the interface. The four distinct layers in figure 25a correspond to the glue, Ag, YBCO, and MgO respectively. The indexed SAD pattern in figure 25c indicates that Ag and YBCO are in the [012] and [010] orientations respectively and the $(002)_{Ag}$ and $(001)_{YBCO}$ are nearly parallel with an offset angle of about 5°. As in the case of ion-milled YBCO, Ag is granular with a constant thickness (about 1500Å). Twins, stacking faults, and dislocation networks are also observed in the Ag layer. However, the thickness of the intermediate layer is no longer constant everywhere. At

higher magnification, figure 25d, the intermediate layer is thicker in the center (about 60Å) than it is at the left side of the micrograph (about 30Å).

This becomes even clearer in figure 26a where Ag is directly bonded to YBCO, right hand side of the micrograph, whereas in the center Ag is bonded to a damaged YBCO surface. The SAD pattern in figures 26b and indexed in figure 26c shows that Ag is in a [233] orientation and exhibits no specific orientation relationship with YBCO.

IV.6 Morphology of YBCO/Ag related to the surface of YBCO

The structure of the YBCO/Ag contact seems to be strongly related to the morphology of the surface of YBCO. Figures 27a and 27b show YBCO/Ag contacts established before and after the YBCO surface was treated. The corresponding SAD patterns are shown in figures 27c and 27d along with their illustrations in figures 27e and 27f. In figure 27a the surface of YBCO is clearly rough and rippled along the whole interface. At certain regions of the interface the perfect structure of YBCO is maintained while at other regions, i.e arrows, the order of the structure is disturbed or completely lost. In this case, the Ag film which exhibits a granular morphology is is in the [123] orientation and the close packed $(111)_{Ag}$ planes are not perfectly parallel to $(001)_{YBCO}$ as indicated in figure 27e. However, beneath the ion-milled surface of YBCO, figure 27b, the structure of YBCO is maintained up to the interface. On the other hand, the Ag layer contains a large twinned grain extending along the entire interface. The close packed $(111)_{Ag}$ planes in this case are perfectly parallel to $(001)_{YBCO}$. However, a uniform layer is created at the surface of YBCO wherein lattice fringes are visible in certain parts of it. By measuring the spacing of those fringes in the bright field image and indexing the extra spots in the SAD pattern this layer is found to be YBCO in the [331] orientation.

Another example illustrating the role of the surface of YBCO on the structural properties of the YBCO/Ag interface is shown in figure 28a. The micrograph shows two grains of YBCO having their (001) planes perpendicular to each other where the surface of YBCO is irregular. The deposited Ag in the [013] zone axis exhibits no orientation relationship with YBCO, as seen in figures 28b and 28c. The same Ag grain grows along the interface on both YBCO grains.

IV.7 Results of sample preparation

The method used to prepare cross section specimens for TEM, described in § III, has proven to be successful for the investigation of the YBCO/Ag interface. In figure 29a a region of about 2.8 μm is transparent to the electron beam. The layers in the micrograph are MgO, YBCO, Ag, glue, Ag, YBCO, and MgO respectively. The thickness of such a specimen is also adequate for HREM. Figure 29b shows a region of the YBCO/Ag interface where the $(001)_{YBCO}$ planes are clearly resolved.

V DISCUSSION

Experimental work on the superconductor-metal interface is still in its infancy, in particular studies of its detailed microstructure. Many experiments have been performed on forming metal contacts to the new class of high T_c superconductors because such a process is extremely important from a scientific as well as from a technical point of view. The results described in this research represent the first systematic studies concerning the structure and the mechanism of metallic contact formation to the superconducting ceramic oxides.

V.1 Morphology of the YBCO/Ag interface

Results of this Ag/YBCO contacts reveal that Ag frequently bonds to YBCO without the formation of any intermediate layer or precipitates at the interface. Direct contact of Ag to YBCO is observed at least in certain regions of the interface, i.e. in figure 11a, where Ag extends over large areas of the interface without any observable reaction products. This result is not surprising since previous work on metal-superconductor contacts [90] indicates that silver yields a better ohmic contact with YBCO than other metals. The electrical results suggest that Ag bonds to the YBCO through direct chemical bonds and reaction products at the interface are few if they exist at all. It is worth mentioning that the Ag/YBCO interface is fairly adhesive and completely free of any voids or cracks even when subjected to different temperatures. These temperatures are liquid nitrogen temperature used during ion-milling and the annealing temperature of 500°C. This suggests that Ag and YBCO have similar thermal expansion coefficients. The Ag/YBCO contact is compared to the Au/YBCO contact in figure 30. The Au contains many

cracks at the interface and there are regions where Au is not bonded to YBCO. Direct contact, however is not observed everywhere at the Ag/YBCO interface. Regions exhibiting different symmetry than that observed in the YBCO film are sometimes encountered. However, those are believed to be related to the roughness of the surface of YBCO rather than to reactions at the interface. The surface of YBCO is well known to react readily with the ambient atmosphere. Such reactions usually lead to decomposition and/or amorphotization of the surface of YBCO.

Usually it is assumed that when surfaces of a metal and a ceramic are in close contact, the bonding occurs spontaneously [104]. In establishing contacts, the formation of an intimate or true interface is the first requirement, especially when the preservation of the bonded compounds are of great importance. This could be achieved whether by van der Waals attractive forces or by an electronic structure across the interface. i.e. chemical bond [8]. The driving force for the formation of an interface is the reduction in the free energy which the system releases as soon as the contact is established. Ceramic/metals interfaces are generally not compatible because redox reactions may occur at the interface involving an oxidation of the metal and a reduction of a cation in the ceramic [105-109]. In the case of an oxide phase, the oxygen released by the reduction of the cation forms an oxide with the metal. Saturation of the interface with the oxide and subsequent formation of a molecular layer oxide results in equilibrium and chemical bonding at the interfaces since the oxide layer is compatible with both its metal and the ceramic.

In the case of Ag/YBCO contacts it is believed that Ag bonds directly to YBCO without any formation of an intermediate oxide layer. If a reaction layer was to exist, one should be able to resolve it by electron diffraction studies.

However, the SAD patterns taken at the Ag/YBCO interface do not reveal any major spots beside those of Ag and YBCO. It may well be that oxygen or other species diffuse from the superconductor and form other compounds with Ag. But this (as we will see later) is believed to occur only in certain region and under special circumstances are available. On the other hand, the occurrence of preferred orientation relationships between Ag and YBCO (as will be discussed later) implies that Ag is directly bonded to the YBCO.

The silver coating exhibits a granular morphology when deposited on the as grown YBCO, i.e. the surface of YBCO is not treated prior to Ag deposition. The morphology of Ag is believed to be directly related to the roughness of the YBCO surface and large grains of Ag are often observed when the YBCO surface gets smoother. Comparison of the morphology of the deposited Ag in figures 9a and 10a supports this conclusion. Where the surface of YBCO appears flat over large areas, figure 9a, the deposited silver contains large grains. However, Ag exhibits relatively smaller grains where the YBCO surface is rough, figure 10a. Ag is also heavily twinned along the Ag/YBCO interface. This twinning usually occurs near a surface ledge, as in figure 9a, and/or when the interface is curved. Twinning is exhibited by the Ag grains when the close-packed planes $(111)_{Ag}$ and $(001)_{YBCO}$ are no longer exactly parallel near a ledge or as the curvature of the surface of YBCO is not atomically smooth.

V.2. Epitaxy at the interface

Epitaxial compatibility would be expected to play a major role in the process of energy minimization at the interface and should be discussed in as much detail as possible. The orientation relationships between Ag and YBCO must be interpreted based on crystallographic considerations. It has been shown by electron diffraction that the deposited Ag tends to adopt a specific

orientation relationship with YBCO over large areas in which the close-packed {111} planes of Ag are always parallel to (001) planes of YBCO. This is not surprising, since locking in of close-packed planes at the interface is suggested [110] to be the principle by which nature constructs favored interfaces between dissimilar solids, rather than a high coincidence density. This is mainly encountered in the case of large lattice misfit which applies to the Ag/YBCO interface.

Angular offsets of a few degrees (1° to 9°) between $(111)_{Ag}$ and $(001)_{YBCO}$ planes are frequently observed. The largest offsets are usually observed in rough surfaces of the YBCO. The $(111)_{Ag}$ planes are mostly oriented such that the <110> directions of Ag are parallel to the [100] or [010] directions of YBCO. However, those close-packed directions are not exactly parallel and angular misorientations on the order of 3° are often observed. Previous studies show that small but definite angular offsets can occur between closed-packed directions or planes in metal/ ceramic interfaces. In Nb/Al_2O_3 interface [111], for instance, it has been found that the close-packed (0001) planes of Al_2O_3 and (011) of Nb are tilted with respect to each other by 3°, and this tilt occurs both in specimens grown by epitaxy and in diffusion bonded ones which were initially adjusted with their close-packed planes in parallel. In diffusion-bonded sandwiches of polycrystalline Cu and Pt foils between identically oriented sapphire crystals, the metal grains developed a preferential orientation with the (111) planes of the metal parallel to the (0001) planes of the sapphire, but with the metal crystals rotated in their own (111) plane by different angles for the two metals [112]. It is not understood why this should occur but it seems that this orientation is of especially low interface energy.

The exact misorientation cannot be directly determined from the SAD patterns since no Kikuchi lines are present. To get a rough estimate of this

deviation, simulated diffraction patterns of Ag and YBCO in the [011] and [010] orientations were compared to the experimental SAD patterns obtained at the Ag/YBCO interface. The best match, as shown in figure 31, was obtained when Ag is tilted about 3° around the [111] zone axis. If the offset angle is larger than 5°, as in figure 31e, the high order reflections, such as (422), are invisible. However, this is not the case in the SAD at the interface, and hence the offset angle is definitely less than 5°. Such a deviation is also observed in other crystallographic orientations wherein the <123> or <112> directions are parallel to the [100] or [010] zone axis of YBCO. The (111) streographic projection in figure 32 shows that [112], [123], and [110] poles belong to the same zone axis, i.e. [111]. The angles between the [110] and [112], and [110] and [123] directions are 30° and 19.11° respectively. Hence transformation of any orientation to another could be accomplished just through a rotation around the [111] zone axis. However, it is believed that the most favorable orientation relationships, such as $[100]_{YBCO}$ (or $[010]_{YBCO}$), are parallel to either $[110]_{Ag}$ or $[123]_{Ag}$.

In all Ag/YBCO interfaces studied the c-axis of YBCO is normal to the interface, however, the preferred limiting plane is not clearly defined. For $(001)_{YBCO}$, four types of planes (denoted I, II, III and IV) can be distinguished in terms of their atomic arrangements, which are shown in figure 33. In the case of an Ag grain growing on an (001)-oriented YBCO substrate, growth could begin on any type of the $(001)_{YBCO}$. An attempt has been made to find the best orientation, in terms of lattice coincidence sites, which Ag would be expected to adopt. The (111) plane of the silver and the most densely packed layer of the (001) plane of YBCO, type (III), are superposed and rotated with respect to each other.

In figures 34a-34d the $[100]_{YBCO}$ direction is parallel to the $[110]_{Ag}$

direction while in figure 34e the $[100]_{YBCO}$ is parallel to the $[123]_{Ag}$. In order to make the recognition of any possible coincidence lattice easier, a Ag atom is placed on top of an O atom at the center in one case, figure 34 a, while in figure 34b a Ag atom is placed on a Cu atom. Consequently, in the direction of $[110]_{Ag}$ or $[100]_{YBCO}$, as the lattice parameters of $(110)_{Ag}$ and $(200)_{YBCO}$ are 2.8894Å and 1.9116Å, respectively, the second Ag atom in the $[110]_{Ag}$ direction coincides almost exactly with the third atom in $[100]_{YBCO}$ direction to within less than 0.8%. The second atom in the $[110]_{Ag}$ is at a distance of 5.7787Å from the origin and the third atom in $[100]_{YBCO}$ is placed 5.7346Å from the origin. This atom could be a Cu or O atom depending on whether the center is placed at an O or Cu site in the $(001)_{YBCO}$ plane, respectively. In the $[112]_{Ag}$ or $[010]_{YBCO}$ direction, normal to the $[110]_{Ag}$, the second Ag atom almost coincides with the fifth atom in the $[010]_{YBCO}$ direction. The second Ag atom in the $[112]_{Ag}$ is at a distance of 10.0091Å from the origin and the fifth YBCO atom in the $[010]_{YBCO}$ direction is at a distance of 9.7155Å within an error of about 3%. When a $(001)_{YBCO}$ plane of type (I) is superposed on a $(111)_{Ag}$ plane, figure 34c, the fourth Ag atom in the $[110]_{Ag}$ direction, distant 11.5575Å from the origin, coincides with the third YBCO atom in the $[100]_{YBCO}$ direction placed at 11.4693Å to within an error of less than 0.8%. In the $[010]_{YBCO}$ direction, however, the same matching positions are maintained as in the case of type (III) layer. Finally when the $(001)_{YBCO}$ of type (II) or (IV), figure 34d, is superposed on a $(111)_{Ag}$ plane, the matching positions in the $[112]_{Ag}$ or $[010]_{YBCO}$ is decreased by a factor of two. Notice that the type (II) and (IV) layers (Y and BaO) exhibit the same symmetry except that in a type (II) layer there is an extra oxygen sublattice shifted 2.7257Å along the $[110]_{YBCO}$ direction. Hence, the matching positions in any type of the $(001)_{YBCO}$ plane are the same but their density decreases as the atomic density $(001)_{YBCO}$

decreases. Consequently, Ag is believed to grow epitaxially from the YBCO surface and the orientation relationship discussed above is not believed to be accidental.

In the case where $(111)_{Ag}$ and $(001)_{YBCO}$ are superposed and the $[123]_{Ag}$ and $[100]_{YBCO}$ directions are parallel, figure 34e, the first Ag atom in the $[123]_{Ag}$ direction, 7.6446Å distant from the center, coincides exactly with the second Cu (or O) atom, distant 7.6462Å from the center. In this case, however, coincidence sites in the other directions are not well defined and at least three possible coincidence site lattices (CSL) could be identified. Their cells are shown in figure 34e. The density of the matching positions again decreases as the atomic density decreases in the different $(001)_{YBCO}$ layers.

The (011) Ag-Ag distance (2.8894Å) and the (011) O-O (2.7257Å) distance, in the $(001)_{YBCO}$, plane differ so little that parallelism of the [100] or $[010]_{YBCO}$ and $[110]_{Ag}$ would be anticipated whenever the surface of YBCO terminates with a type (III) layer. Such a coincidence lattice configuration has a lattice mismatch ratio of 9:10 indicating an almost perfect match. However, such an orientation relationship was never encounter.

V.3. Structure of the Ag/YBCO interface

The results obtained by HREM indicate that the interface planes possess high atomic density and are usually the close-packed planes of the Ag and YBCO lattices, (111) and (001) respectively. It is very difficult to draw a criterion for low energy boundaries in Ag/YBCO, but it appears that parallelism of close-packed directions across the interface is important. It has been demonstrated [113] that low energy configurations between noble metals and ionic crystals are established when there is parallelism of low index planes and close-packed directions across the interface. There are two

components relevant to the discussion of the structure and bonding of the Ag/YBCO interface. First, there is the issue of surface structure of the YBCO in the sense of topography, whether intimate contact is established or not, and in the sense of the precise surface crystallography and atomic relaxations at the surface. Secondly, there is the issue of chemistry, whether chemical bonds form between Ag and YBCO, and what species in YBCO bond to Ag.

Direct contact of Ag to YBCO is evident at least in certain parts of the Ag/YBCO interface, i.e. figures 11a and 12a. In such parts there is a distinct boundary between Ag and YBCO in which the interface is perfectly flat over large areas and the $(111)_{Ag}$ planes are locked-in to $(001)_{YBCO}$ planes. This crystallographic configuration is maintained despite the presence of planar steps and ledges along the surface of YBCO. The presence of those irregularities at the surface of YBCO leads to deviation of the boundary of the interface from the exact $(111)_{Ag}$ or $(001)_{YBCO}$ planes and sometimes to twinning of the Ag grains. Along the faces of the ledges the image contrast of the Ag structure changes quite drastically even for the same thickness and the same defocus. Such change in contrast is most probably produced by the strain observed along the interface. This may point to the importance of the lock-in structure at the Ag/YBCO interface instead of gaining stability from the relatively weak epitaxial compatibility. It is quite possible that offset angles observed in certain parts of the Ag/YBCO interface develop to accommodate the misorientation of the planes of the two lattices when the surface of YBCO is not perfectly flat. Nevertheless, the joining (111) planes of silver are not bent over these steps. The misorientation of the metal against the superconducting oxide may be accommodated by dislocations in the metal, allowing its close-packed planes to be exactly parallel to that of the YBCO. Study of the interface of gold islands on (001) oriented MgO shows that the lattice misfit is taken up

by interface dislocations whose spacing is in agreement with calculations based on minimization of elastic strain in the whole island. Although such a structural configuration could not be confirmed in the present study, it could be applicable for the Ag/YBCO interface.

The structure of YBCO is mostly preserved up to the Ag contact with few exceptions in which a line defect is seen. This defect is thought to be related to the YBCO growth rather than to be a result of the Ag deposition. Such defects as well as others which propagate through the surface of YBCO are often observed mainly at regions close to the MgO substrate. It is also noticed that the defect density is independent of whether or not a direct contact between Ag and YBCO is observed. The extra spots in the electron diffraction patterns in some areas of the Ag/YBCO interface indicate that there are changes in the local crystallographic orientation of the surface of YBCO near the interface. The spacing relative to those spots match exactly those of the (013) and (103) of YBCO. Whether this change in the crystallographic orientation occurs during or prior to the the Ag deposition is not known. The fact that the same orientation is preserved up to Ag contact at certain regions of the interface suggests that contamination of the surface prior to the Ag deposition is the cause of the change of the YBCO crystallographic orientation near the Ag/YBCO interface.

Ion-milling occurs with different erosion for the metal and the superconducting oxide and therefore thin sections suitable for atomic resolution at the interface have been very difficult to obtain. The difference in the thinning rate also makes computer simulation studies at the interface almost impossible since Ag and YBCO exhibit different thicknesses near the interface. Hence it is very hard to draw any conclusion about the nature of the chemical bonding between Ag and YBCO.

V.4. Stability of the interface

Once the Ag/YBCO is structurally characterized it is essential to investigate its stability. For practical applications, such as establishing ohmic contacts, the driving force for the formation and stability of an interface must be increased. This could be achieved by an increase in temperature or change of the atmosphere during or after bonding. In the case where the driving force is a thermodynamical potential of the components (or elements) the formation of the interface is characterized by charge transport across the interface and may also involve mass transport and diffusion. Because the Ag is sputtered on YBCO, defects are expected to exist both in the YBCO and the Ag near the interface. Annealing, hence, can lead to defect motions near the interface. The defect motion does not need to mean atomic or ionic motion through the interface but simply rearrangement of atoms or transfer of electrons from one defect to another. In this section the structure, morphology and reaction products at the interface are discussed based on HREM results obtained from the annealed Ag/YBCO interface.

V.4.1 Morphology and structure of the annealed Ag/YBCO interface

There are three components relevant to the discussion of the stability of the Ag/YBCO interface: structure of YBCO, structure of Ag, and possible reaction at the interface. The YBCO structure is found to be intact when heat-treated in an oxygen atmosphere at 500°C for two hours. There are no defects added to the structure of YBCO besides those already observed before annealing. The perfect structure of YBCO can be easily recognized in YBCO and is often maintained up to the interface. The temperature, however, does not seem to enhance the quality of the surface of YBCO which appears to maintain

its roughness, i.e. figure 13a. Regions near the interface where the structure of YBCO is disturbed after annealing, i.e. figure 15a, are sometimes observed. It is not clear whether the change in the YBCO structure near the interface is activated by the temperature or occurs before the heat-treatment.

There is evidence of grain growth of the deposited Ag upon heat-treatment. The micrograph in figure 13a, for example, shows a single twinned grain extending along the whole interface. Such a large grain size was not observed prior to the heat-treatment of the interface. The bright speckles, about 20Å across, observed in the micrograph are most probably defects generated during the preparation of the specimen, by ion beam bombardment, or generated during imaging.

The Moire fringes observed at certain region of the interface indicate a good epitaxy between Ag and YBCO. This is also confirmed in the SAD pattern taken at the interface where the $(111)_{Ag}$ and $(001)_{YBCO}$ planes are exactly parallel. However, similar to what is found before annealing, the $(111)_{Ag}$ plane seems to be slightly rotated around the normal to the interface, i.e. $[010]_{YBCO}$ or $[011]_{Ag}$. In figure 18a Ag develops facets parallel to the $(001)_{YBCO}$ planes retaining a 3° tilt of the two lattices. Since this offset angle occurs after annealing the interface this crystallographic configuration might be one of especially low interface, energy and indicates good adhesion between Ag and YBCO.

It becomes more evident upon inspection of more highly enlarged portions such as in figures 13d and 14a, that there is an enhancement of the quality of the Ag/YBCO interface wherever the the perfect structure of YBCO is maintained at its surface. At regions where Ag is bonded to YBCO there is a clear boundary at the interface. Changes in the contrast along the interface often observed before annealing are no longer visible. It is obvious that not

every atom in YBCO is coincident with one in Ag a circumstance which must result in elastic strain at the interface. Possible relaxation events may involve shuffling of non-coincident $(111)_{Ag}$ planes along the interface. It seems that relaxation to relieve lattice mismatch between the two lattices does occur along the interface since dislocations with a defined periodicity are clearly seen along the flat facets. The temperature seems to increase the mobility of the atomic species and also the mobility of the dislocations in the deposited Ag. Based upon these findings it is believed that the improvement of contact resistivity achieved by heat-treatment [90] of the Ag/YBCO interface is related to the enhancement of the structure of the interface, namely grain growth of the deposited Ag and atomic rearrangement near the interface. Increasing the grain size of Ag decreases the grain boundary area resulting in better conductivity in Ag as well as higher electron injection through the interface when the defect concentration is lowered.

V.4.2 Chemical stability of the Ag/YBCO interface

It is extremely important to notice that bonding between Ag and YBCO occurs without an intermediate reaction layer. In all the HREM results obtained at the Ag/YBCO interface, Ag is directly bonded to YBCO. This is mainly observed where the structure of the surface of YBCO is perfectly ordered. Where the surface of YBCO is disordered and/or rough, however, it is found that Ag_2Y and Ag_2O compounds grow at or near the Ag/YBCO interface. These phases are strictly present at certain regions of the interface and do not form continuous layers along the Ag/YBCO interface. Hence the growth of these compounds at the interface is thought to be strongly related to the poor quality of the surface of YBCO. It is not clear how the formation of these compounds occurs but since they form after the interface has been annealed it

is believed that these compounds form by diffusion of Y and O into Ag.

The roughness of the surface of YBCO does not seem to be the only reason for the growth of those phases since no such phases are observed near the curved interface in figure 13a. However, the steps and ledges as well as regions of disordered structure at the interface may act as nucleation sites for the reaction products. When an epitaxial relationship is involved low energy interfaces exist if the boundary between the two lattices is ordered. Hence when a disordered region is present near the Ag/YBCO interface the temperature may provide the activation needed for a transition of the energetically anisotropic boundary structure to an isotropic one. Both Ag_2Y and Ag_2O are found to exhibit specific orientation relationships with Ag and YBCO in which the close-packed planes are parallel. Such a transformation could occur via the rearrangement of atoms/molecules or interdiffusion of certain species through the interface.

Closer examination of the structure of YBCO around the interface reveals that the $(001)_{YBCO}$ are often bent where Ag_2Y or Ag_2O are present, i.e. figure 18a. On the other hand, the strict periodicity of the $(001)_{YBCO}$ planes is completely lost where these phases form as in figures 16f, 16g, and 17a. These observations strongly suggest that yttrium and oxygen diffuse out from YBCO during the heat-treatment of the Ag/YBCO interface. Upon cooling the Ag is supersaturated with Y or O and precipitation of Ag_2Y and Ag_2O occurs. The phase diagram of Ag-Y in figure 35 shows that Ag_2Y is an intermetallic compound which forms between 960°C and room temperatures. The Ag-O phase diagram, on the other hand shows that Ag_2O forms at low temperatures, 190°C and room temperature. The mechanism of formation of Ag_2Y and Ag_2O, although thermodynamically acceptable is not yet well understood. Particularly, it is uncertain whether the oxygen present during annealing is

responsible for Ag_2O formation or whether it occurs by diffusion of O from YBCO.

It is not understood why diffusion is limited to Y and O and does not involve other species such as Ba. Barium may also diffuse from YBCO but if this happens it is believed to be in much less quantity than Y or O. The linear defects often observed in YBCO near the interface may act as channels for Y and O diffusion. It is also found that Ag_2Y, i.e. in figure 20a, forms along the steps of the surface of YBCO. This suggests that the diffusion path of Y is likely parallel to $(001)_{YBCO}$ planes. A conclusive explanation of such an observation is hard to reach at this early stage of study. However, it is thought that the relatively smaller atomic sizes of Y and O, compared to that of Ba, might be one of the reasons why diffusion is restricted to Y and O only. For more quantitative understanding of stability and hence better control of the Ag/YBCO interface the activity of all species of YBCO must be theoretically determined as well as their interdiffusion profiles.

V.5. Treatment of the YBCO surface before Ag deposition

One would assume that the quality of the surface of YBCO should have a strong influence on the contact resistivity of Ag/YBCO interface. In the mean time the structure of YBCO must not be altered especially at its surface. First, we have the possibility of reducing the contamination of the surface of YBCO by depositing Ag in the same chamber where YBCO has been grown. For unknown reasons, the result of such an experiment was deceiving since improvement of the YBCO surface was not accomplished, i.e. figure 19. It is believed that the time required to bring the temperature of the grown YBCO down to room temperature and to evacuate the chamber for Ag deposition is enough to cause the surface of YBCO to be contaminated. Furthermore, failure

to reach room temperature might result in interaction of the outdiffusing yttrium with the deposited Ag. This is likely to occur where the surface of YBCO exhibits steps or ledges such as in figure 20a.

Secondly, one might try ion radiation to "clean" the surface of YBCO and hence improve the quality of the Ag/YBCO interface. The process of ion-bombardement proves to be appropriate for obtaining flat surfaces such as in figure 21a. Such a smooth surface of YBCO leads to the growth of large Ag grains. However, the improvement of the morphology of the surface results in damaging a layer of the YBCO surface. This damage is not well defined and varies from partial disorder to complete loss of crystallinity of the YBCO structure. Nevertheless, at certain region of the Ag/YBCO interface, orientation relationships between YBCO and Ag are observed, similar to the one found prior to the ion-milling process. These orientation relationships suggest that crystallinity of YBCO is preserved at certain regions of the surface of YBCO. Preferential etching near the interface may occur leading to a shadow effect which results in a contrast seam along the interface. However, for the Ag/YBCO interface since this kind of layer is not observed when the surface of YBCO is not treated. Away from the interface the structure of YBCO is maintained and there no evidence of new defects generated by the process of ion-bombardment. So in order to obtain a more thorough cleaning of the surface of YBCO the ion-bombardment parameters such as the ion accelerating voltage and the impinging angle must be carefully studied.

Thirdly, the surface of YBCO is sputter-etched after it is ion-milled. The purpose of such a process is to remove the undesirable surface defects resulting from ion-bombardment. However, this process is not found to enhance the structure of YBCO near the Ag/YBCO interface. The results obtained so far suggest that sputter-etching is likely to result in further

damage of the YBCO surface and may cause other defects such as near-surface charged defects to occur.

VI CONCLUSIONS

The structural properties of the Ag/YBCO interface were investigated by HREM to determine its morphology and structure as well as the orientation relationships between Ag and the high T_c superconductor YBCO. The major conclusions drawn from this investigation are summarized as follow:

1. The as-deposited Ag film exhibited a granular morphology in which the Ag grains are often twinned along the (111) plane.

2. The morphology of Ag was strongly related to that of the surface of the YBCO substrate which was rough and different in structure from the underlying YBCO film.

3. The Ag contact to YBCO occurred without formation of any intermediate phase layer or particles at the interface. Furthermore it was found by electron diffraction that the close-packed $(111)_{Ag}$ were always parallel to the $(001)_{YBCO}$ planes and the $[011]_{Ag}$ or $[123]_{Ag}$ directions were parallel to the $[100]_{YBCO}$ or $[010]_{YBCO}$ directions.

4. Annealing of the Ag/YBCO interface resulted in an outdiffusion of yttrium and oxygen mainly at regions where the surface of YBCO was rough. This diffusion, however did not result in the formation of continuous layers at the Ag/YBCO interface but only to growth of Ag_2Y and Ag_2O particles. This implies that the stability of the Ag/YBCO depends on the quality of the surface of YBCO, especially its structure. On the other hand, the heat-tretment of the interface

resulted in grain growth and a decrease in the density of the structural defects of the deposited Ag.

5. Treatment of the surface of YBCO by ion-bombardment yielded flat surfaces but damaged a layer of about 30Å. However, the same orientation relationships between Ag and YBCO were observed after such a cleaning process and probably implies that the destruction of the structure at the surface is only partial. Such a cleaning process, however, improved the quality of the deposited Ag since the Ag grains were larger and contained lower defect concentration.

6. Further treatment of the surface of YBCO by sputter-etching did not result in any enhancement of the quality of the surface.

7. Deposition of Ag in the same chamber where YBCO was grown minimized the contamination of the surface of YBCO but did not improve the structure of the Ag/YBCO interface. The roughness of the surface of YBCO did not decrease and the quality of the Ag deposited by laser ablation was worse than that deposited by sputtering.

8. The improvement of the morphology and structure of the Ag/YBCO interface and hence the contact resistivity of Ag to YBCO, requires a flat and perfect surface with perfect YBCO prior to metal deposition. Thus finding a method to treat the surface of YBCO is the clue to establishing good ohmic contacts to the YBCO superconductor.

9. The results obtained by HREM are incomplete without more quantitative information which requires more detailed studies of the relations between internal structure and surface energy of the materials involved. Furthermore, other characterization methods, such as chemical investigation of the metal/superconductor are required for fully understanding the properties and stability of such interfaces. Finally structural studies must be correlated to the electrical properties for technological applications.

REFERENCES

1. J. B. Bednorz and K. A. Mueller, Z. Phys. **B64,** 189 (1986).

2. K. Kishio, K. Kitazawa, S. Kanbe, I. Yasuda, N. Sugii, H. Takagi, S. I. Uchida, K. Fueki, and S. Tanaka, Chem. lett. (Japan) 429 (1987).

3. M. K. Wu, J. R. Asburn, C.J. Torng, P.H. Hor, R.L. Meng, L. Gao, Z.J. Huang, Y.Q. Wang, and C.W. Chu, Phys. Rev. Lett. **58**, 908 (1987).

4. E. A. Giess, K. N. Tu and D. R. Uhlmann, Eds., Electronic Packeging Materials Science, MRS Symp. Proc., **40** (Marerials Research Society, Pittsburg, 1985)

5. J. M. Gibson and L. R. Dawson Eds., Layered Structures, Epitaxy and Interfaces, MRS Symp. Proc. **37** (Marerials Research Society, Pittsburg, (1985)

6. M. Ruhle, R. W. Balluffi, H. Fischmeister and S. L. Sass, Eds Proc. Intern. Conf. on the Structure and Properties of Internal Interfaces [J. Physique Colloq. **46** (1985) C4].

7. M. G. Nicholas, "Bonding Ceramic-Metal Interfaces and Joints" pp. 349-357 in Ceramic Microstructures '86: Role of Interfaces. Edited by J. A. Pask and A. G. Evans. Plenum, NewYork, 1987.

8. J. A. Pask. Am. Ceram. Soc. Bull. **66,**(11) 87 (1987).

9. K. Suganuma, T. Okamoto, M. Koizumi, and M. Shimada, J. Am. Ceram. Soc., **68**[12], C334 (1985).

10. J. T. Klomp in Ceramic Microstructures '86: Role of Interfaces. Edited by J. A. Pask and A. G. Evans. Plenum, New York, (1987).

11. J. T. Klomp, Am. Ceram. Soc. Bull., **51(9)**, 683 (1972).

12. M. Ruhle, K. Burger, and W. Mader, J. Micros. Spectrosc. Electron., **11,** 163 (1986).

13. J. F. Burgess, C. A. Neugebauter, and G. Flanagan, J. Electrochem. Soc.**122**[5], 688 (1975).

14. H. J. DeBruin, A. F. Moodie, and C. E. Warble, J. Mat Scien. **7,** 909 (1972).

15. W. Tojkowski and H. Gleiter, J. Physique **46**, Suppl. C4-89 (1985).

16. N. H. Fletcher, Adv. Mat. Research **5**, 281 (1971).

17. R. M. Pilliar and J. Nutting, Phyl. Mag. **16**, 181 (1971).

18. K. Takayanagi, K. Yagi and G. Honjo, Thin Solid Films **48**, 137 (1978).

19. C. A. M. Mulder and J. T. Klomp, J. Physique **46**, C4-111 (1985).

20. U. Erb, W. Abel, H. Gleiter, Scripta Metall. **16**, 1317 (1982).

21. H. Gleiter, J. Physique **46**, C4-393 (1985).

22. H. J. Fecht, W. Lojkowski and H. Gleiter, J. Physique **46**, Suppl. C4-107 (1985).

23. R. H. Hoel, Surf. Sci. **169**, 317 (1986).

24. T. Clomp, Brit. Ceram. Proc. **34**, 239 (1984).

25. S. Morozumi, M. Kikuchi and T. Nishino, J. Mater. Sci. **16**, 2137 (1981).

26. M. Florjancic, W. Mader, M. Ruhle and M. Turwitt, J. Physique **46**, Suppl. C4-129 (1985).

27. R. J. Cava, et al, Phys. Rev. Lett., **58**, 1676, (1987).

28. H. W. Zandbergen et al, Phys. Stat. Soli. (a) **103(45)** (1987).

29. J. E. Greedon et al, Phys. Rev., B **35**, 8843 (1987).

30. O. K. Antson, P .E. Hiismaki, H. O. Poyry, A. T. Tiitta, K. M. Ullakko, V. A. Trunov, and V. A. Ul'yanov, Sol. St. Comm. **64**, 757 (1987).

31. F. Beech, S. Miraglia, A. Santoro, and R. S. Roth, Phys. Rev. **B35**, 8778 (1987).

32. M. A. Beno, L. Soderholm, D. W. Capone, D. G. Hinks, J. D. Jorgensen, J. D. Grace, and I. K. Schuller, Appl. Phys. Lett. **51**, 57 (1987).

33. G. Calestani and C. Rizzoli, Nature **328**, 606 (1987).

34. J. J. Capponi, C. Chaillout, A. W. Hewat, P. Lejay, M. Marezio, N. Nguyen, B. Raveau, J. L. Soubeyroux, J. L. Tholence, and R. Tournier, Europhys. Lett. **3**, 1301 (1987).

35. D. E. Cox, A. R. Moodenbaugh, J. J. Hurst, and R. H. Jones, J. Phys. Chem. Sol. **49**, 47 (1988).

36. G. E. Greedan, A. H. O'Reilly, and S. V. Stager, Phys. Rev. **B 35**, 8770 (1987).

37. J. D. Jorgensen, M. A. Beno, D. G. Hinks, L. Soderholm, K. J. Volin, R. L. Hitterman, J. D. Grace, I. K. Schuller, C. U. Segre, and M. S. Kleefisch, Phys. Rev. **B 36**, 5731 (1987).

38. T. Siegrist, S. Sunshine, D. W. Murphy, R. J. Cava, and S. M. Zahurak, Rev. **B 35**, 7137 (1987).

39. R. Yoshizaki, H. Sawada, T. Iuwazumi, Y. Saito, Y. Abe, H. Ikeda, K. Imai, and I. Nakai, Jpn. J. Appl. Phys. L1703 (1987).

40. Q. W. Yan, P. L. Zhang, L. Jin, Z. G. Shen, J. K. Zhao, Y. Ren, Y. N. Wei, T. D. Mao, C. X. Liu, T. S. Ning, K. Sun, and Q. S. Yang, Phys. Rev. **B 36**, 5599 (1987).

41. H. You, R. K. McMullan, J. D. Axe, D. A. Cox, J. Z. Liu, G. W. Crabtree, and D. J. Lam, Sol. St. Comm. **64**, 739 (1987).

42. H. Bakker, D. O. Welch, and O. W. Lazareth, Jr. Sol. Comm. **64**, 237 (1987)

43. R. Beyers, G. Lim, E. M. Engler, V. Y. Lee, M. L. Lamirez, R. J. Savoy, R. D. Jacowitz, T. M. Shaw, S. La Placa, R. Boehme, C. C. Tsuei, S. I. Park, M. W. Shafer, and W. J. Gallagher, Appl. Phys. Lett. **51**, 614 (1987).

44. M. O. Eatough, D. S. Ginley, B. Morosin, and E. L. vanturini, Appl. Phys. Lett. **51**, 367 (1987).

45. T. Iwazumi, R. Yosizaki, H. sawada, Y. Saito, H. Ikeda, Y. Abe, and E. Matsuura, Jpn. J. Appl. Phys. **26**, 1065 (1987), Suppl. 26-3.

46. J. D. Jorgensen, B. W. Veal, W. K. Kwok, G. W. Crabtree, A. Umezawa, L. J. Nowicki, and A. P. Paulikas, Phys. Rev. **B 36**, 5731 (1987).

47. J. Jorgensen, Jpn. j. Appl. Phys., **26,** Supll. 26-3 (1987).

48. J. D. Jorgensen, H. B. Schttler, D. G. Hinks, D. W. Capone, II, K. Zang, M. B. Brodsky, and D. J. Scalapino, Phys. Rev. lett. **B 58**, 1024 (1987).

49. G. S. Grader, P. K. Gallagher, E. M. Gyorgy, Appl. Phys. Lett., **51,** 1115 (1989).

50. I. K. Schuller, D. G. Hinks, M. A. Beno, D. W. Capone, II, L. Soderholm, J. P. Locquet, Y. Bruynseraede, C. U. Segre, and K. Zhang, Sol. St. Comm. **63**, 385 (1987).

51. C. C. Torardi, E. M. McCarron, P. E. Bierstedt, A. W. Sleight, and D. E. Cox, Sol. St. Comm. **64**, 497 (1987).

52. G. van Tendeloo, and S. Amelinckx, Phys. Stat. Sol. **103**, K1 (1987).

53. N. Fukushima, et al, Jpn. j. Appl. Phys., **26 (5),** L719 (1987).

54. Y. H. Liang, J. Chen, and D. Feng., Appl. Phys. Lett., **54(4),** 368 (1989).

55. H. Sawada, et al, Jpn. J. Appl. Phys. **26(6),** L1054 (1987).

56. I. W. Chen, S. J. Keating, X. Wu, J. Xu, P. E. Reyes-Morel, T. Y. Tien, Sol. St. Comm. **63**, 997 (1987).

57. W. K. Kwok, G. W. Crabtree, A. Umezawa, E. E. Alp, L. Morss, and L. Soderholm,Jpn. J. Appl. Phys. **26,** Suppl. 26-3 (1987).

58. J. Narayan, V. N. Shukla, S. J. Lukasiewicz, N. Biunno, R. Singh, A. F. Schreiner, and S. J. Pennycook, Appl. Phys. Lett., **51**, 940 (1987).

59. A. Ourmazd, J. C. H. Spence, M. O'Keefe, R. J. Graham, D. W. Johnson, Jr, J. A. Rentschler, and W. W. Rhodes, **MRS** Ahaheim Symp. (1987).

60. H. W. Zandbergen, K. Wang, and R. Gronsky, **MRS** Boston Symp. (1987).

61. A Brokman, Sol. St. Comm. **64**, 257 (1987).

62. C. S. Pande, A. K. Singh, L. Toth, D. U. Gubser, and S. Wolf, Phys. Rev. **B 36**, 5669 (1987).

63. B. Raveau, C. Michel, and M. Hervieu, ACS Symp. (1987), p. 122.

64. M. Sarikaya, B. L. Thiel, I. A. Aksay, W. J. Weber, and W. S. Frydrych, J. Mater. Res. **2**, 736 (1987).

65. H. W. Zandbergen, G. van Tendeloo, T. Okabe, and S. Amelinckx, Phys. Stat. Sol. **103**, K1 (1987).

66. R. L. Barns and R. A. Laudise, Appl. Phys. Lett., **51**(17) 1373 (1989).

67. H. K. Onnes, Commun. Phys. Lab. Univ. Leiden Nos. 119b, 120b, 122b (1911).

68. W. Meissner, and R. Ochsenfeld, Naturwissenschaften **21**, 787 (1933).

69. G. B. Yntema, Phys. Rev. **98**, 1197 (1955).

70. D. L. Martin, M. G. Benz, C. A. Bouch, and C. H. Rosner, Cryogenics **3**, 161 (1963).

71. D. Dew-Hughes in "Treatise on Materials Science and Technology Vol. 14: Metallurgy of Superconducting Materials" pp.1, Edited by T.Luhman and D. Dew-Hughes.

72. A. R. Kantrowitz and Z. J. J. Stekly, Appl. Phys. Lett., **6**, 56 (1965).

73. C. Laverick, Proc. Int. Symp. Magn. Technol., Stanford pp. 560 (1965).

74. C. N. Whetstone, IEEE Trans. Magn. **MAG-2**, 307 (1966).

75. R. W. Meyerhoff, Ieee Trans. Power Apparatus Syst. **PAS-94**, 1734 (1975.

76. S. C. Lee, J. H. Lee, B. J. Suh, S. H. Moon, C. J. Lim, and Z. G. Khim, Phys. Rev. **B 37**, 2285 (1988).

77. J.W. Ekin, A. J. Panson, and B. A. Blankenship, Appl. Phys. Lett., **52**, 331 (1988).

78. D. L. Kaiser, F. Holtzberg, B. A. Scott, T. R. McGuire, Appl. Phys. Lett., **51**, 1040 (1987).

79. D. L. Kaiser, F. Holtzberg, M. F. Chisholm, and T. K. Worthington, J. Cryst. Growth **85**, 593 (1987).

80. M. Okada, A. Okayama, T. Morimoto, T. Matsumoto, K. Aihara, and S. Matsuda, Jpn. J. Appl. Phys. **27**, L185 (1988).

81. N. Koura, Denki Kagaku **56**, 208 (1988).

82. C. T. Chu and B. Dunn, Appl. Phys. Lett., **55(5)**, 492 (1989).

83. J. van der Mass. V. A. Gasparov, and D. Pavuna, Nature **328**, 603 (1987).

84. R. Caton, R. Selim, A. M. Buoncristiani, and C. E. Byvik, Appl. Phys. Lett., **52**, 1014 (1988).

85. A.D. Wieck, Appl. Phys. Lett., **52**, 1017 (1988).

86. K. Takeuchi, Y. Okabe, M. Kawasaki, and H. Koinuma, Jpn. J. Appl. Phys. **26**, L1017 (1987).

87. K. Muzushima, M. Sagoi, T. Miura, and J. Yoshida, Appl. Phys. Lett. **52**, 1101 (1988).

88. J. W. Ekin, T. M. larson, N. F. Bergren, A. J. Nelson, A. B. Swartzlander, L. L. Kazmerski, A. J. Panson, and B. A. Blankenship, Appl. Phys. Lett. **52(21)**, 1819 (1988).

89. J. R. Gavaler, A. I. Braginski, J. Talvacchio, M. A. Janocko, M. G. Forrester, and J. Greggi, In High Temperature Superconductors II, edited by D. W. Capone, W. H. Butler, B. Batlogg, and C. W. Chu (MRS, Pittsburgh, 1988), p.193.

90. A. C. Rastogi, S. T. Lakshmikumar, Pramana J. Phys. **31**, L67 (1988).

91. P. Chaudhri, R. H. Coch, R. B. Laibowitz, T. R. McGuire, and R. J. Gambino, Phys. Rev. Lett. **58**, 2684 (1987).

92. J. W. Ekin, A. J. Panson, and B. A. Blankenship, in High Temperature Superconductors, edited by M. B. Brodsky, H. L. Tuller, R. C. Dynes, and K. Kitazawa (MRS, Pittsburgh, PA 1988) Symp. Proc. No. 99, pp. 283.

93. Y. Tzeng, A. Holt, and R. Ely, Appl. Phys. Lett. **52**, 155 (1988).

94. S. T. Lakshmikumar, A. C. Rastogi, Appl. Phys. A **48**, 325 (1989).

95. R Y. Suzuki, T. Kusaka, T. Aoyama, T. Yotsuya, and S. Ogawa, Appl. Phys. Lett. **54(7)** (1989).

96. G. Chung and L. W. Barr, Solid State Commun. **67**, 123 (1988).

97. T. Ttakabatake and M. Ishikawa, Solid State Commun. **66**, 413 (1988).

98. S. X. Dou, N. Savvides, X. Y. Sun, A. J. Bourdillon, C. C. Sorrell, J. P. Zhou, and K. E. Easterling, J. Phys. C **20**, L1003 (1987).

99. Yu A. Bashkirov, A. A. Golub, and O. V. Grimalski, J. Phys. D **21**, 622 (1988).

100. R. D. Ray II and E. E. Hellstrom, J. Appl. Phys. **66**(2), 325 (1989).

101. S. B. Newcomb, C. B. Boothroyd, and W. M. Stobbs J. Microsc. **140**:195 (1985).

102. J. C. Bravman, and R. Sinclair Journal of Electron Microscopy Technique, **1**:53-61 (1984).

103. A. Garulli, A. armigliato, and M. Vanzi, J. Microsc. Spectrsc. Electrn. **10**(2):135-144 (1985).

104. K. Burger, W. Mader, and M. Ruhle, Ultramicrosc. **22**, 1 (1987).

105. A. P. Tomsia and J. A. Pask, Dent. Mater. **1** (2), 10 (1986).

106. M. G. Nicholas and D. A. Mortimer, Mater. Sci. Technol. **1** (9), 657 (1985).

107. S. M. Rekhson, Glass Technol. **20** (1), 27 (1979).

108. S. M. Rekhson, ibid., **20** (4), 132 (1979).

109. A. K. Varshneya, in Treatise on Materials Science and Technology, Vol. 22. Academic Press, New York, 1982 pp.241-306.

110. P. H. Pumhrey, Scripta Metall. **6**, 107 (1972).

111. W. Krakov, D. A. Smith, J. Mater. Res. **1**, 47 (1986).

112. T. Klomp, Brit. Ceram. Proc. **34**, 239 (1984).

113. V. P. Dravid, C. E. Lyman, M. R. Notis, and A. Revcolevschi, Ultramicros. **29**, 60 (1989).

114. C. P. Poole, Jr., T. Datta, H. A. Farach, Copper Oxide Superconductor, John Wiley, New York, 1988.

115. Graeme-Barber et al Cryogenics **12**, 317 (1972).

116. G. Bogner and P. Penczynski, Cryogenics **16**, 355 (1976).

117. Max Hansen, Constitution of Binary Alloys, 2nd ed. New York McGraw-Hill (1986).

FIGURE CAPTIONS

Figure 1: (a) Yttrium copper oxide (YBCO) orthorhombic unit cell. (b) Layering scheme of the YBCO superconductor structure. The layers are perpendicular to the c axis. The extent of puckering of the median Cu_2O layers is indicated [114]. XBL 905-1615

Figure 2: Coaxial pair of niobium-clad copper tubes developed at the Central of Electricity Research Laboratories, England. Outer diameters are 63.5 and 100 mm. Inset: etched cross section showing one of the 50 μm niobium surface on top of the copper [115]. ZBB 905-3701

Figure 3: Niobium flexible ac coaxial cable developed at Siemens, Erlangen, West Germany [116]. ZBB 905-3701

Figure 4: A schematic illustration showing the different steps followed during the cutting stage of TEM cross sectional samples. XBL 904-1316

Figure 5: Shows that when the specimen is inserted in the ion-mill chamber it is oriented such that the ion-beam (arrows) is perpendicular to the interface. XBL 904-1316

Figure 6: Curve of resistivity versus temperature for the YBCO superconducting thin film. XBL 904-1317

Figure 7: (a) High resolution TEM micrograph of the interface between (001) oriented MgO and YBCO film in the [010] zone axis. Stacking faults can be seen at mark (i) and bending of the $(001)_{YBCO}$ planes are visible at mark (ii). At mark (iii) a region of different symmetry is also visible. (b) SAD pattern of the YBCO/MgO interface. (c) Indexed SAD pattern. XBB 903-2437

Figure 8: (a) Lattice image of two YBCO grains (I) and (II) oriented such that $(001)_{YBCO}$ planes are respectively parallel and normal to the interface and perpendicular to each other. The $(001)_{YBCO}{}^{II}$ planes are heavily bent along the grain boundary. (b) The micrograph shows two adjacent grains of YBCO in the [100] orientation and illustrate again the polycrystallinity of the grown YBCO film. While the c-axes in both grains are, normal to the incident beam, they form a 44° angle. (c) SAD pattern for (a) and illustrated in (d). XBB 903-2418

Figure 9: (a) A low magnification electron micrograph of a typical contact between silver and the high critical temperature superconductor $YBa_2Cu_3O_7$. Although the Ag film appears to be heavily twinned along the whole interface, no visible intermediate layer could be seen. (b) SAD pattern taken near the Ag/YBCO interface. (c) The indexed SAD pattern showing Ag and YBCO in the [011] and [100] zone axes respectively. (d) HREM micrograph of the Ag/YBCO interface. Both two sets of $\{111\}_{Ag}$ as well as $(001)_{YBCO}$ planes are resolved. XBB 903-2436

Figure 10: (a) Shows another interface and illustrates the roughness of the surface of YBCO. In this micrograph YBCO has uniform structure up to the the

interface, despite the roughness of its surface, and the Ag film appears to have granular morphology. (b) SAD pattern of the corresponding interface. (c) the indexed SAD pattern indicate a 9° offset angle between the close packed planes $(111)_{Ag}$ and $(001)_{YBCO}$ and shows that Ag and YBCO are in the [123] and [100] zone axes respectively. XBB 903-2435

Figure 11: (a) shows a lattice fringe image of an Ag/YBCO interface with a sharp boundary extending over large areas without any intermediate layer. The micrograph illustrates parallelism of the close-packed planes $(111)_{Ag}$ and $(001)_{YBCO}$ with an offset angle of about 1.5°. (b) The corresponding SAD pattern. (c) the indexed SAD pattern. XBB 903-2434

Figure 12: (a) Another orientation of the Ag/YBCO interface. Here again the close packed $(111)_{Ag}$ planes are stacked parallel to the $(001)_{YBCO}$ planes with no offset angle. (b) Corresponding SAD pattern indexed in (c). XBB 903-2433

Figure 13: (a) A lattice image of a typical region of an annealed Ag/YBCO interface for two hours at 500°C in an oxygen atmosphere. The interface is well defined without any extended transition region between the two Ag and YBCO. The YBCO grain is in a [100] orientation while the Ag region consists of a [011] oriented grain and its twin along the (111) plane. (b) The inset box I shown at higher magnification. (c) shows the specimen after tilting around $[010]_{YBCO}$, which brings the interface closer to an edge-on orientation. (d) shows the other inset box (II) at higher magnification. (e) and (f) SAD pattern and its illustration. XBB 903-2441 and XBB 903-2431

Figure 14: (a) A lattice image of another region of the annealed Ag/YBCO interface. (b) SAD pattern taken near the interface. The Ag/YBCO contact exhibits a sharp interface along the whole micrograph with occasional unit steps due to local growth perturbations of the YBCO film. (c) Indexed SAD pattern. XBB 903-2432

Figure 15: A HREM image of the annealed Ag/YBCO interface in which the $(111)_{Ag}$ is rotated 4° with respect to the $(001)_{YBCO}$. Notice that YBCO and Ag overlap near the interface i.e. at the arrow and in the inset box. (b) The inset box at higher magnification showing a sharp and atomically smooth boundary. (c) Corresponding SAD pattern showing three grains of Ag in the [011] orientation and YBCO in the [100] orientation. (d) One Ag grain and YBCO are indexed. XBB 903-2430

Figure 16: (a) A HREM micrograph showing a [123] oriented grain of Ag in contact to YBCO in the [100] orientation and two regions (I) and (II) where Ag_2Y form. (b) SAD pattern taken at region (II). (c) Indexed SAD pattern. (d) illustrates the orientation relationship between YBCO and Ag_2Y. (e) Illustrates the orientation relationship between YBCO and Ag. (f) and (g) are the inset boxes (I) and (II) at higher magnification. Lattice distortions at the contact are limited to a very narrow region, preferentially, in YBCO. Notice the sharp and atomically smooth interface between the Ag_2Y and Ag at the arrow mark. XBB 903-2429 and XBB 903-2428

Figure 17: (a) Another example showing that Ag_2Y forms along the curve interface. (b) The SAD pattern taken at the interface and indexed in (c). (d)

and (e) illustrate the orientation relationships between Ag_2Y and YBCO and Ag and YBCO respectively. XBB 903-2427

Figure 18: (a) Shows the nucleation of an Ag_2O particle at the Ag/YBCO interface. Facets along the YBCO/Ag contact are also visible. (b) The corresponding SAD pattern and (c) its illustration. (d) and (e) illustrate the orientation relationships between Ag_2O and YBCO and Ag and YBCO respectively. XBB 903-2426

Figure 19: (a), (b), and (c) are a series of HREM images taken at different regions of the Ag/YBCO in which was laser ablated in the same chamber where YBCO was grown. Notice that in both micrographs the $(111)_{Ag}$ planes are randomly oriented with respect to the interface and a layer of disordered YBCO, of different thicknesses, extends along the interface. XBB 903-2440

Figure 20: (a) A lattice image showing steps of one to four atomic layers along the whole surface of YBCO illustrating its irregularity and where Ag_2Y is found to nucleate along the surface of YBCO. Notice that the Ag_2Y phase does not seem to be continuous along the surface of YBCO but rather distributed as clusters. (b) The corresponding SAD pattern and (c) its illustration. XBB 903-2424

Figure 21: (a) Show a low magnification TEM image of the Ag/YBCO where the the surface of YBCO was ion-milled before the deposition of Ag. Notice the nearly flat boundary and the bright seam along the interface. (b) The corresponding SAD pattern. (c) the indexed SAD pattern. XBB 903-2423

Figure 22: (a) A lattice image of an Ag/YBCO interface after treatment of the YBCO surface. Lattice fringes, i.e. the arrow mark, are visible in some regions of the intermediate layer and seem to originate in the YBCO and extend up to the Ag. The micrograph also shows that the silver grain is heavily twinned along the interface. Stacking faults and bending of (001) are also observed in the YBCO film.(b) The corresponding SAD pattern and (c) its illustration. XBB 903-2422

Figure 23: (a) and (c) show two other regions of the Ag/YBCO interface in which the intermediate layer is always present and where at the Ag is in the [112] and [123] orientations. In both cases the close packed planes of Ag are stacked parallel to the $(001)_{YBCO}$ planes with an offset angle of about 8° and 15° in the first and second example respectively. (b) and (d) are the SAD patterns for (a) and (c) which are illustrated in (e) and (f). XBB 903-2421

Figure 24: (a) Shows a region in which the YBCO surface is still rough and contains steps after it was ion-milled. (b), (c), and (d) Three different regions (I, II, and III) along the interface examined at higher magnification. Lattice fringes running across the intermediate layer are visible. Along the interface, in both three micrographs, there is a noticeable change in the contrast in both Ag, the intermediate layer, and YBCO while Ag grains exhibit different orientation with respect to interface. XBB 903-2443 and XBB 903-2439

Figure 25: (a) A typical Ag/YBCO interface at low magnification in which the surface of YBCO was ion-milled then sputter-etched before the coating with Ag. The Ag and YBCO are in the [012] and [010] orientations respectively and

the $(002)_{Ag}$ and $(001)_{YBCO}$ are nearly parallel with an offset angle of about 5°. Notice that the intermediate layer is thicker in the center (about 60Å) than it is at the left side of the micrograph (about 30Å). (b) A SAD pattern taken near the interface. (c) Illustration of the SAD pattern. XBB 903-2417

Figure 26: (a) A HREM micrograph illustrating the irregularity of the YBCO surface. Ag is directly bonded to YBCO, in right hand side of the micrograph, whereas in the center of the image Ag is bonded to a damaged YBCO surface. (b) The corresponding SAD pattern and indexed (c) shows that Ag, in the [233], exhibits no orientation relationship with YBCO. XBB 903-2420

Figures 27: (a) and (b) show the Ag/YBCO interface before and after the YBCO surface was treated. Notice that in (a) the surface of YBCO is clearly rough and rippled along the whole interface whereas in (b) the interface is flat while a uniform layer is created at the surface of YBCO. (c) and (d) The corresponding SAD patterns for (a) (b) respectively. XBB 903-2442

Figure 28: (a) A lattice image showing Ag in contact to two grains of YBCO having their (001) planes perpendicular to each other. The surface of YBCO is irregular and the deposited Ag in the [013] zone axis exhibits no orientation relationship with YBCO. (b) The corresponding SAD pattern and its illustration in (c). XBB 903-2419

Figure 29: (a) A TEM micrograph sowing a whole region of about 2.8 μm transparent to the electron beam. (b) Shows that the thickness of such specimen are also adequate for HREM. XBB 903-2438

Figure 30: (a) A TEM micrograph shows an Au/YBCO interface and (b) its corresponding SAD pattern. XBB 905-3561

Figure 31: A series of computed SAD of an [111] oriented Ag grain tilted around the [111] zone axis by an angle of 0°(a), 1°(b), 2°(c), 3°(d), 4°(e), and 5°(f) respectively. XBL 904-1315

Figure 32: [111] Stereographic projection for a cubic crystal showing the 011, 112, and 123 poles. XBL 905-1616

Figure 33: Atomic structure of (001) layers (a) of type I or CuO, (b) type II or BaO, (c) type III or Cu_2O, and (d) type IV or Y. XBL 904-1617

Figure 34: Coincidence lattice of a (111) Ag layer on top of an (001) YBCO layer. (a) The $[011]_{Ag}$ and $[100]_{YBCO}$ directions are parallel while one Ag atom is placed on top of a copper atom in the (001) of type III (Cu_2O) layer. (b) Same as in (a) but Ag is placed on an oxygen atom. (c) Same as (a) but $(001)_{YBCO}$ is of type (II) while in (d) it is of type (IV). (e) Same as (a) but $[123]_{Ag}$ and $[100]_{YBCO}$ directions are parallel. XBL 904-1318 to 1322

Figure 35: (a) Ag-Y and (b) Ag-O phase diagrams [117]. XBL 905-1623

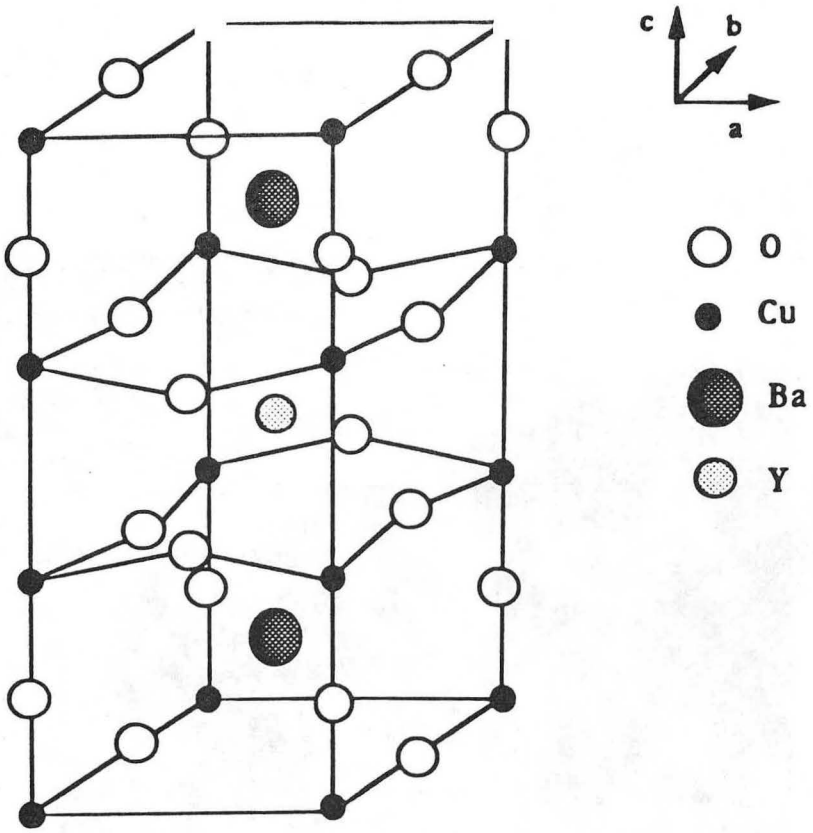

(a)

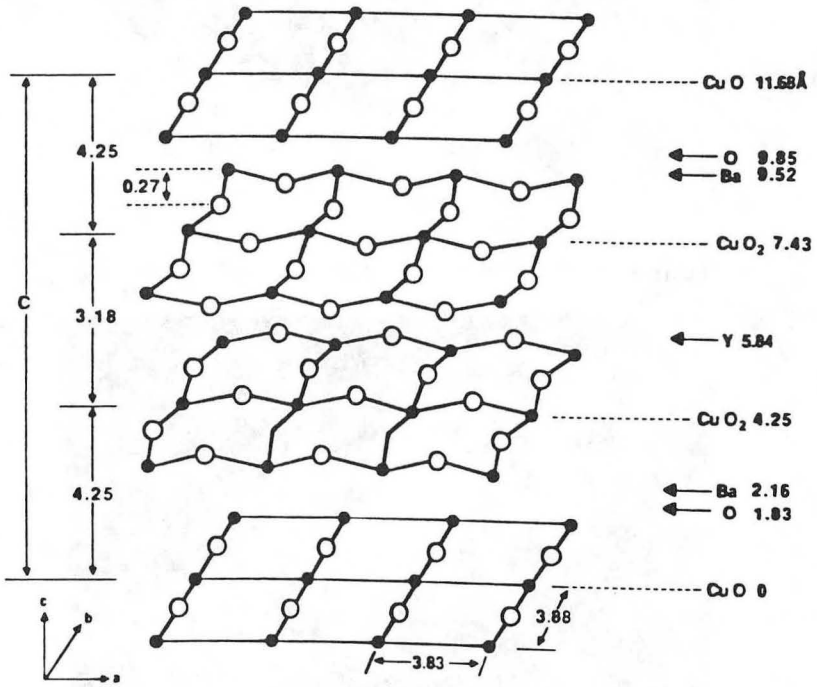

Figure1

XBL 905-1615

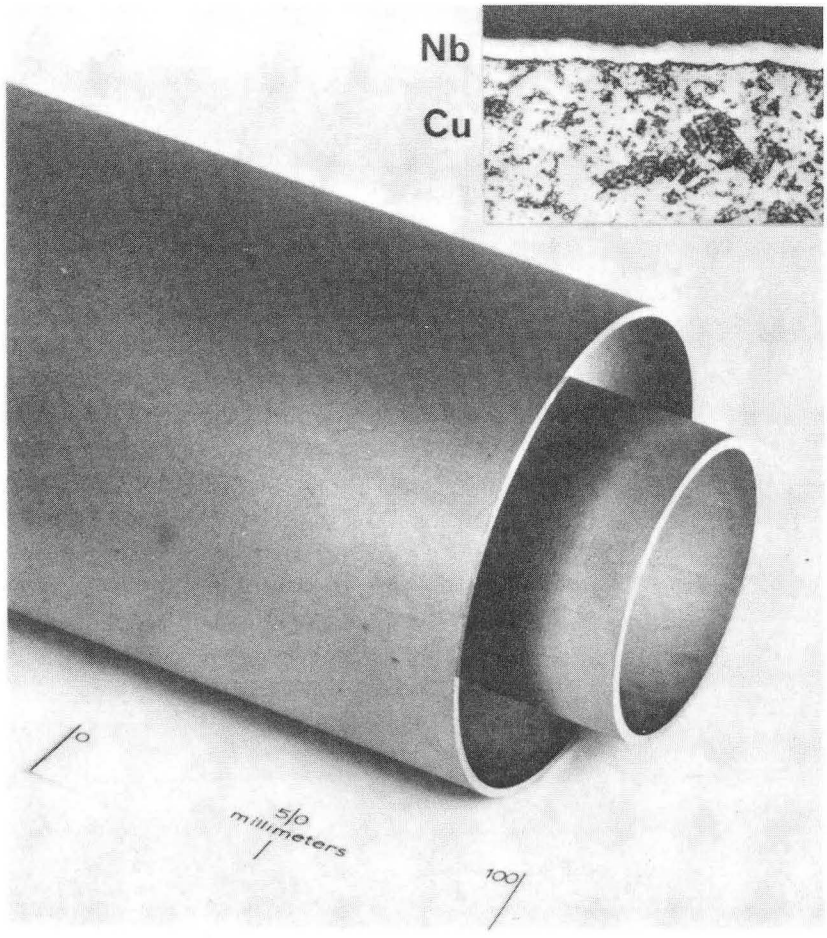

Figure 2

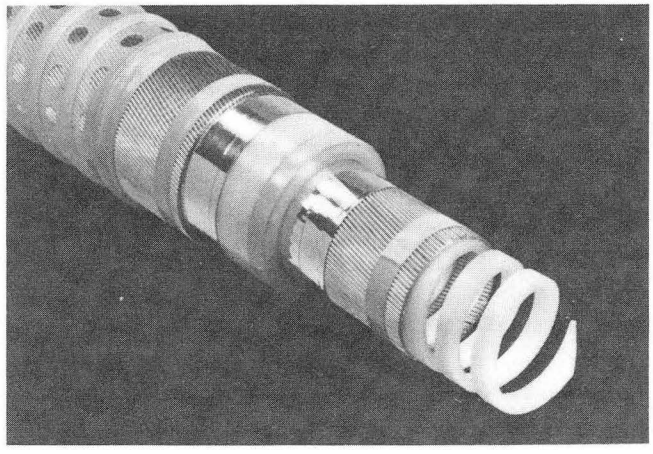

Figure 3

ZBB 905-3701

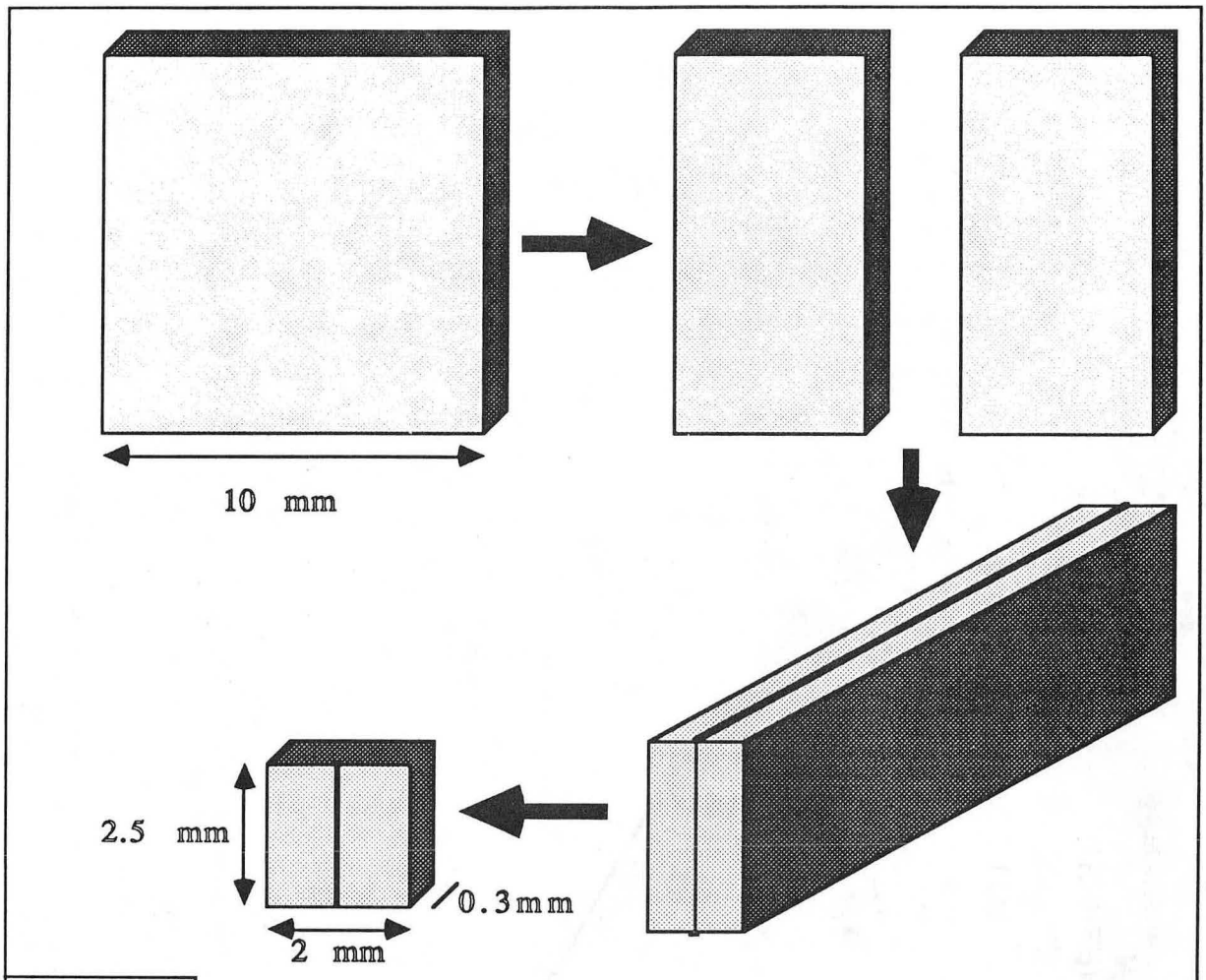

Figure 4

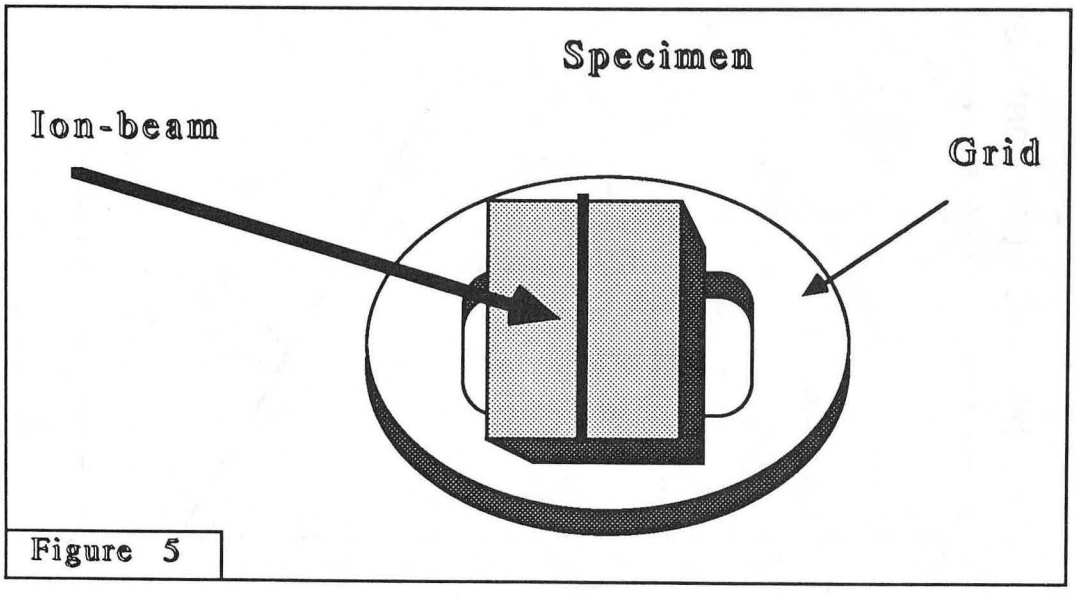

Figure 5

XBL 904-1316

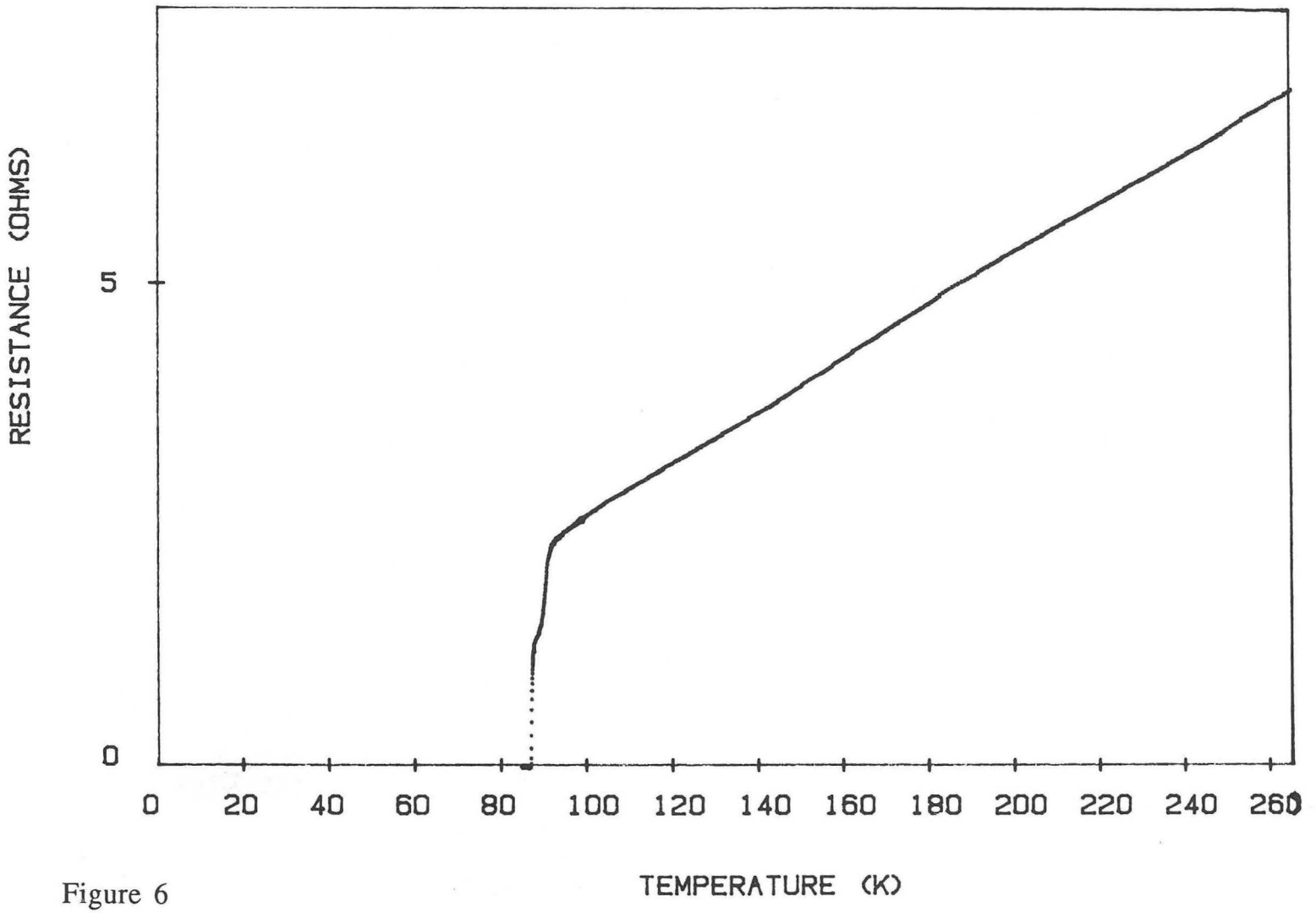

Figure 6

XBL 904-1317

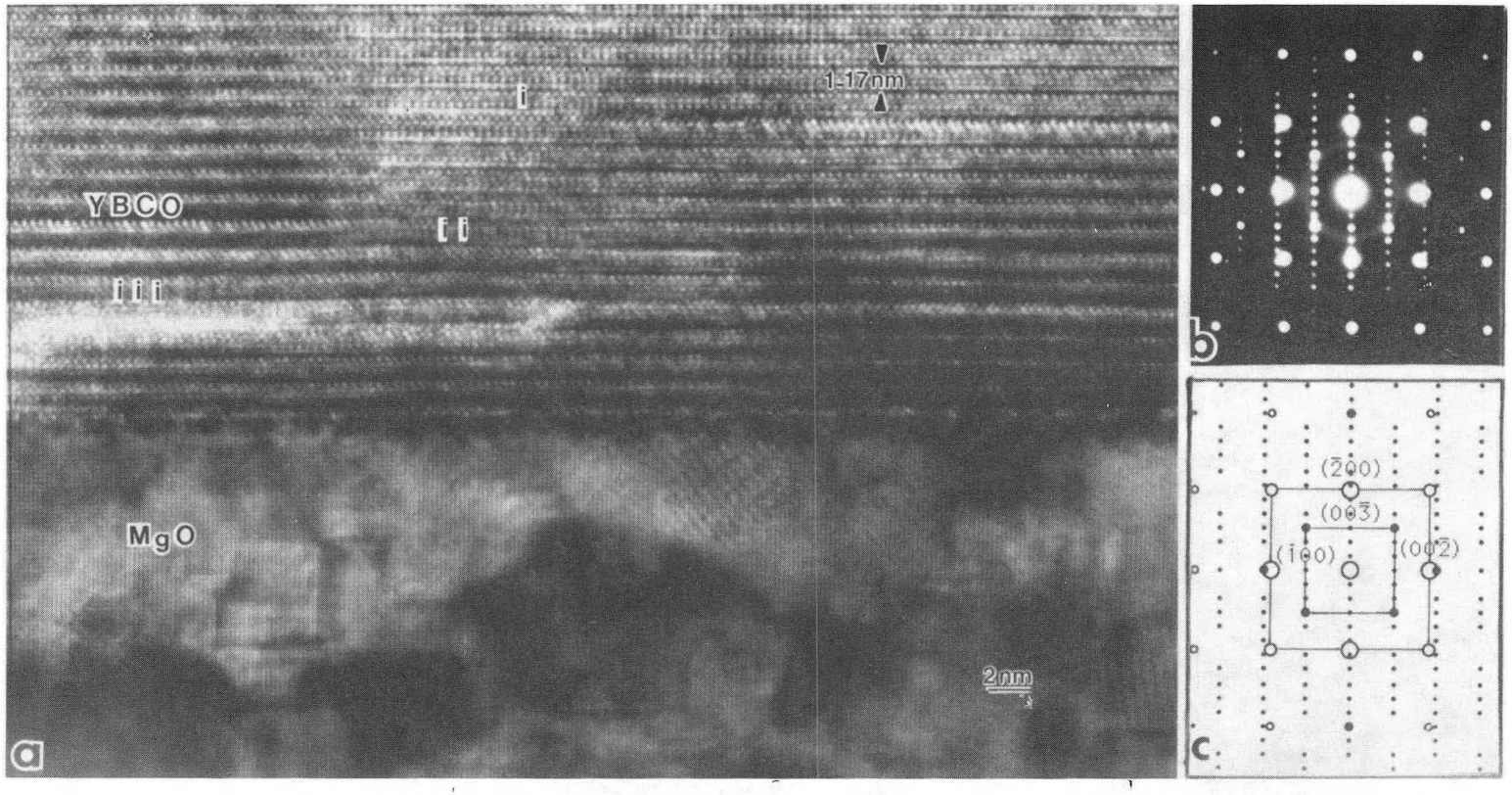

Figure 7

XBB 903-2437

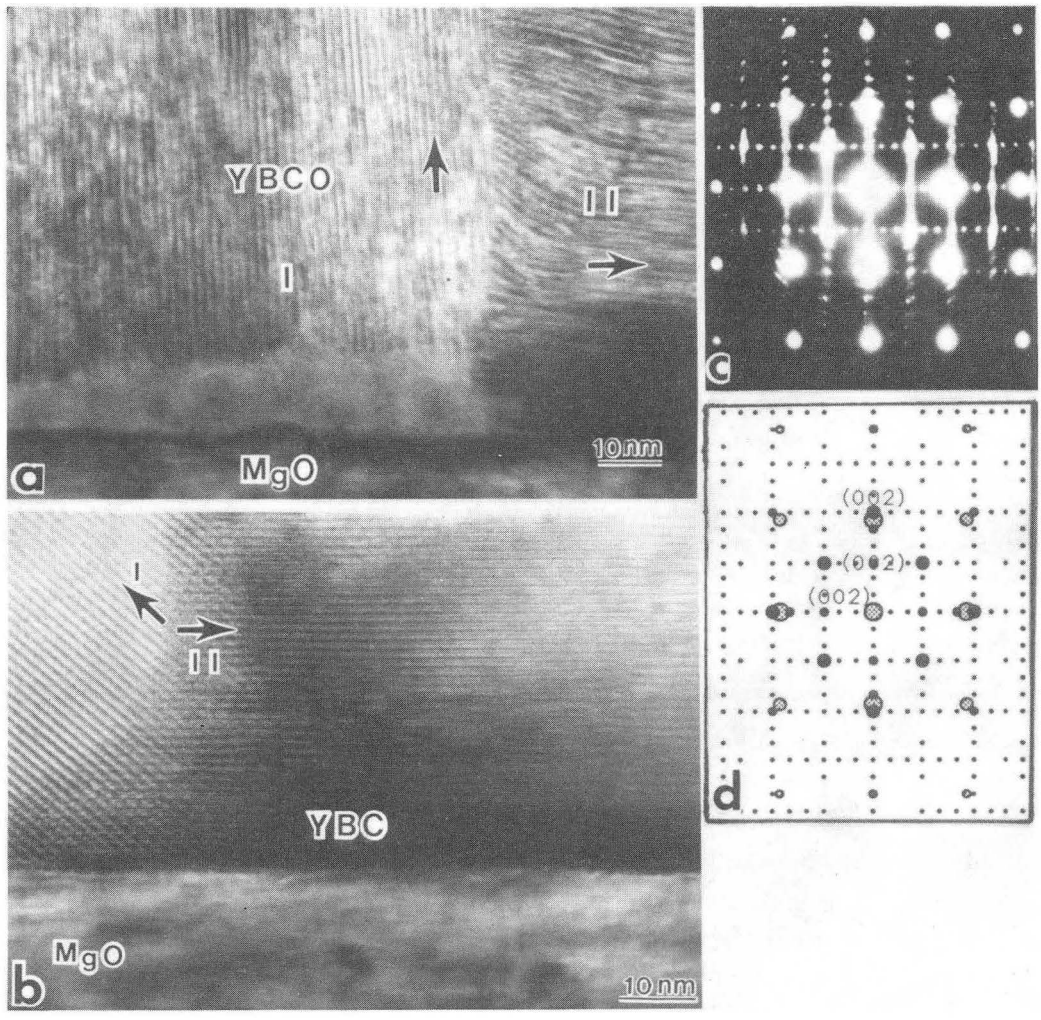

XBB 903-2418

Figure 8

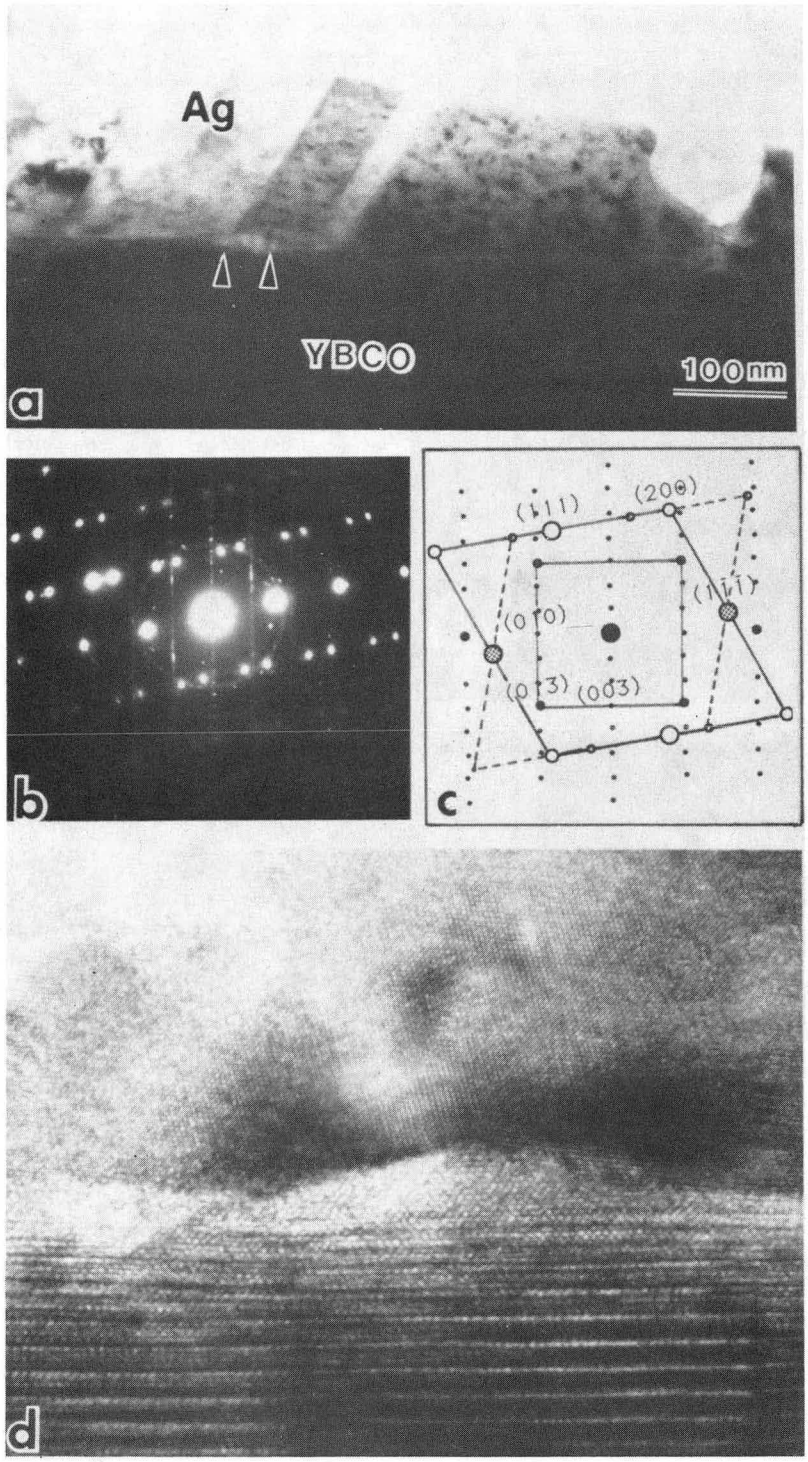

XBB 903-2436

Figure 9

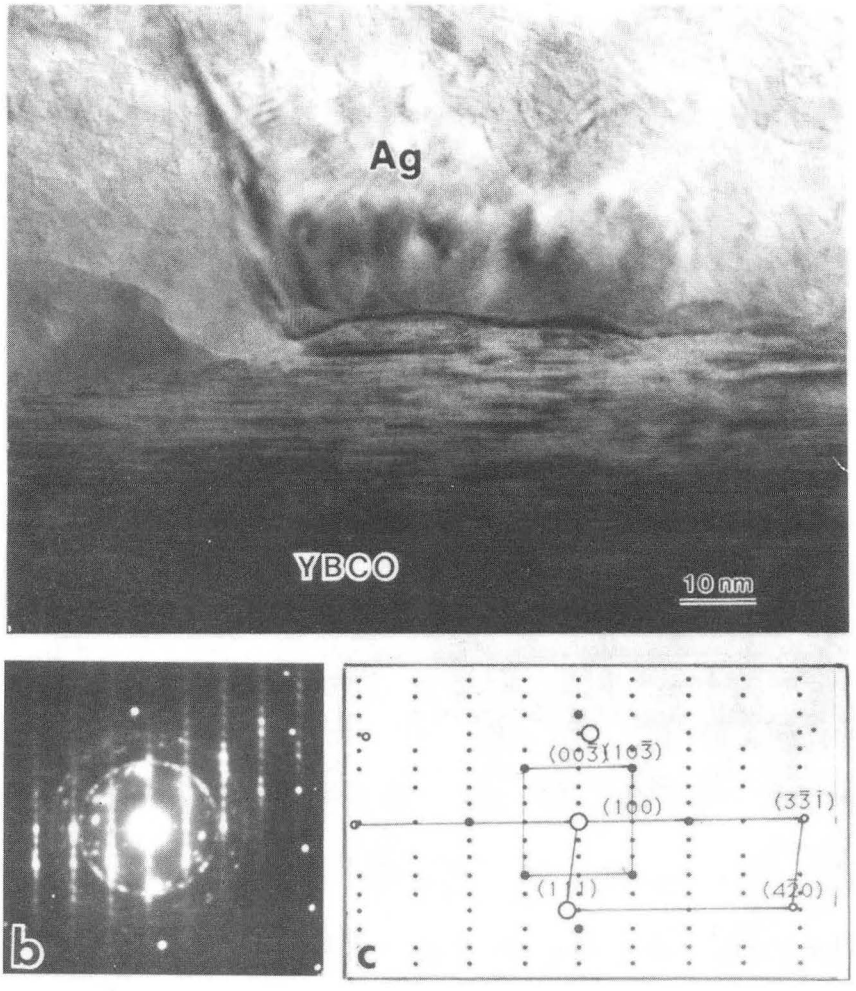

Figure10 XBB 903-2435

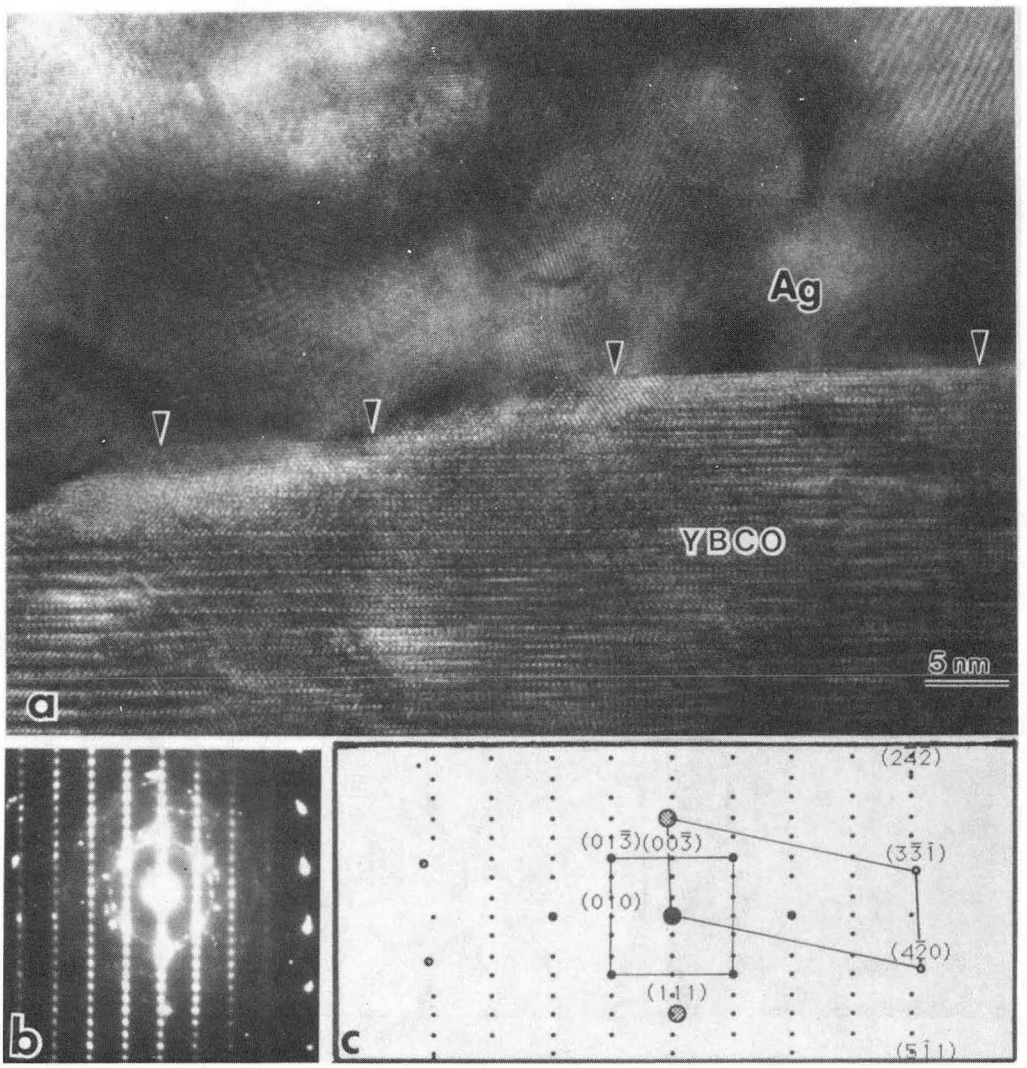

XBB 903-2434

Figure 11

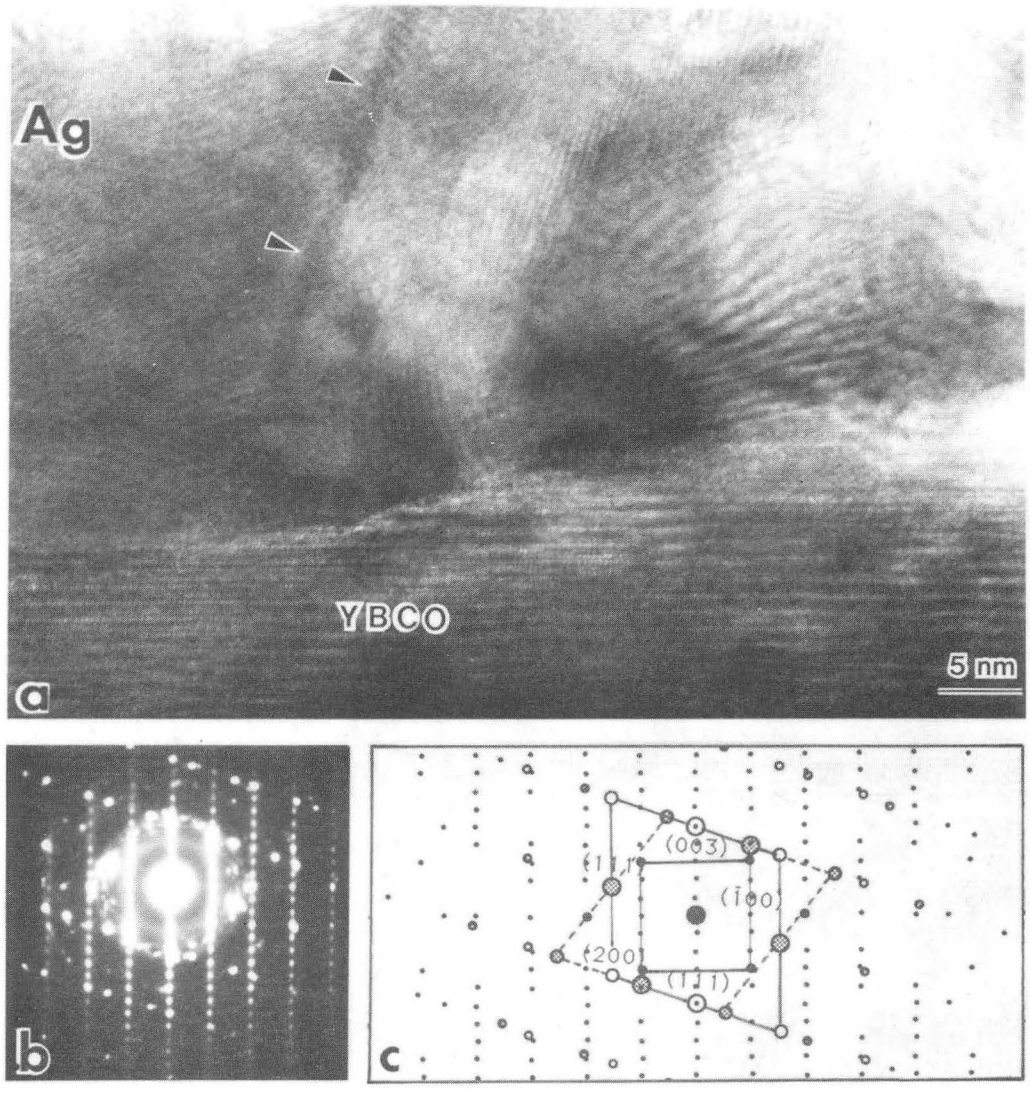

XBB 903-2433

Figure 12

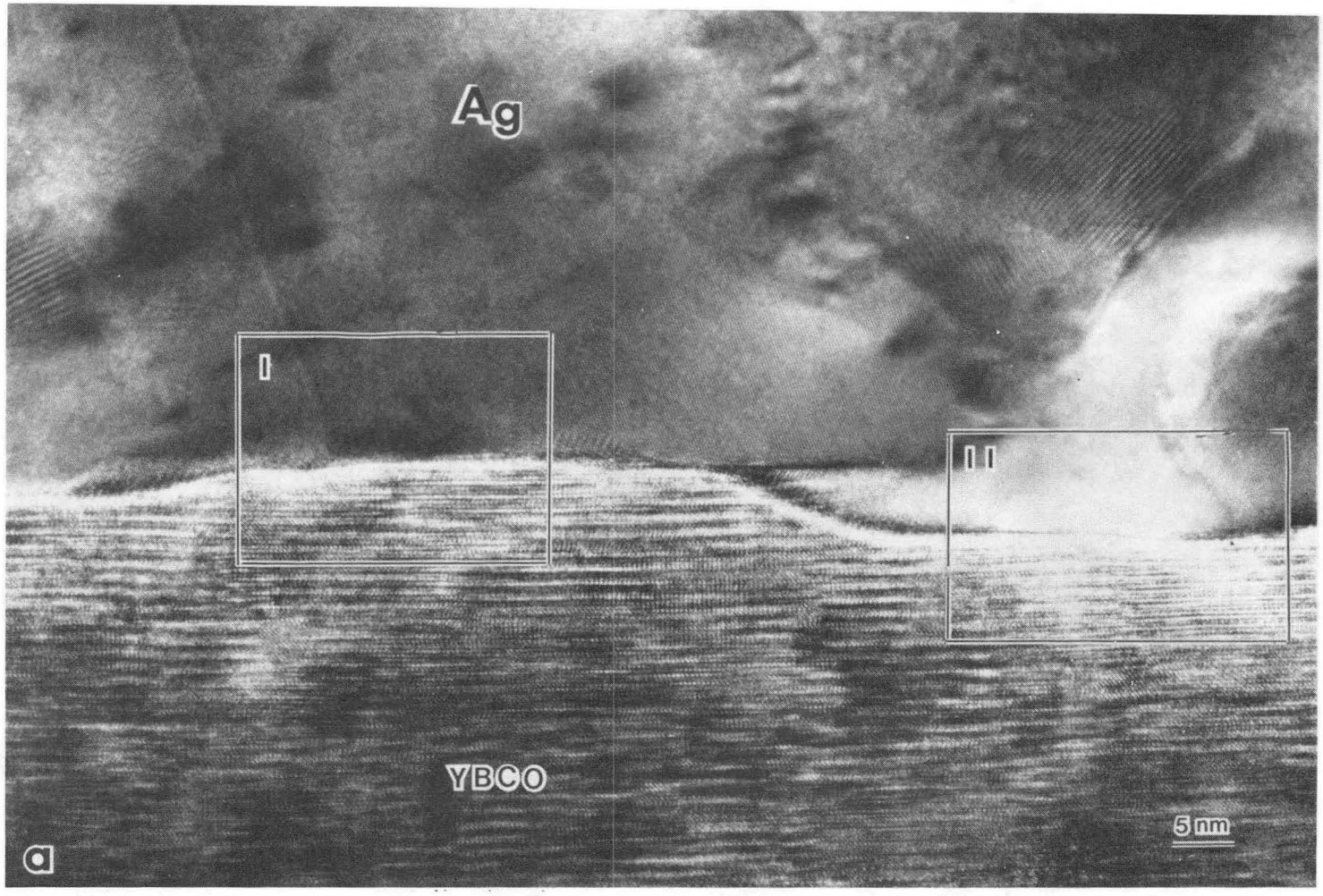

Figure 13

XBB 903-2441

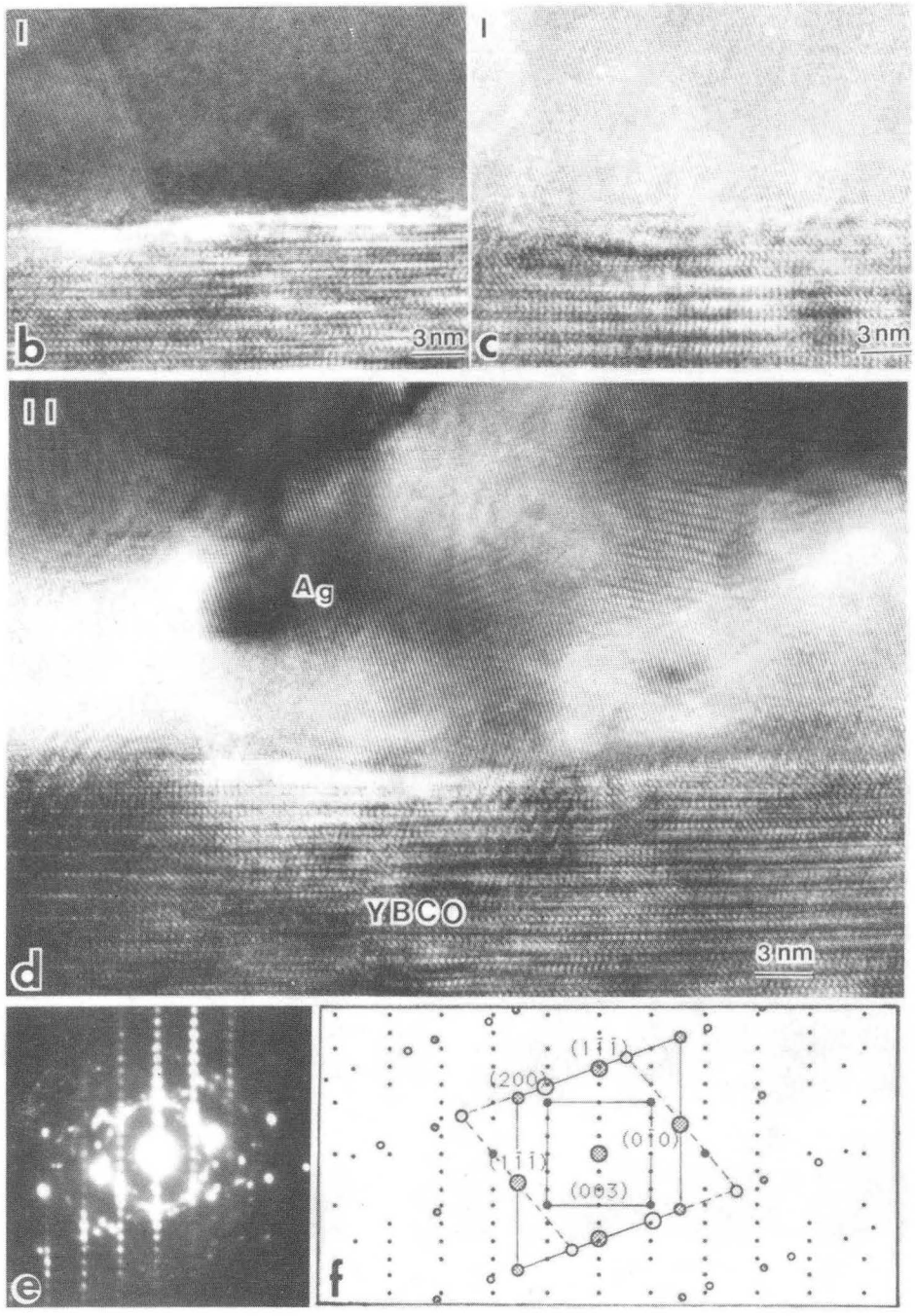

Figure 13 (Cont)

XBB 903-2431

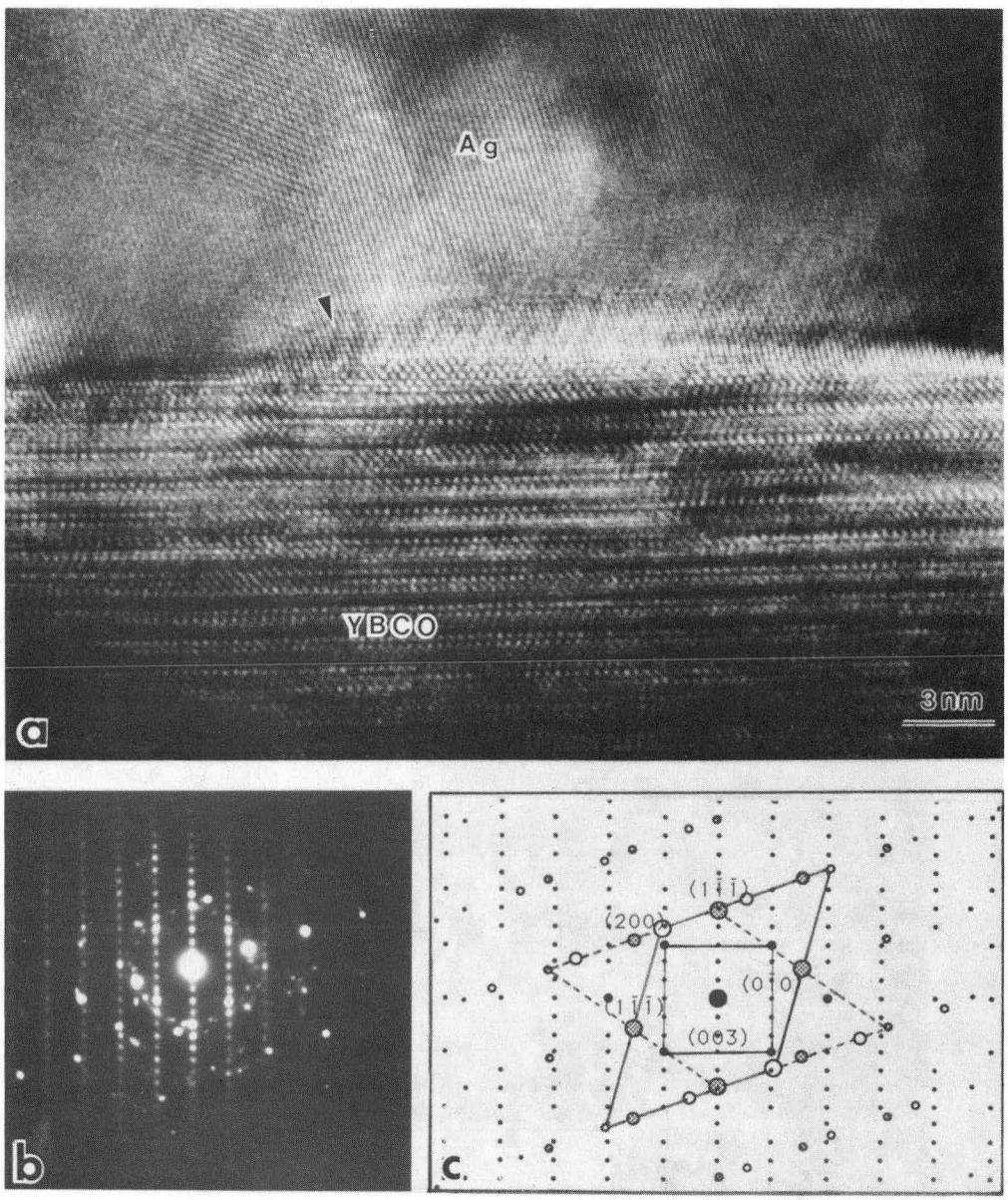

XBB 903-2432

Figure 14

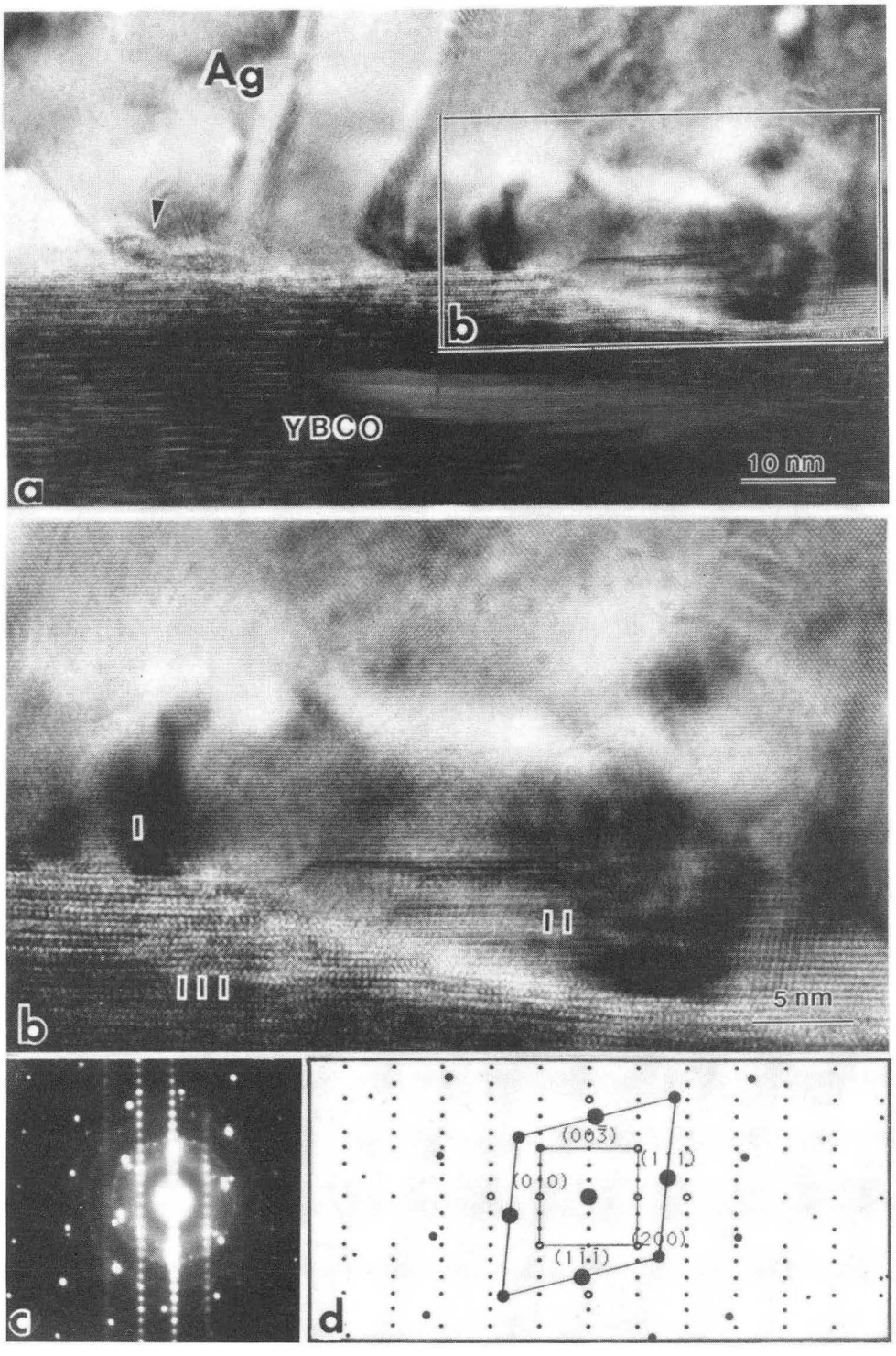

Figure 15

XBB 903-2430

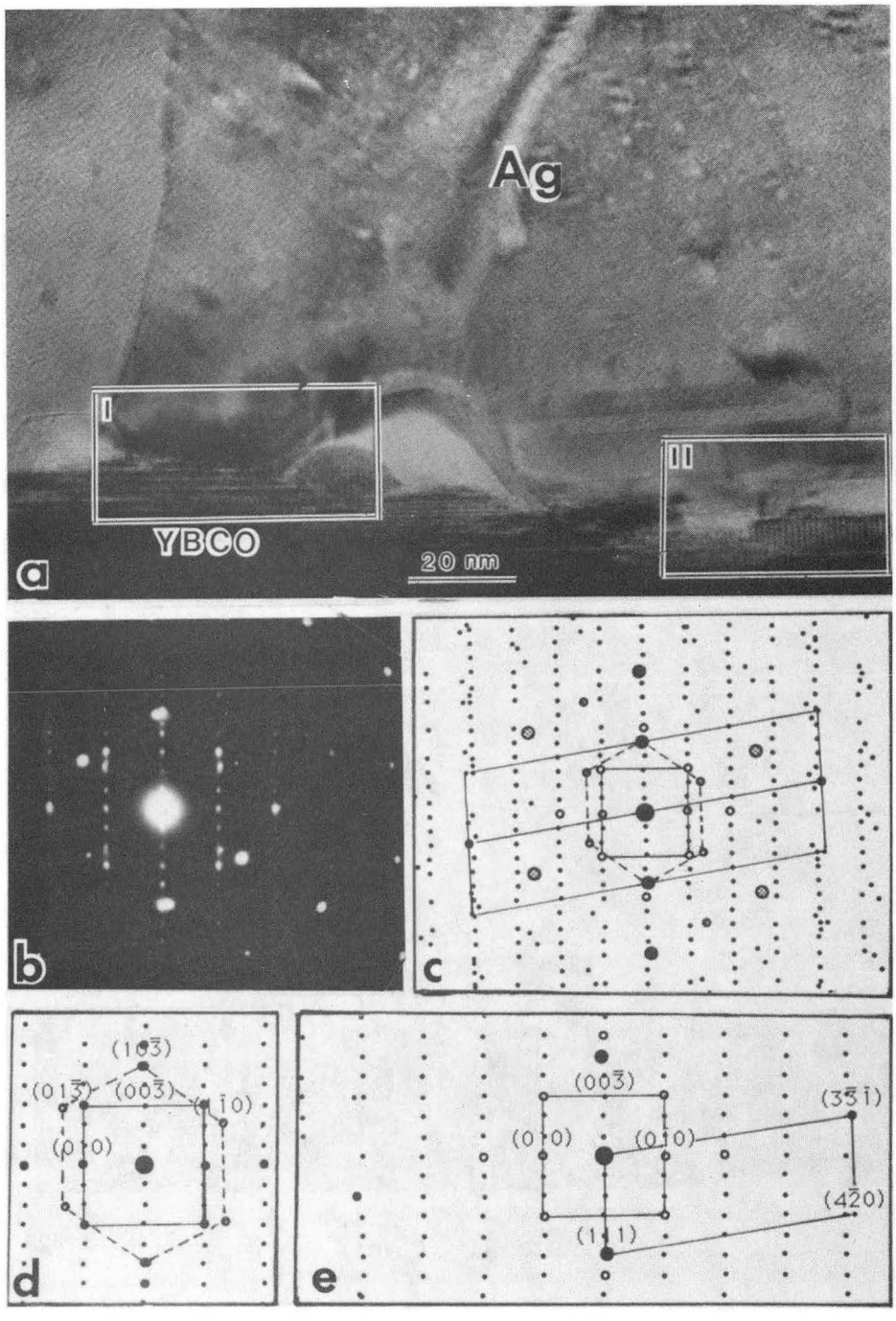

XBB 903-2429

Figure 16

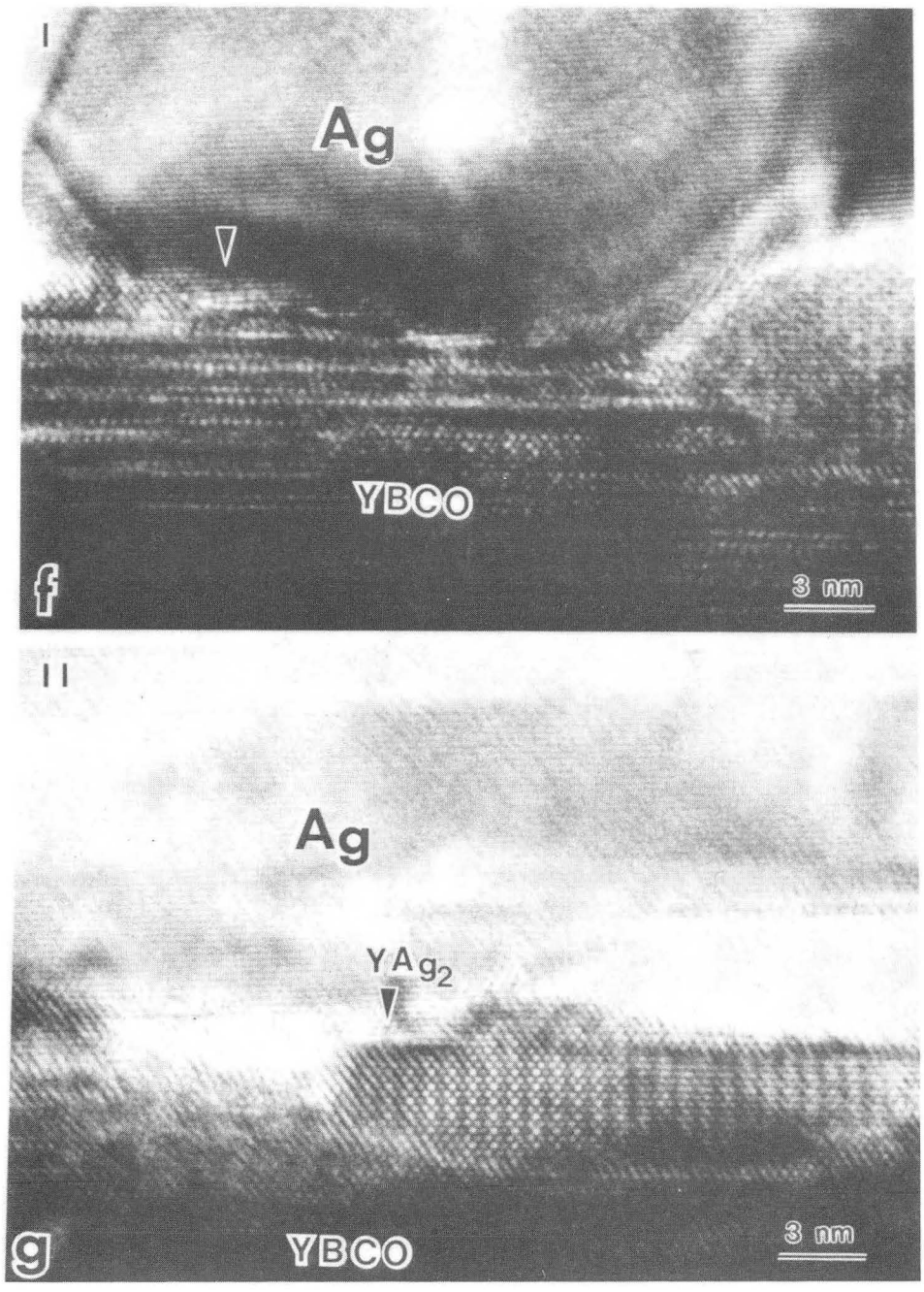

Figure 16 (Cont)

XBB 903-2428

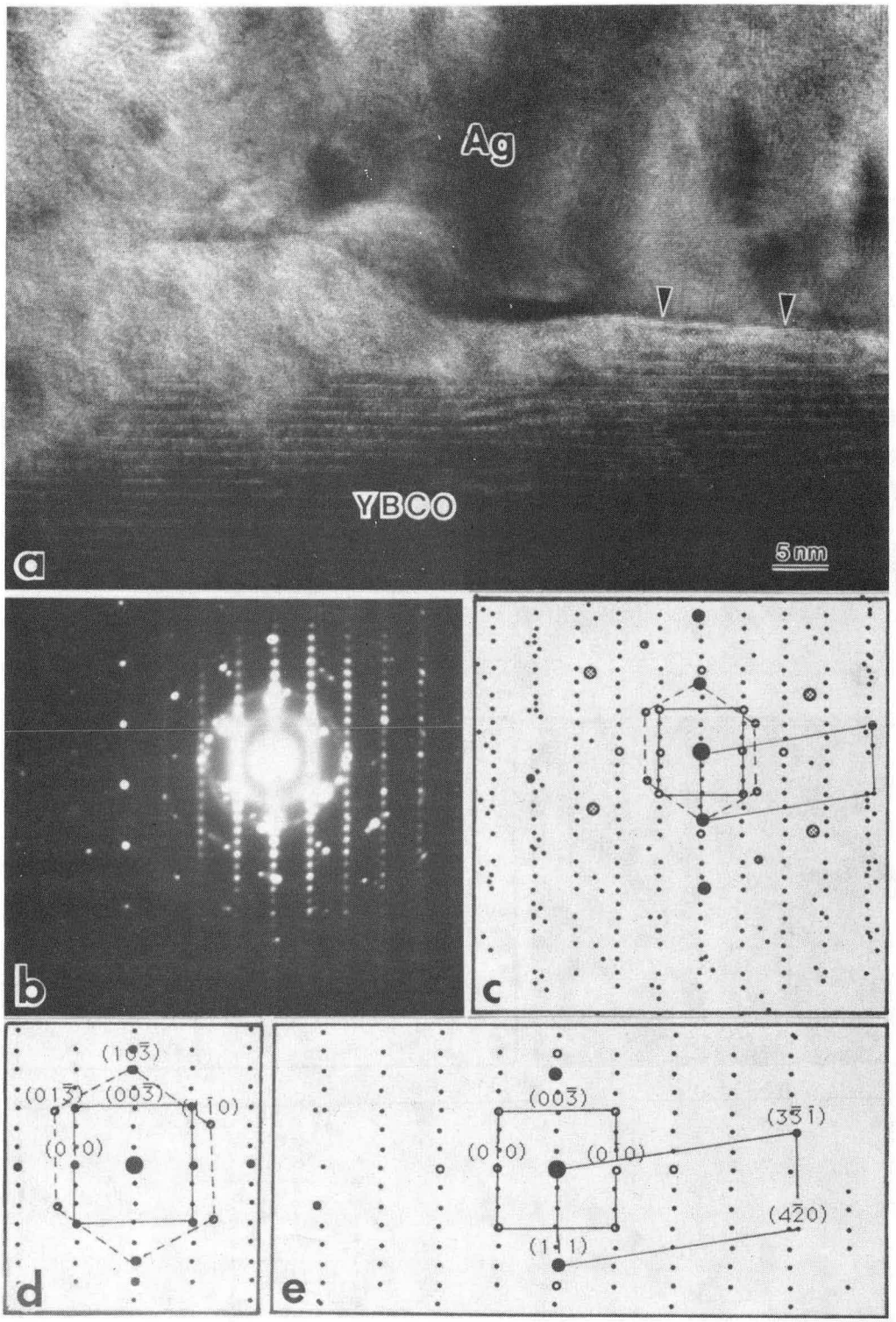

XBB 903-2427

Figure 17

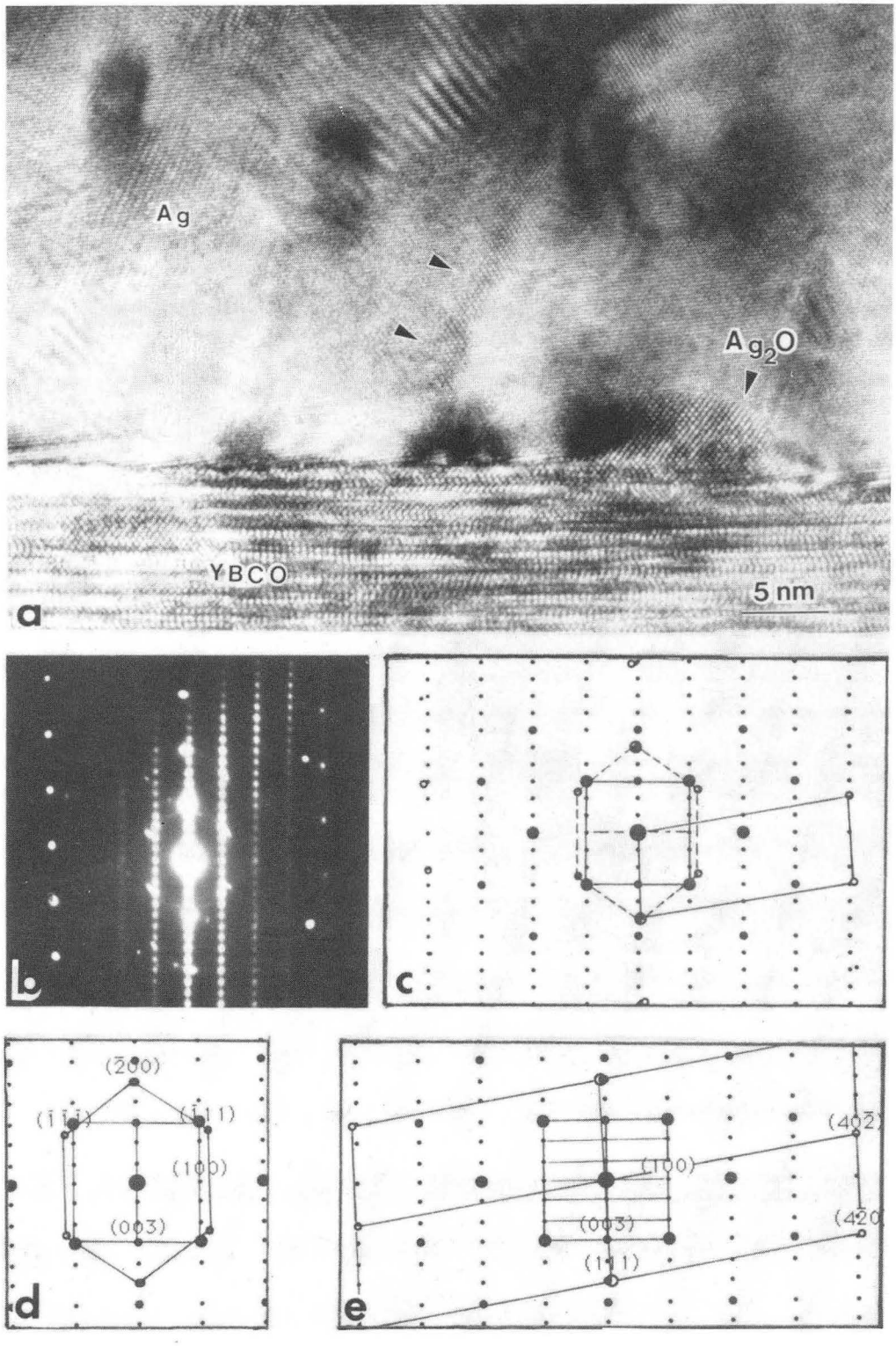

Figure 18

XBB 903-2426

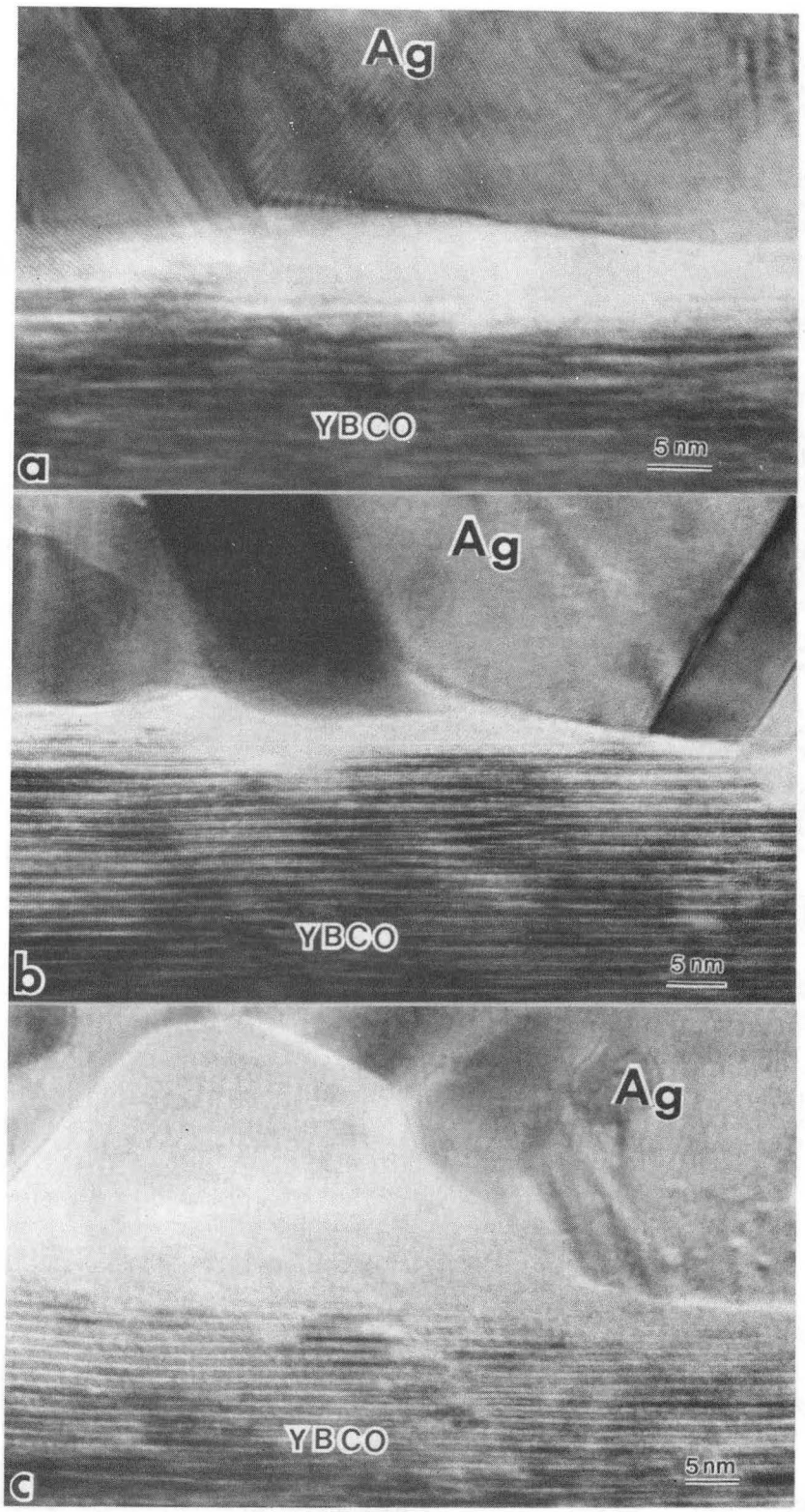

Figure 19

XBB 903-2440

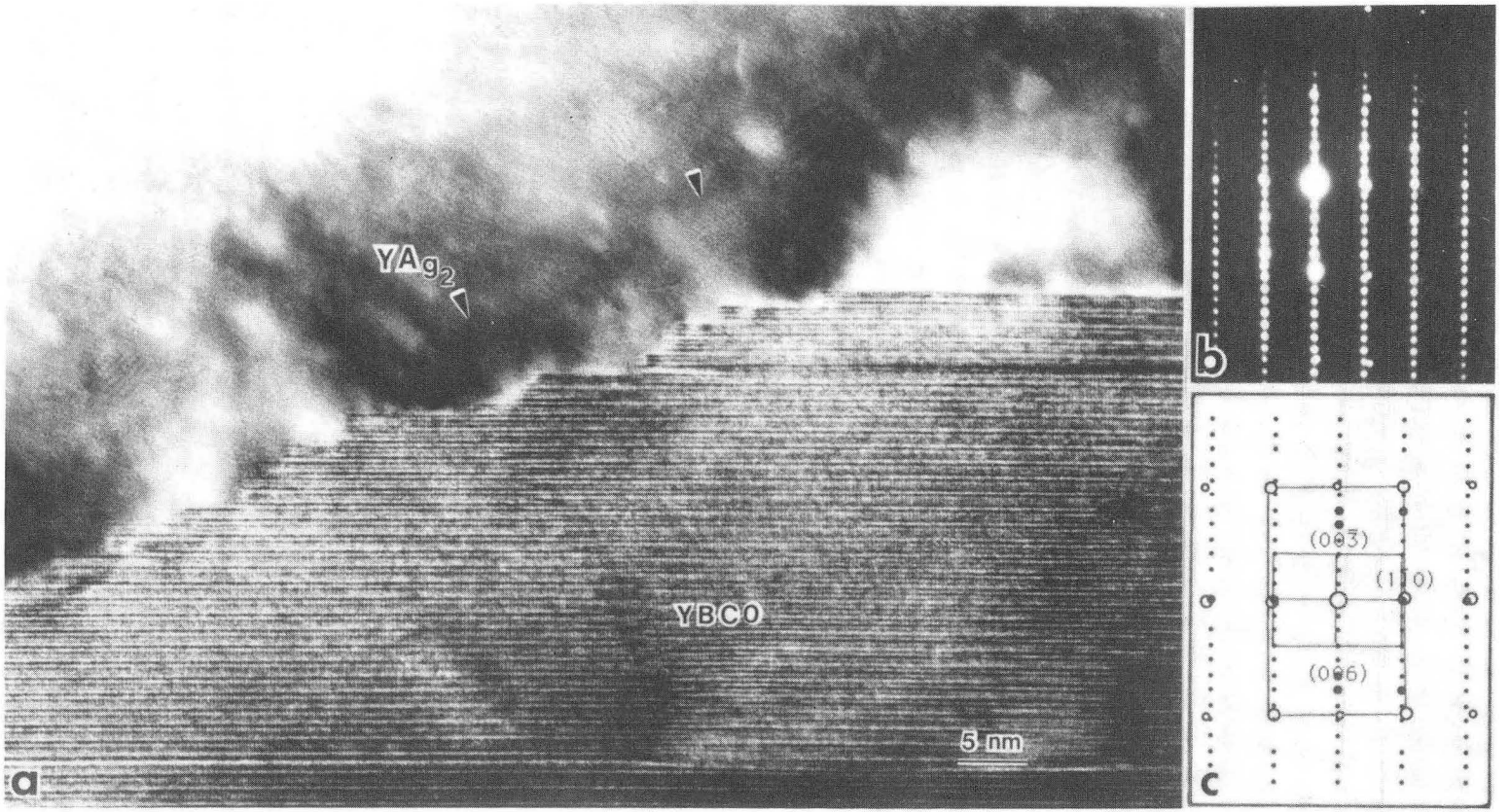

Figure 20

XBB 903-2424

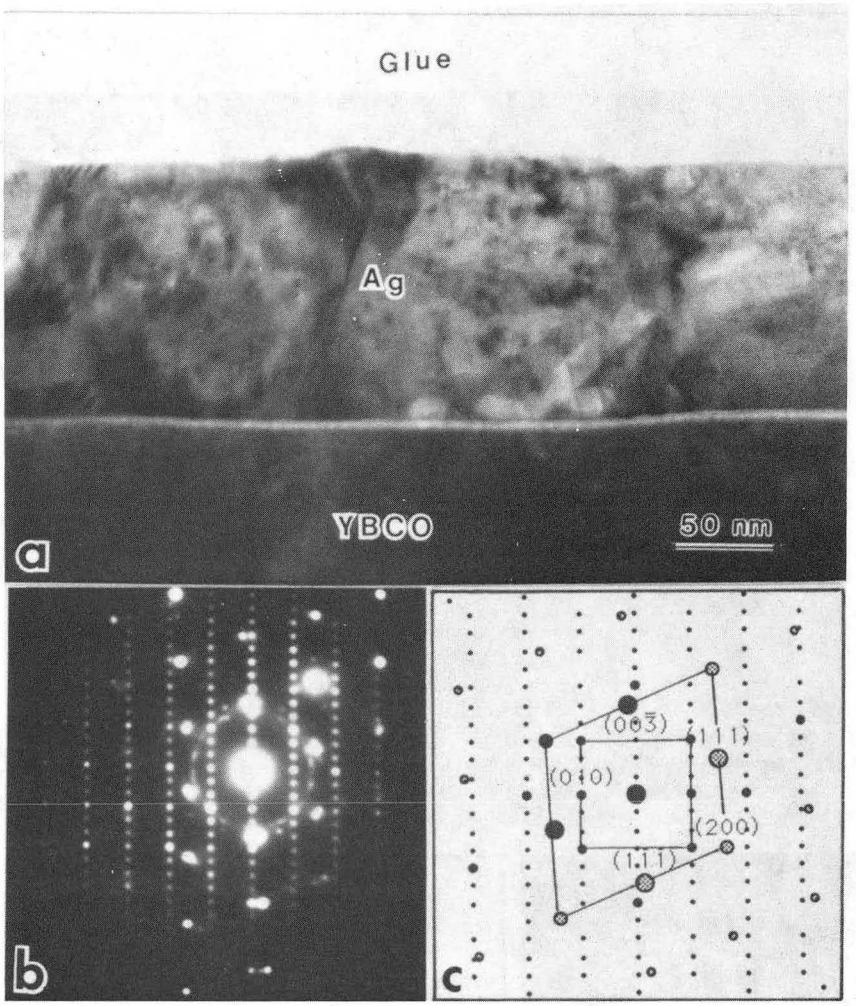

XBB 903-2423

Figure 21

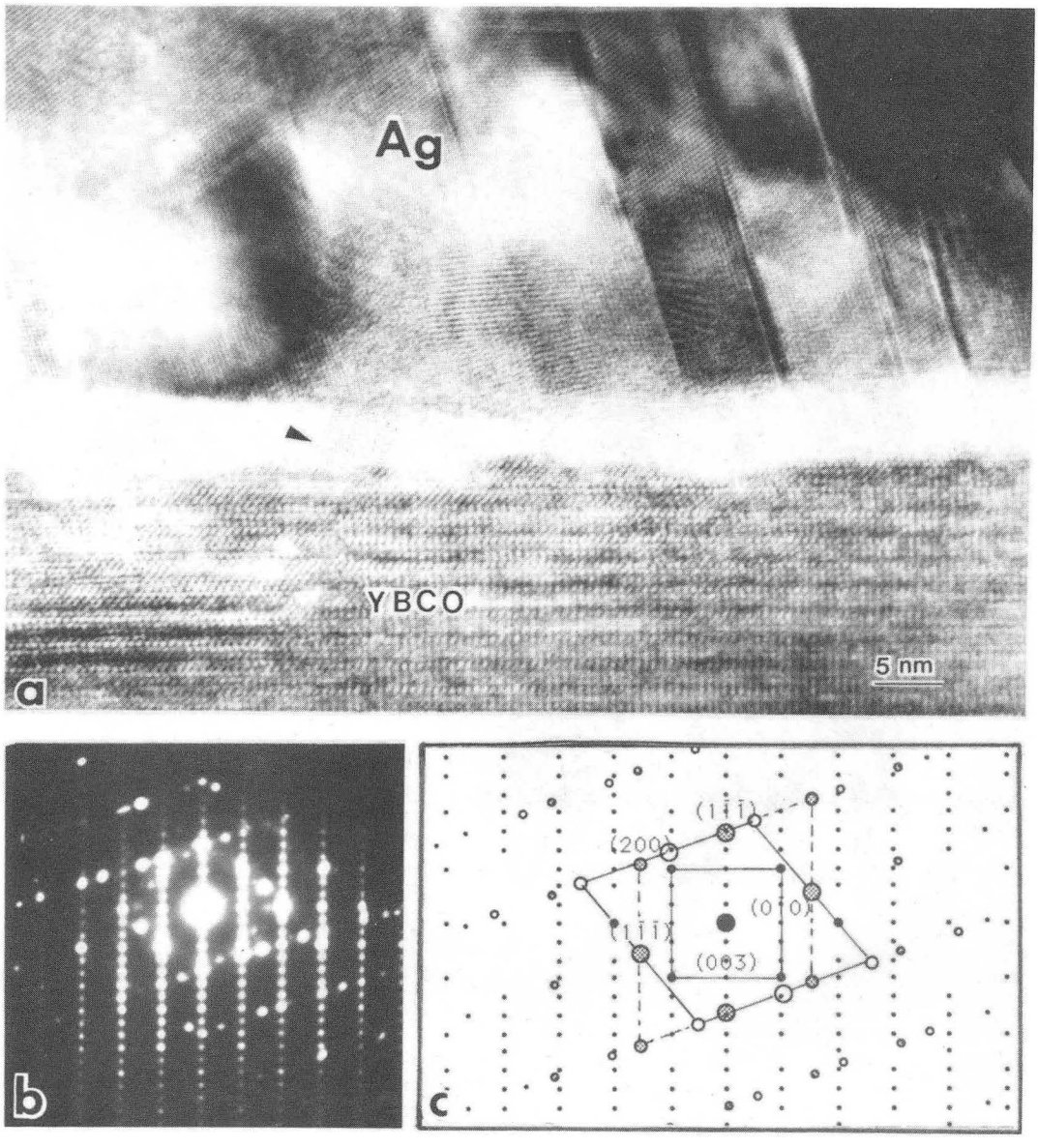

XBB 903-2422

Figure 22

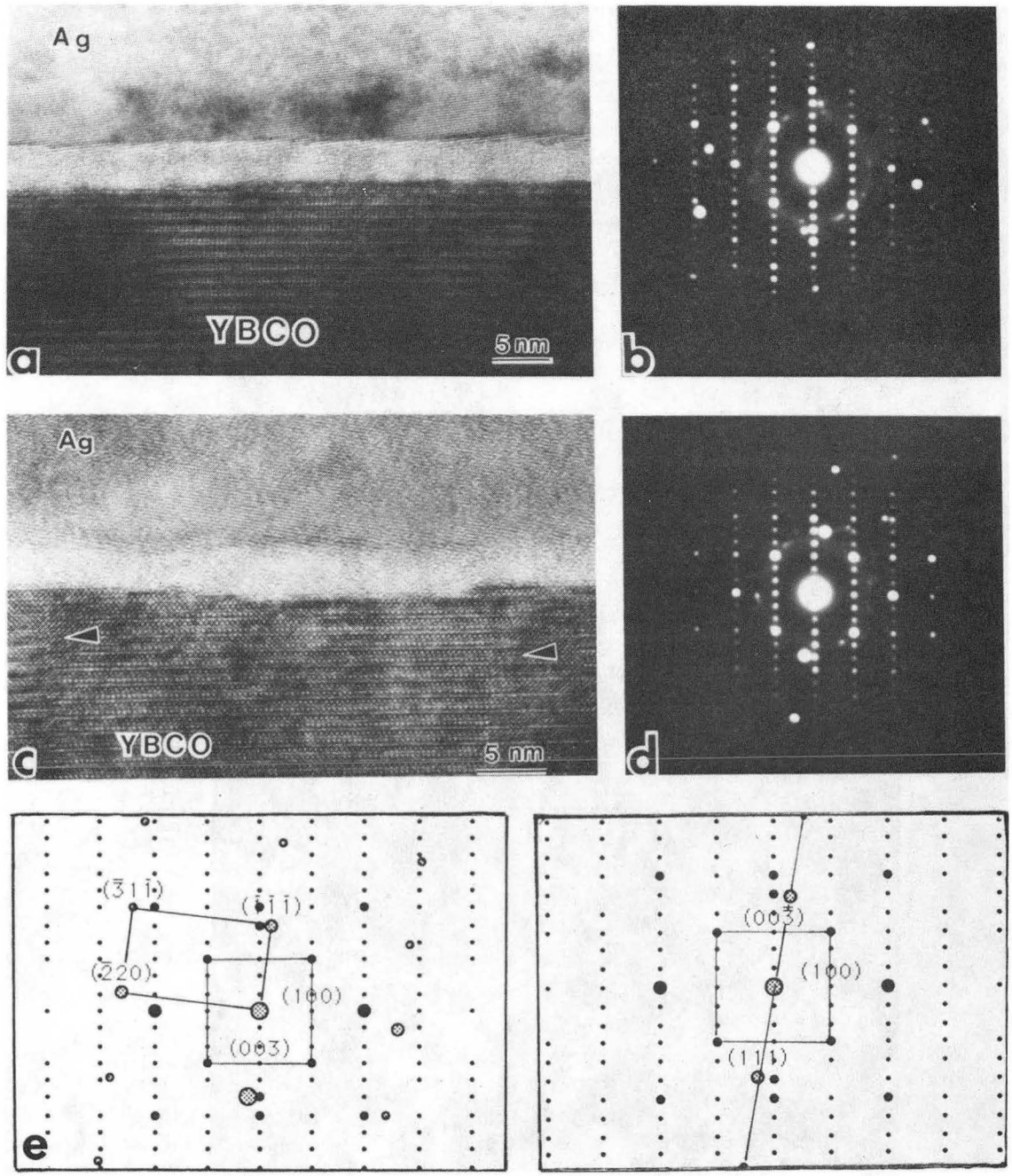

Figure 23

XBB 903-2421

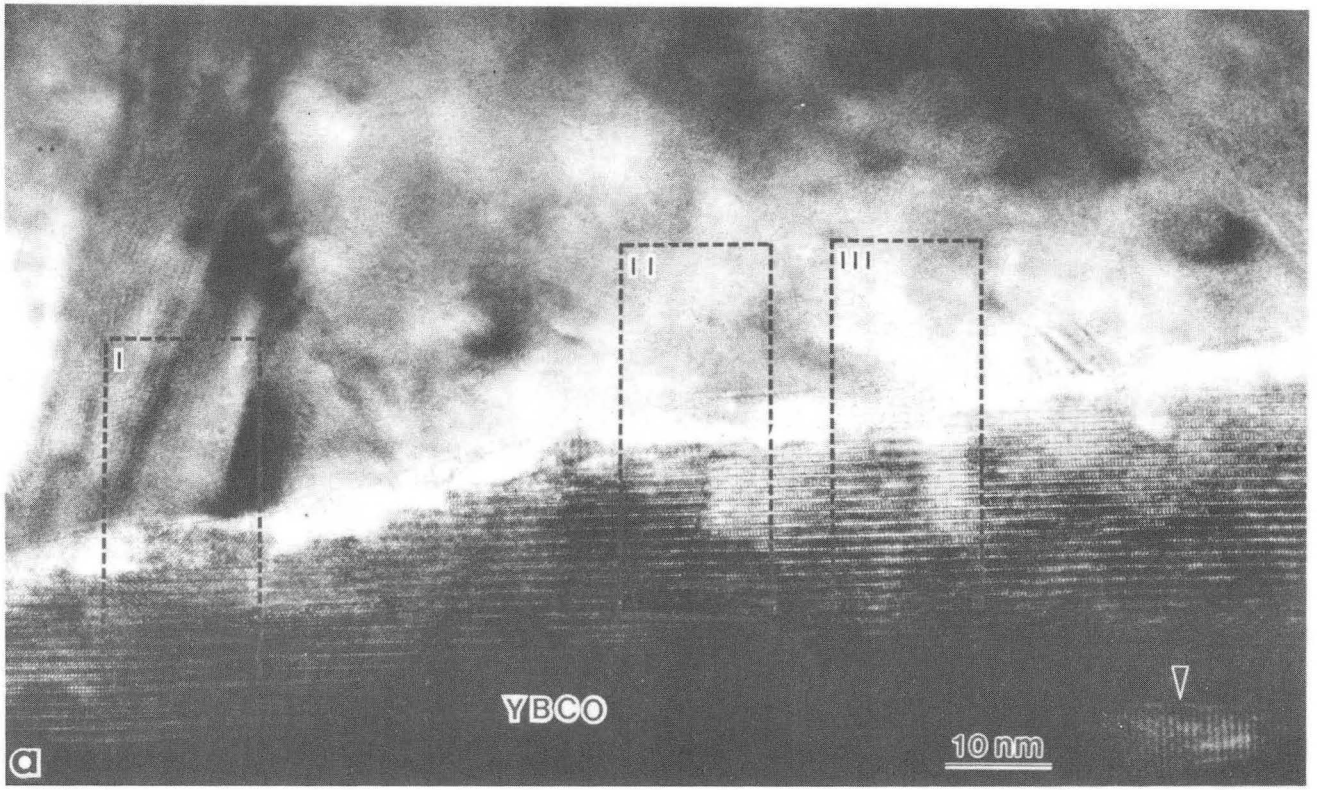

Figure 24

XBB 903-2443

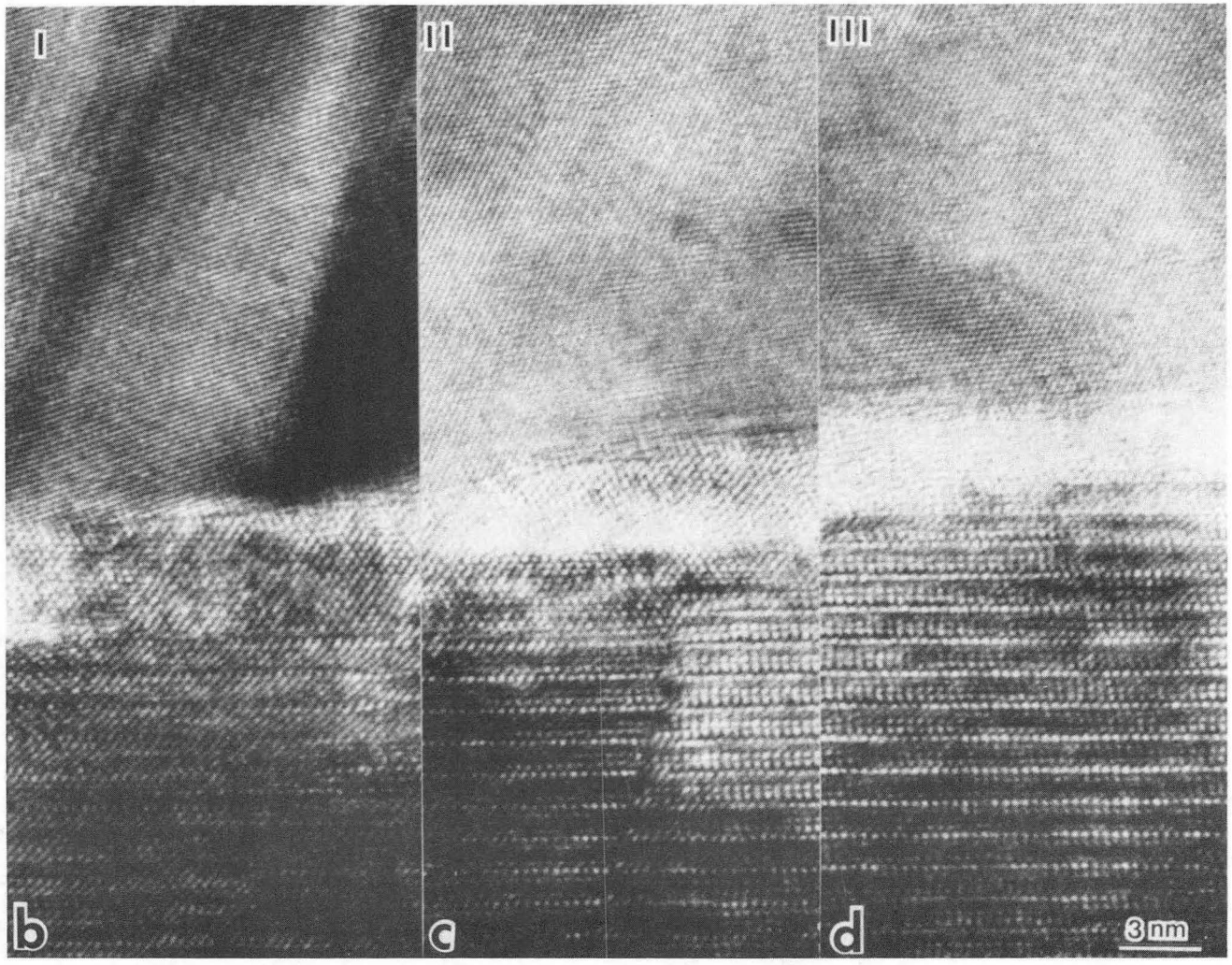

Figure 24 (Cont)

XBB 903-2439

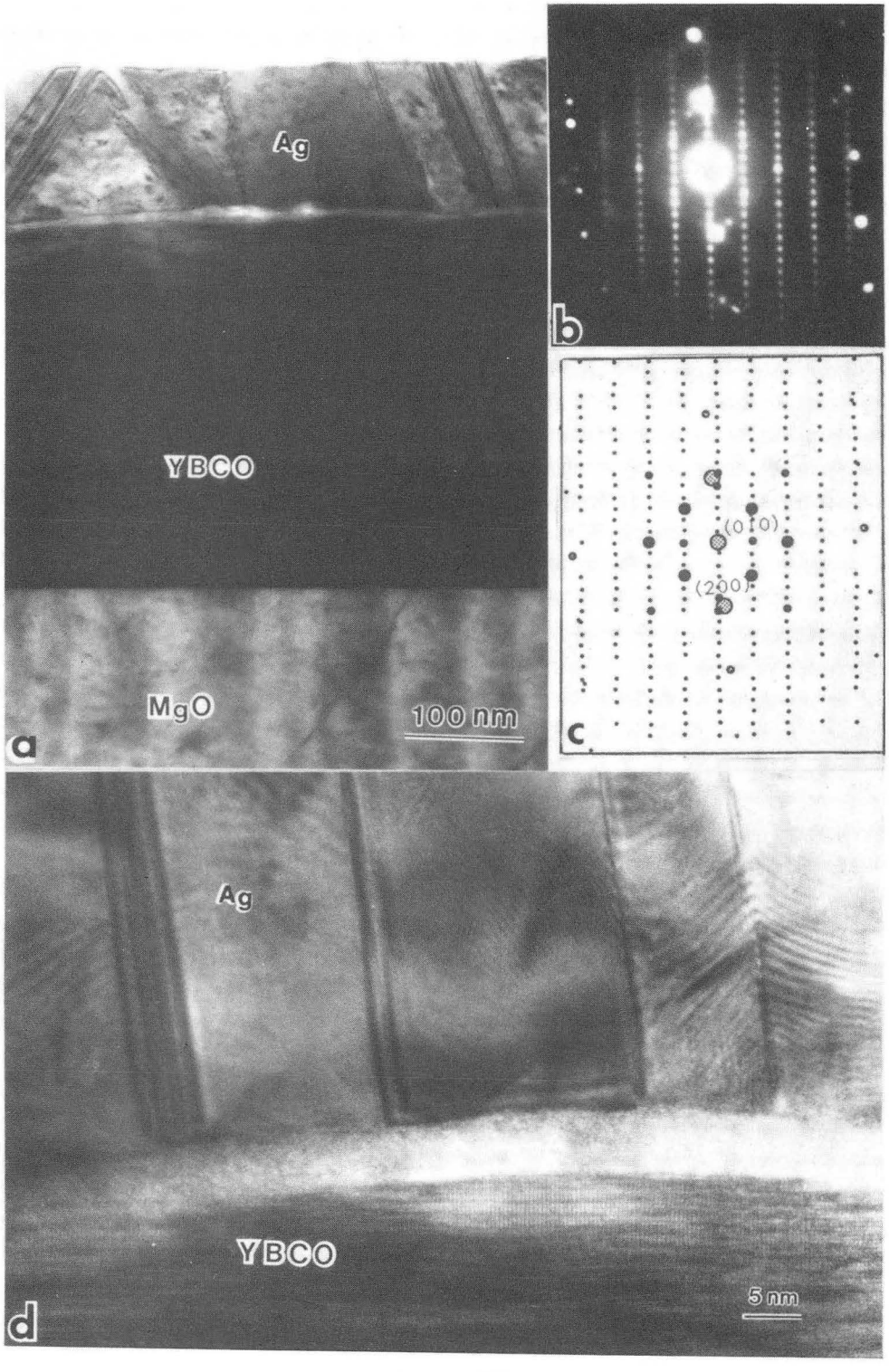

Figure 25

XBB 903-2417

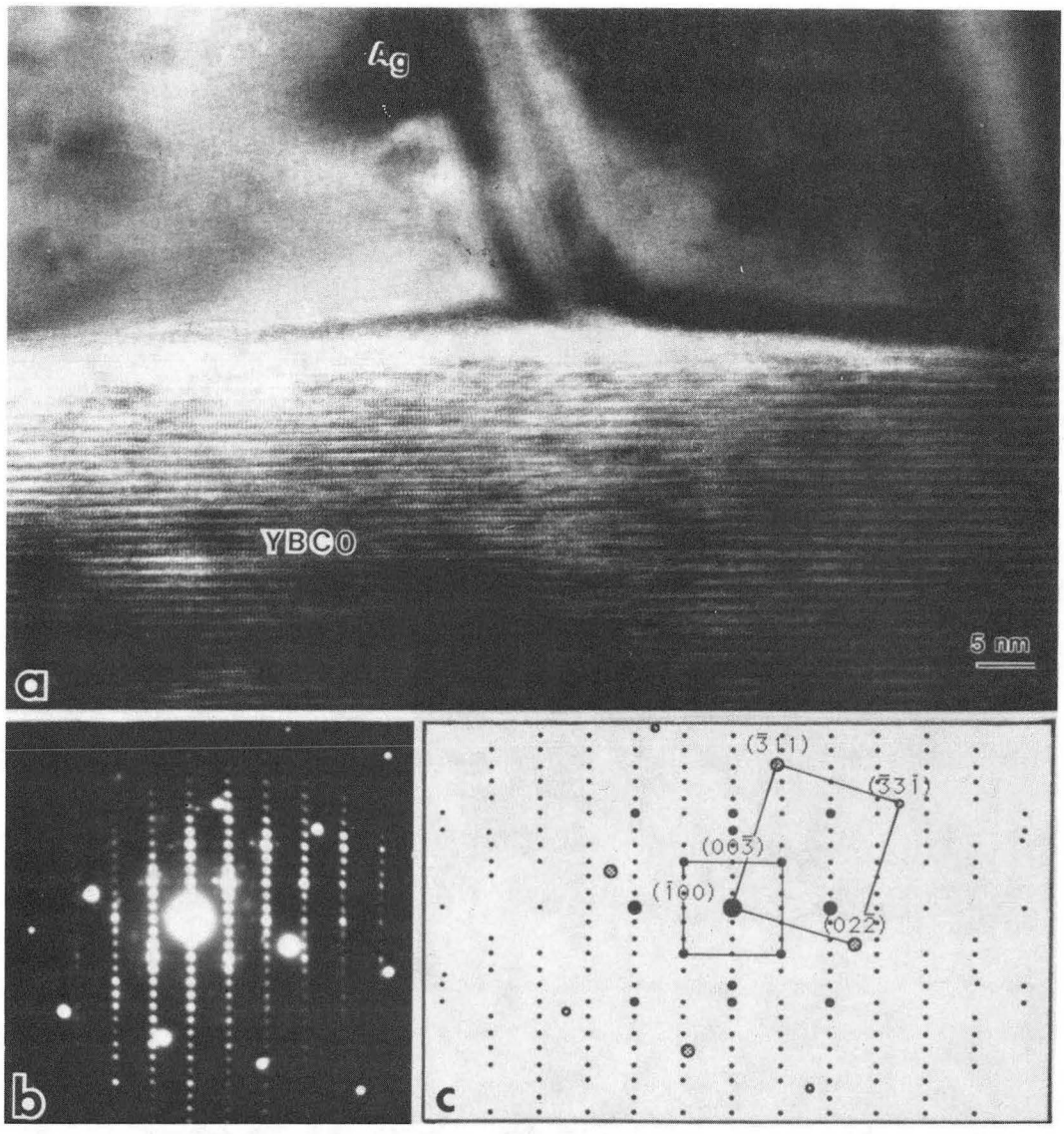

XBB 903-2420

Figure 26

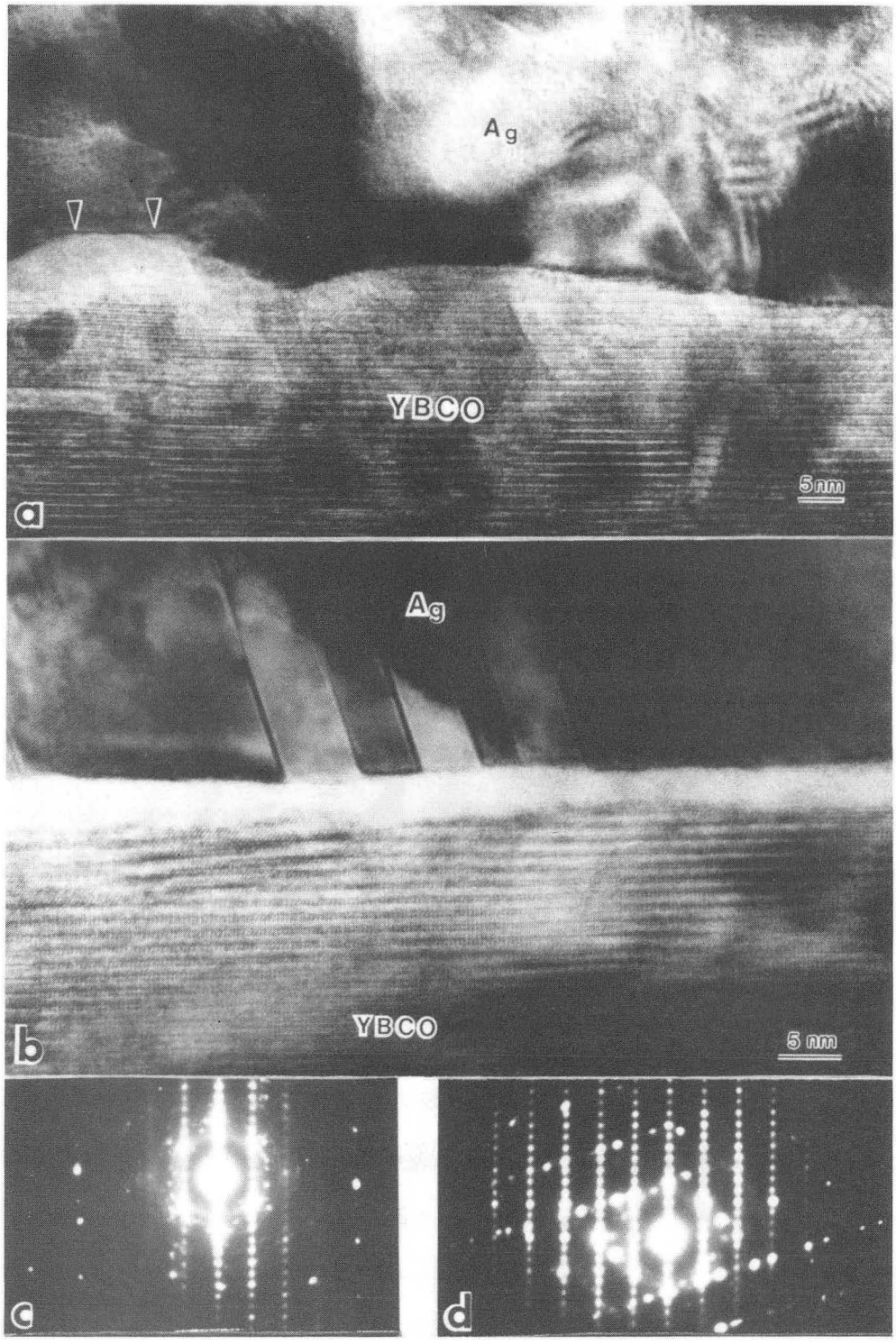

Figure 27

XBB 903-2442

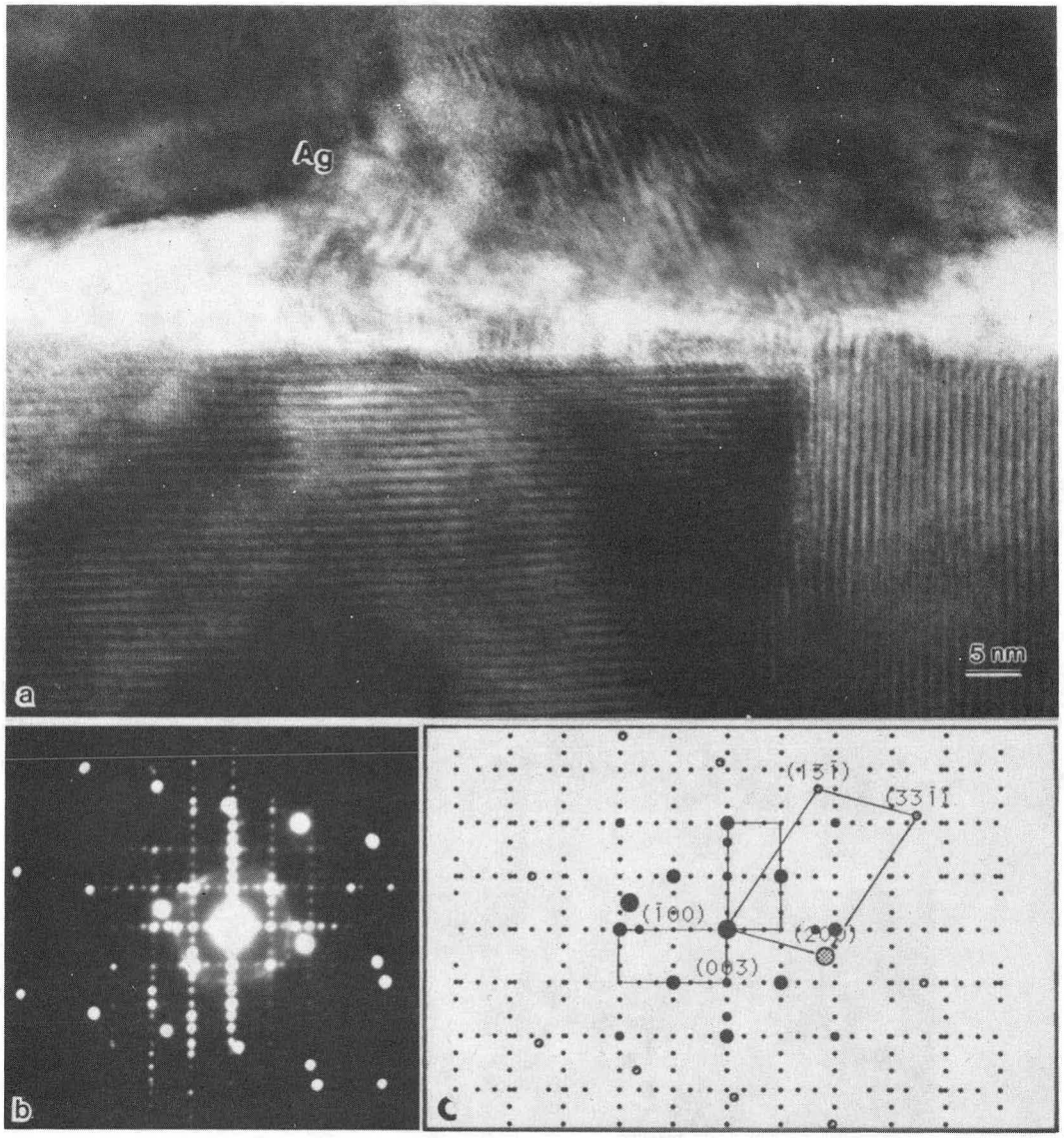

Figure 28

XBB 903-2419

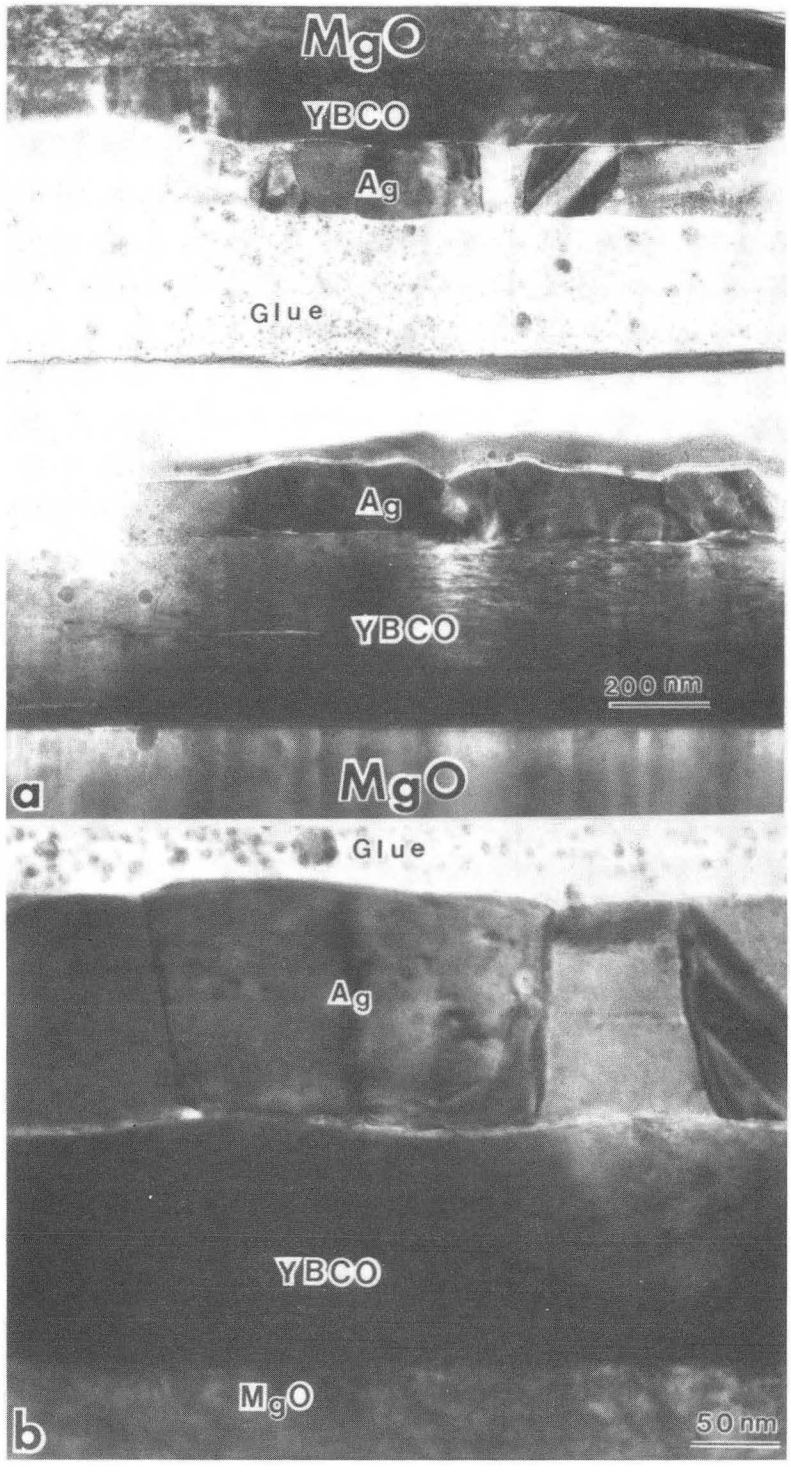

Figure 29 XBB 903-2438

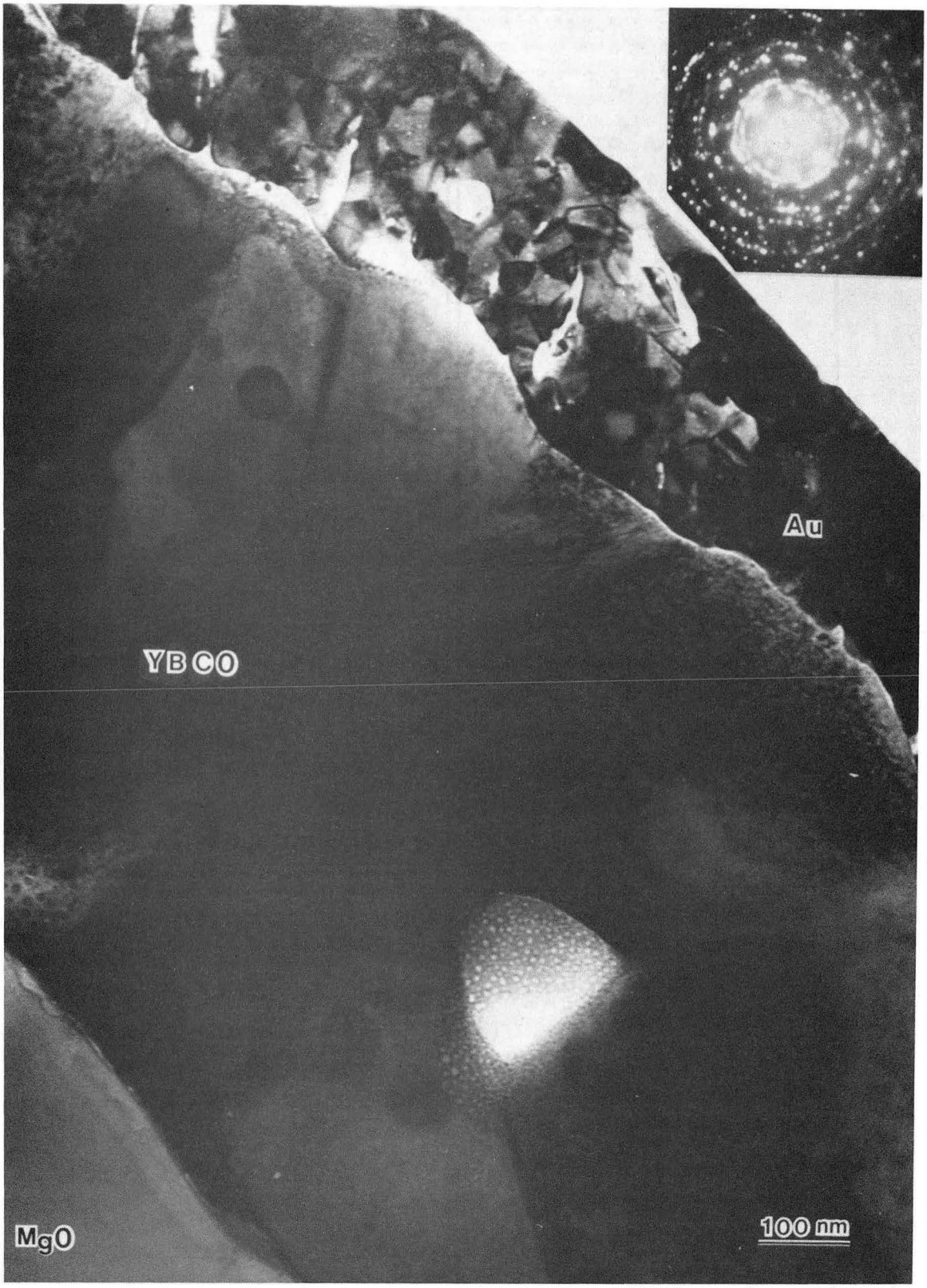

XBB 903-3561

Figure 30

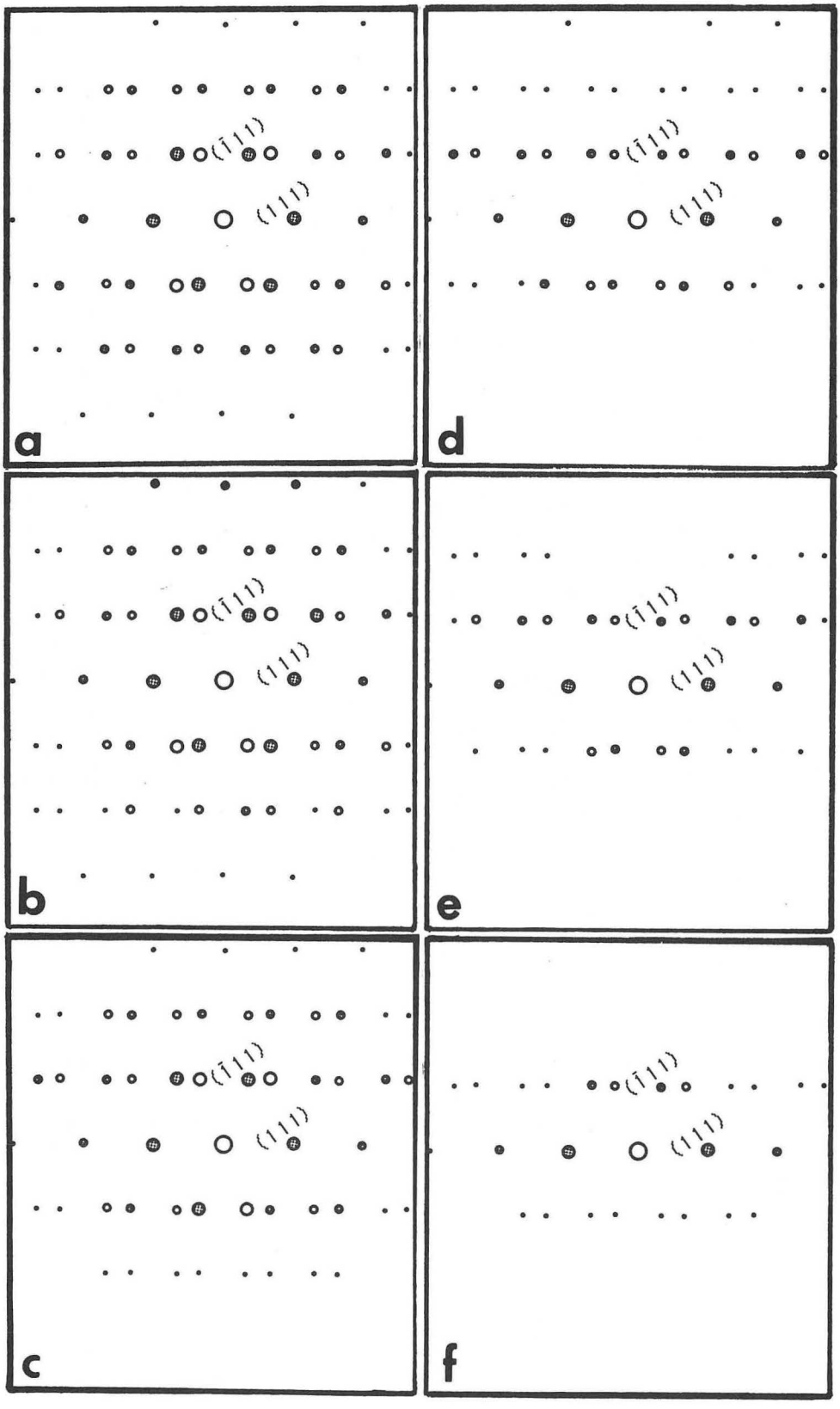

Figure 31

XBL 904-1315

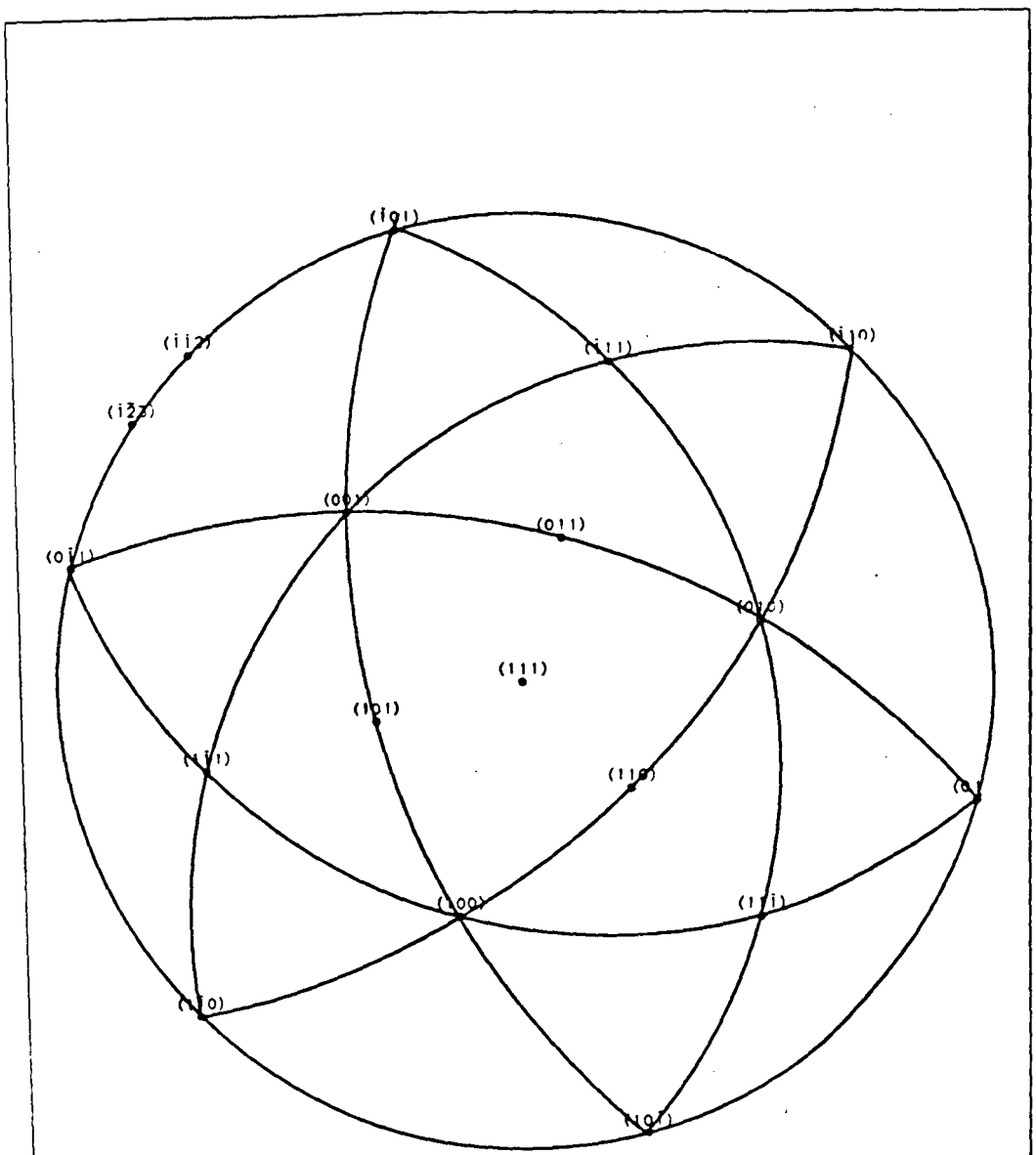

Figure 32

XBL 905-1616

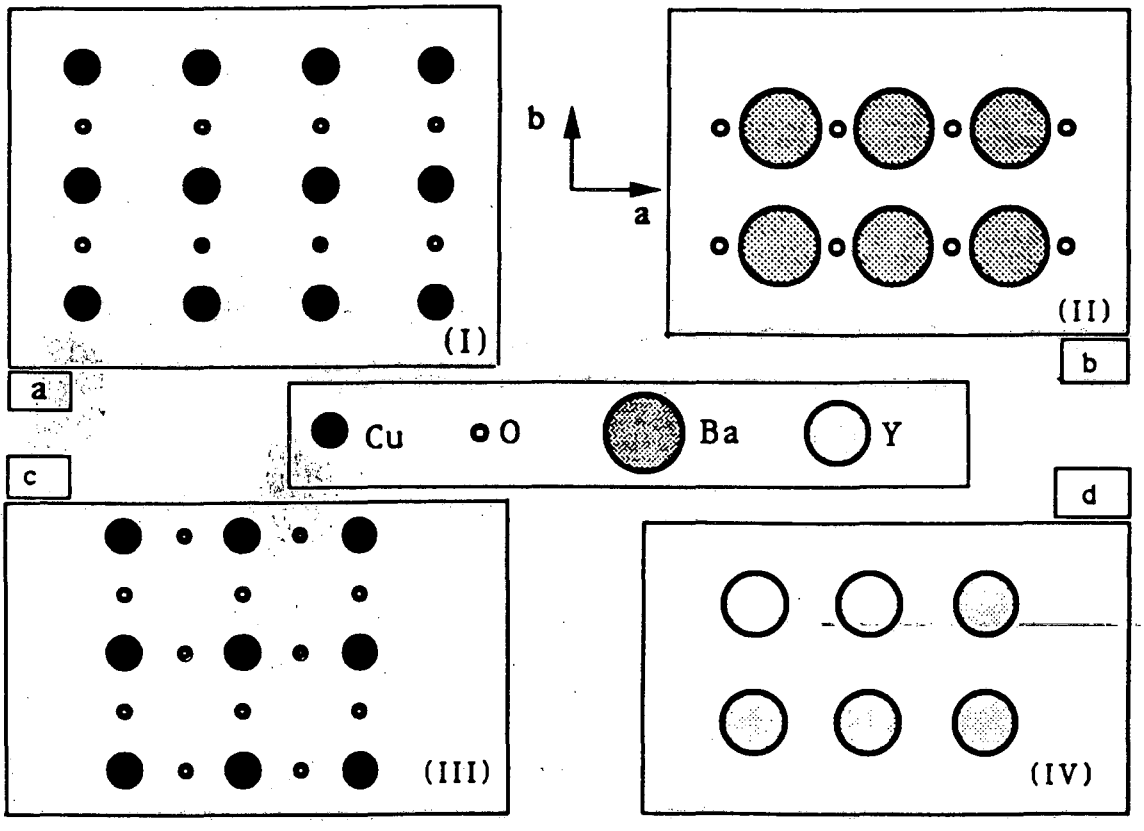

XBL 905-1617

Figure 33

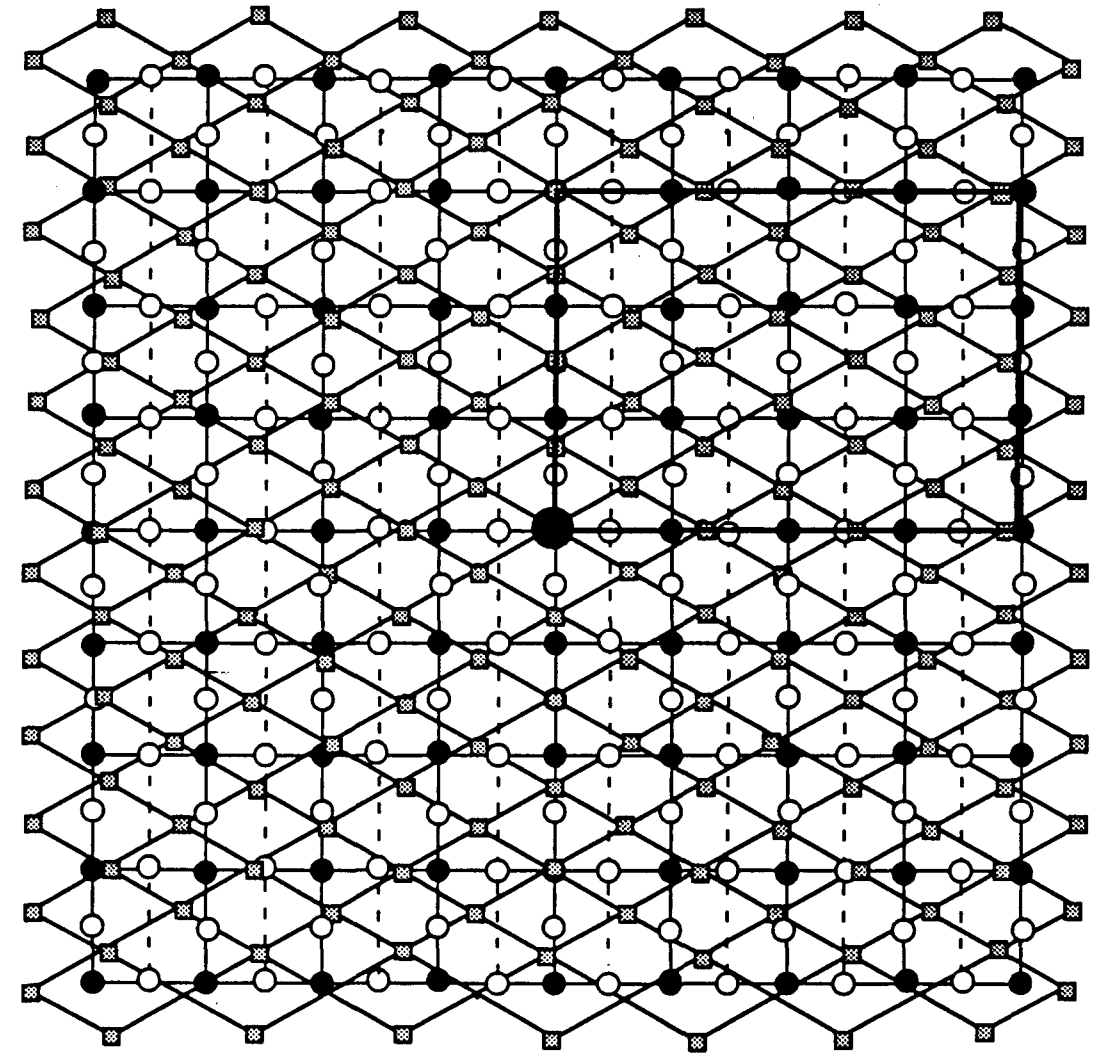

XBL 905-1618

Figure 34a

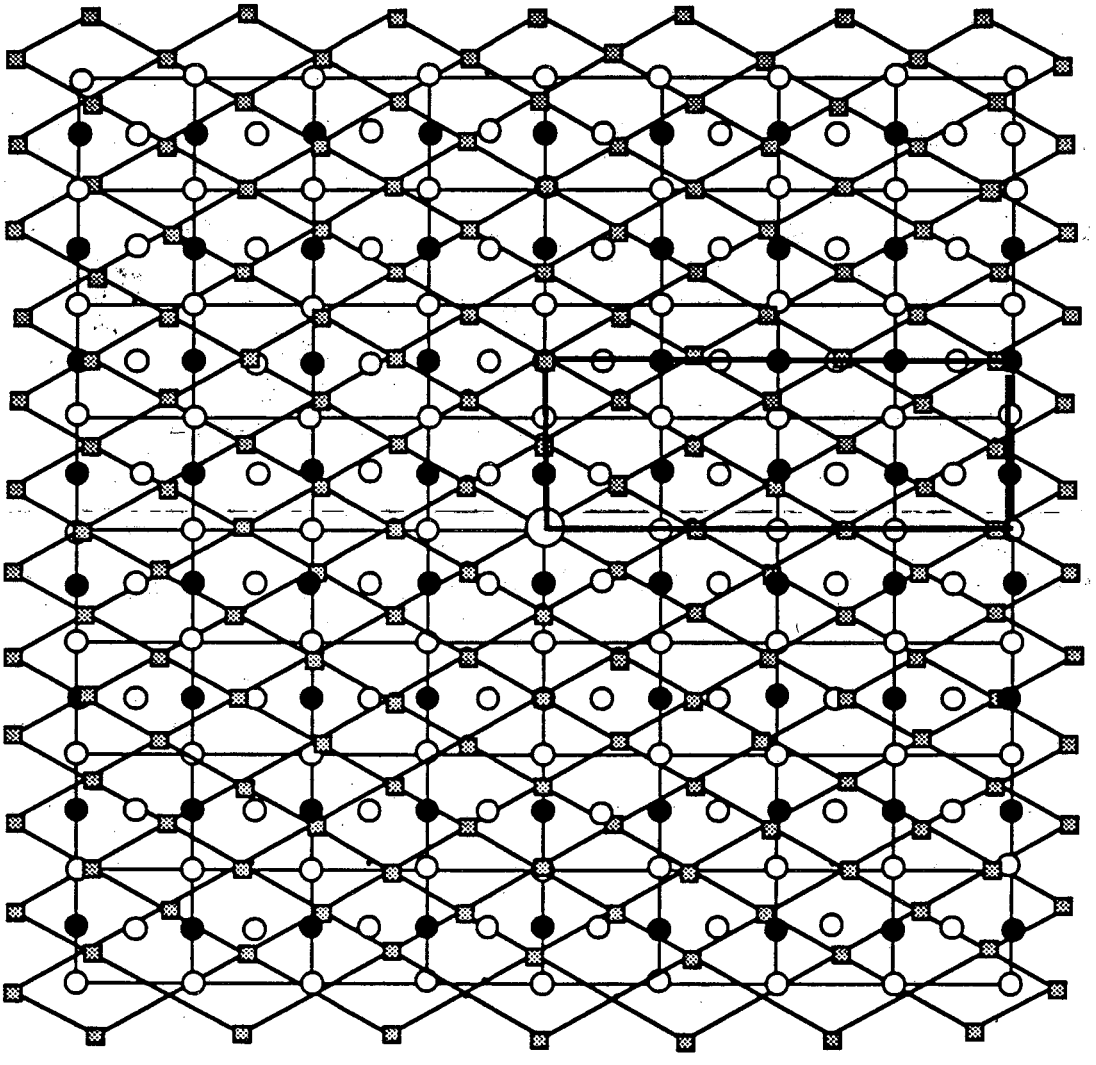

XBL 905-1619

Figure 34b

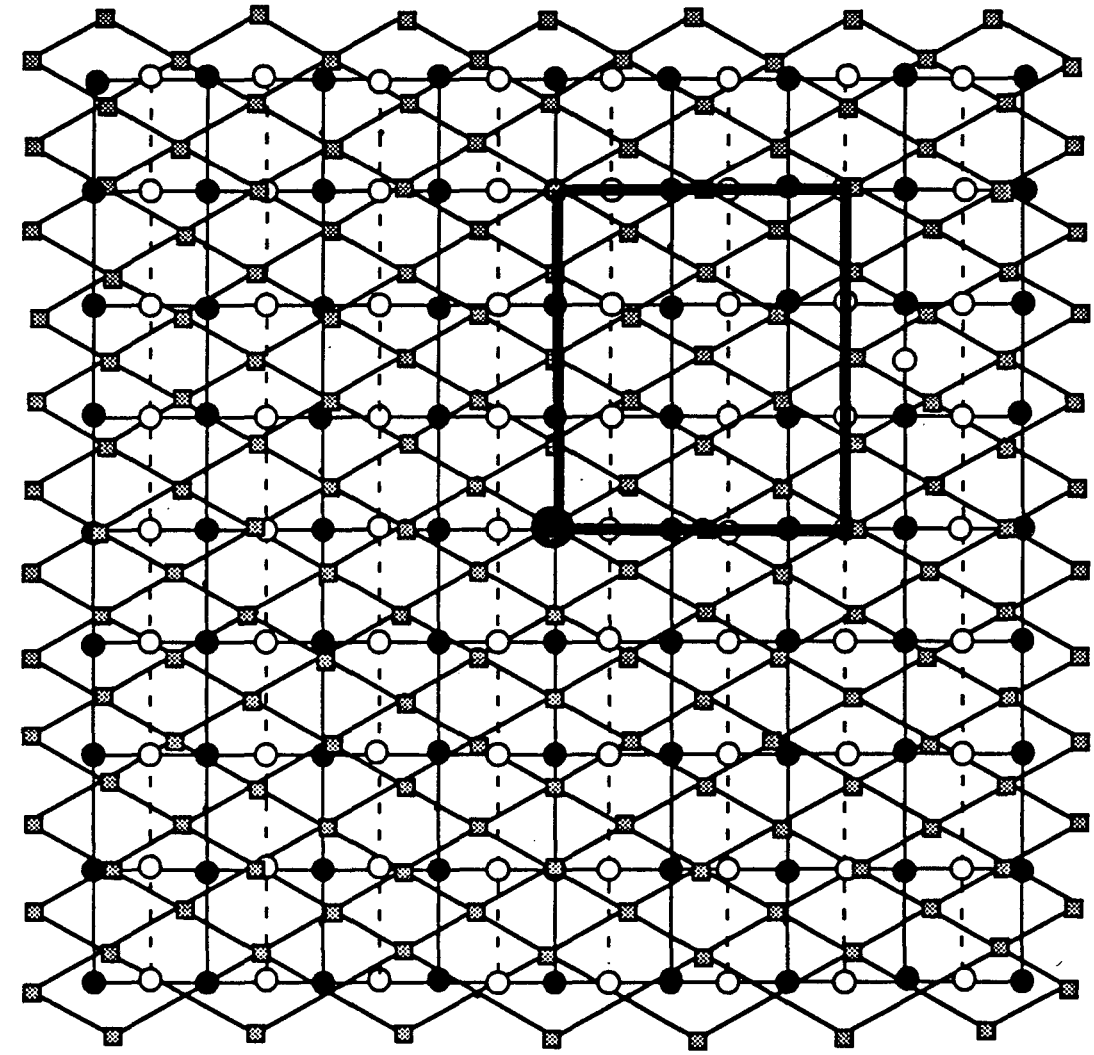

Figure 34c

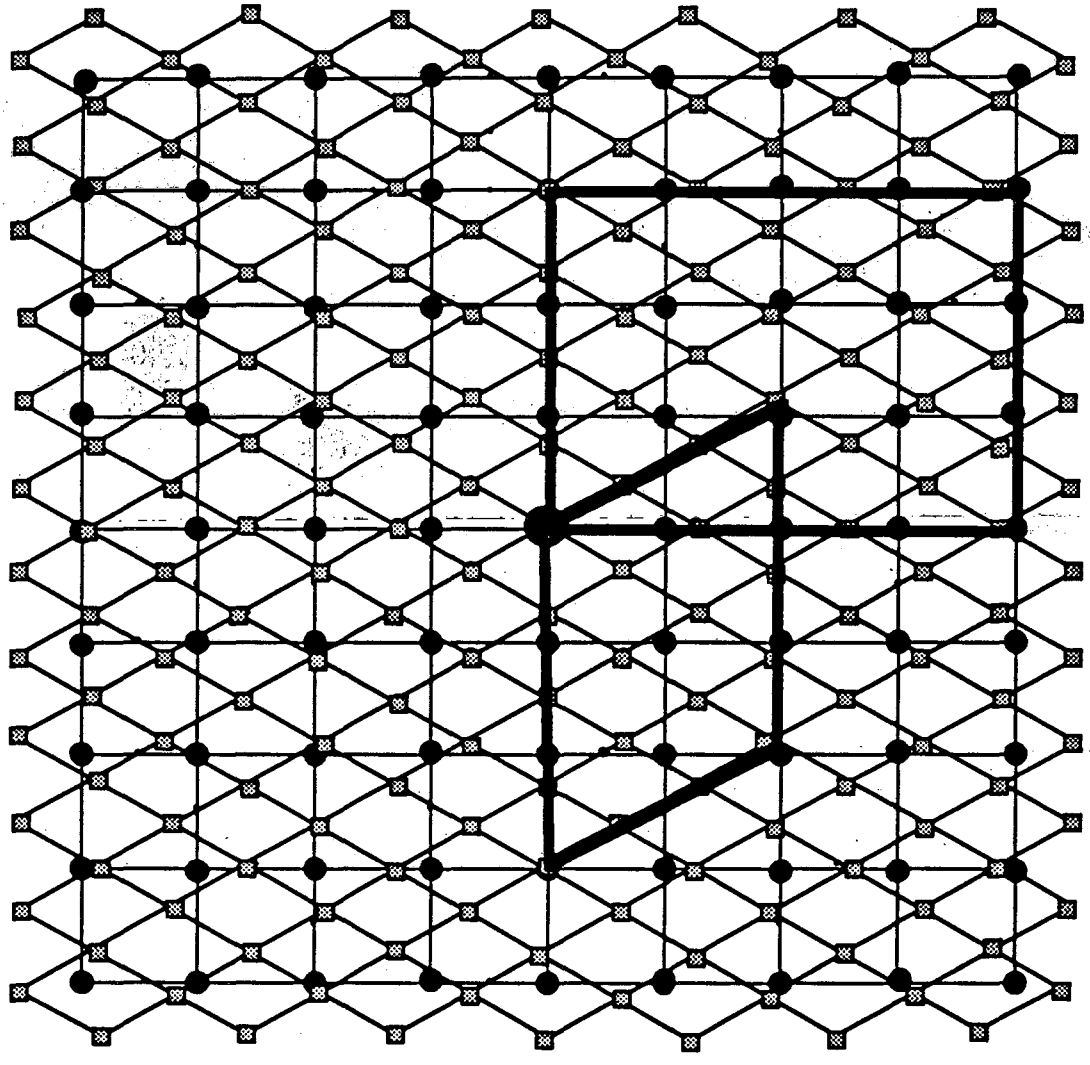

Figure 34d

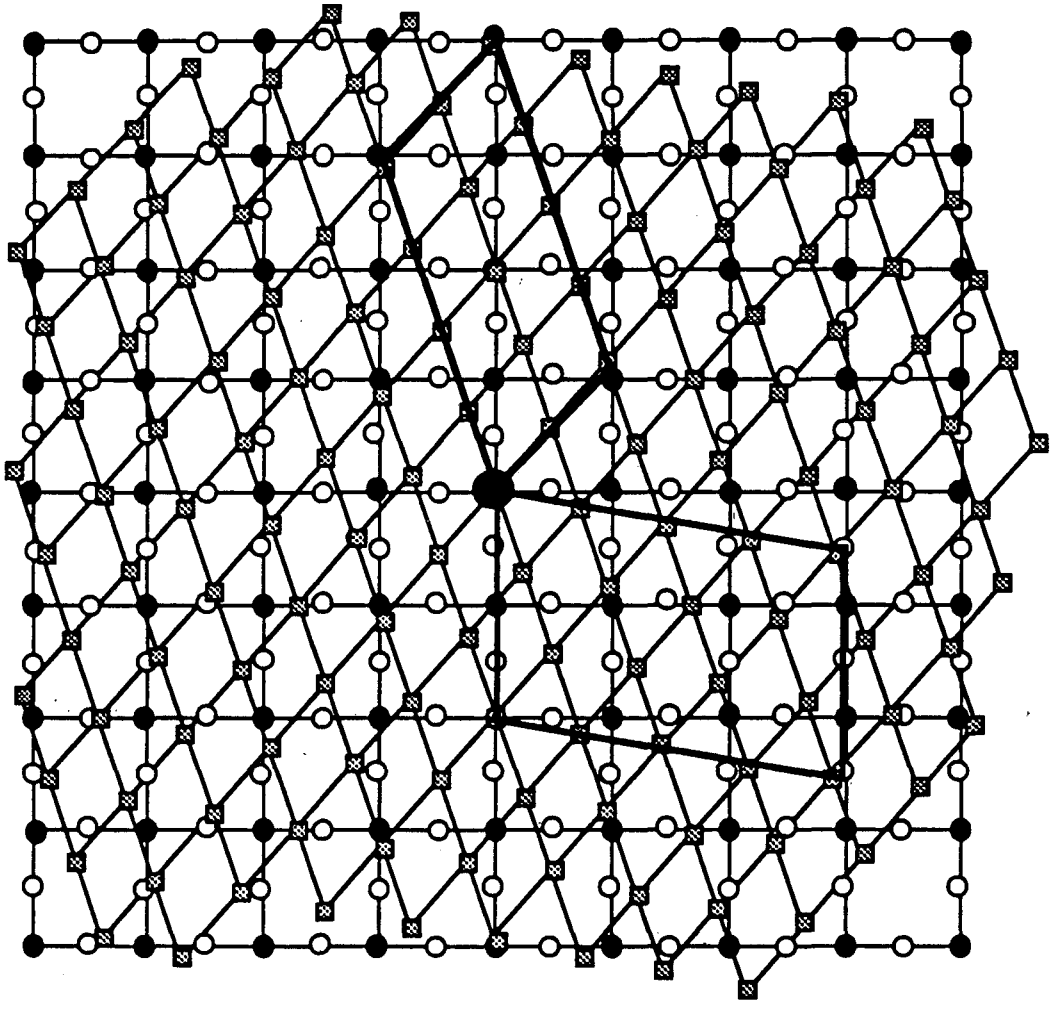

Figure 34e

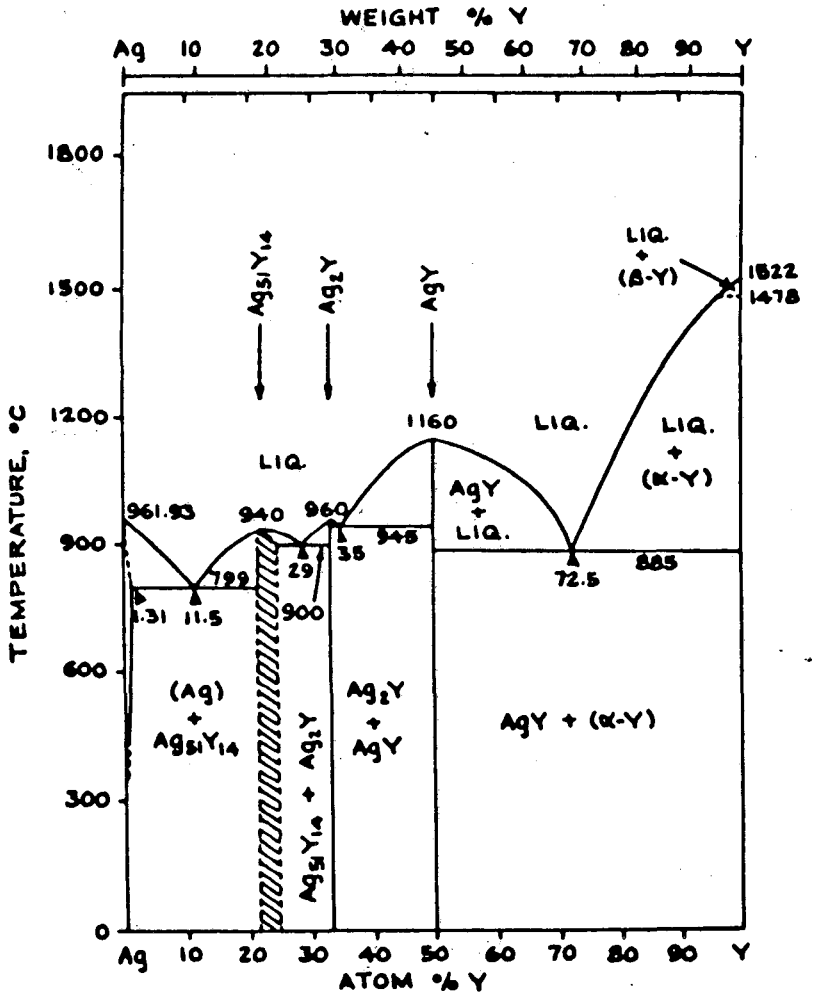

(a)

Figure 35

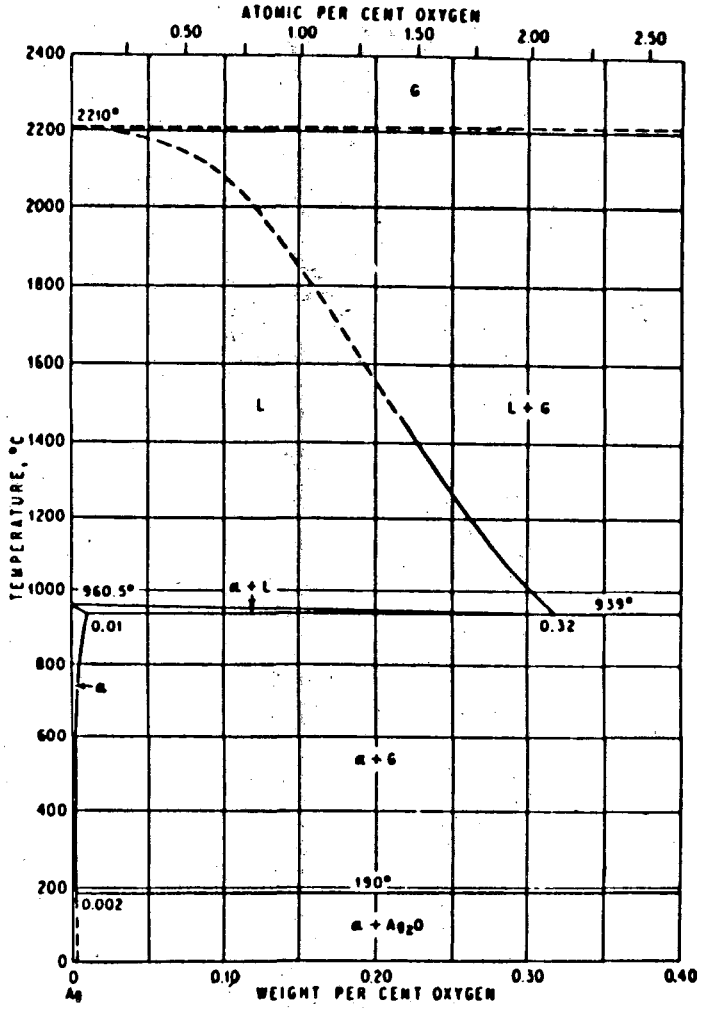

Fig. 22. Ag-O. (According to H. C. Vacher.)

(b)

XBL 905-1623

LAWRENCE BERKELEY LABORATORY
UNIVERSITY OF CALIFORNIA
INFORMATION RESOURCES DEPARTMENT
BERKELEY, CALIFORNIA 94720